UNIVERSITY OF SOUTHAMPTON

FACULTY OF ENGINEERING

Department of Ship Science

MEASUREMENT OF THE WAVE PATTERN RESISTANCE OF ASYMMETRIC HULL FORMS BY THE LONGITUDINAL CUT METHOD

by

D. A. Colman

Thesis for the

degree of

Master of Philosophy

ACKNOWLEDGEMENT

The author wishes to thank his supervisor, Dr. J. F. Wellicome for all his invaluable advice and assistance throughout the course of this work. Also he wishes to thank Mr. J. R. Gibbons for his advice and maintenance on all the electronic equipment and Mrs. M. Z. Strickland for typing this work.

C O N T E N T S

ABSTRACT

FACULTY OF ENGINEERING

SHIP SCIENCE

Master of Philosophy

MEASUREMENT OF THE WAVE PATTERN RESISTANCE OF ASYMMETRIC HULL FORMS BY THE LONGITUDINAL CUT METHOD

by Derek Alan Colman

Much work has been done on the measurement of the wave pattern resistance of hulls and a completely automated system has been developed by Hogben at N.P.L. However, this work has been concerned almost entirely with symmetric hull forms and wave patterns. This present work is concerned with the measurement of both symmetric and asymmetric wave patterns and thus establishing the wave pattern resistance of symmetric and asymmetric hull forms.

The wave pattern is measured by four wave probes spaced across the tank such that the first and fourth are equidistant from the centre-line and similarly for the second and third. Thus the symmetric and antisymmetric components of the asymmetric wave pattern are found respectively by halving the sum and difference of each pair of probes and their contribution to resistance is then calculated separately. The wave pattern expansion is as a Fourier series and the analysis makes a least squares fit over points measured, followed by the Gauss-Seidel method to solve the resulting simultaneous equations, in order to find the coefficients in the expansion. In general the analysis of the symmetric component is good but in the antisymmetric case the weaknesses of the method are more pronounced and the results consequently poor.

Plots of the total resistance and wave pattern resistance for the upright symmetric model show that their difference, the viscous resistance, is of the magnitude and behaviour expected. Previous wind tunnel results imply that the total wave pattern resistance should increase with yaw. However, results show that any increase is in fact small so the greater increase with yaw in total resistance in the tank over that in the tunnel must be sought within the viscous and induced resistances.

NOTATION

b	tank breadth
e	tank depth
g	gravitational acceleration
U	model velocity
x,y,z	coordinate axes
	x parallel to model direction, positive astern
	y perpendicular to x and horizontal
	z vertical, positive upwards
u,v,w	velocity perturbations in directions x, y, z
ℓ	L.W.L. of model
d	model draught
A	wetted surface area
S	underwater plan area
ζ	wave elevation, positive upwards
ζ_s	symmetric wave elevation
ζ_a	antisymmetric wave elevation
θ	wave angle
λ	wavelength
c	wave velocity = $U \cos \theta$
γ	$= 2\pi/\lambda$
ω_n	$= \gamma_n \cos \theta_n$ in expansion of symmetric wave pattern
Γ_m	$= \gamma_m \cos \theta_m$ in expansion of antisymmetric wave pattern
ξ_n, η_n	coefficients in expansion of symmetric wave pattern
μ_m, ν_m	coefficients in expansion of antisymmetric wave pattern
N	number of symmetric wave harmonics
M	number of antisymmetric wave harmonics
h	distance between sampling positions in x-direction
K	number of samples taken from each wave probe

R_T total resistance of model

R_v viscous resistance

R_I induced resistance

R_w wave pattern resistance

R_{ws} symmetric wave pattern resistance

R_{wa} antisymmetric wave pattern resistance

δR_w resistance component of one wave harmonic

$C_{D_{tank}}$ resistance coefficient in the towing tank $= R/\frac{1}{2}\rho U^2 S$

$C_{D_{tunnel}}$ resistance coefficient in the wind tunnel

F_r Froude number $= \frac{U}{\sqrt{g\ell}}$

Re Reynold's number $= \frac{U\ell}{\nu}$ ν kinematic viscosity

Λ quality of fit $\frac{\text{r.m.s. residual}}{\text{r.m.s. wave height}}$

1. INTRODUCTION

Essential to the model testing of hull forms in the towing tank is an understanding of the components of the total resistance to motion experienced by the model.

Following William Froude's early hypothesis that the total resistance can be divided into two components, the skin-friction resistance due to the tangential shear forces acting on the hull surface and a residuary resistance, due to normal pressure forces, mainly comprised of wave pattern resistance, Kelvin made a great step forward in the understanding of the wave pattern when, in 1904, he published his linearised theory of ship waves. In spite of the rather drastic approximation of representing the ship by a single point disturbance the wave pattern so produced bears a close resemblance to the general wave pattern shape of a real ship. Havelock continued theoretical work on wave patterns (ref. 3) and considered a wave pattern moving at velocity U comprised of waves moving with the wave pattern but at an angle θ to its direction and obtained

$$\zeta = \int_{-\pi/2}^{\pi/2} F(\theta) \sin\{K \sec^2\theta(x \cos\theta + y \sin\theta + \varepsilon(\theta))\}d\theta$$

where $K = \frac{2\pi c^2}{g}$, $F(\theta)$ is the amplitude factor and $\varepsilon(\theta)$ is phase, for the wave elevation.

By drawing lines representing the crests of waves at various values of θ, Havelock found that the envelope of these lines produced the typical wave pattern comprising both diverging and transverse waves, as seen behind a ship.

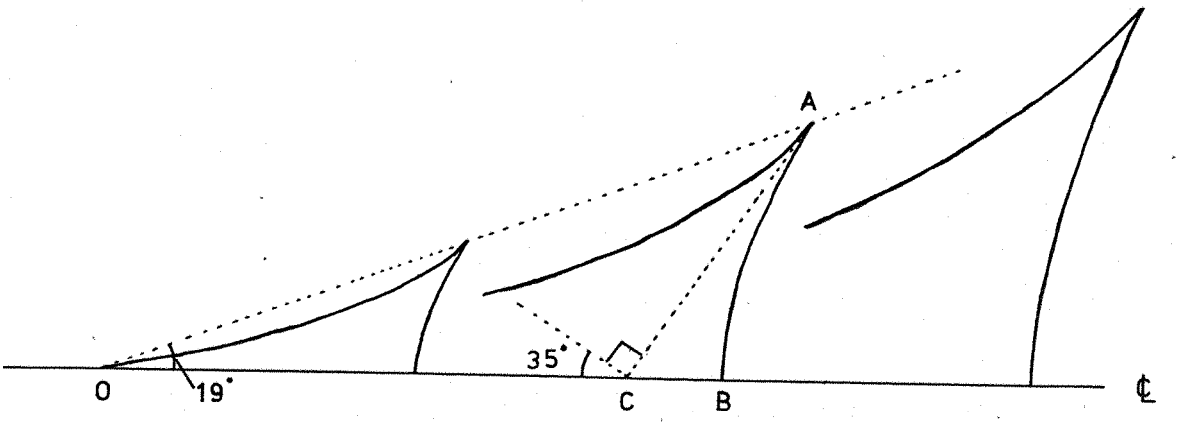

WAVE PATTERN BEHIND A SHIP

AC is parallel to crests of waves of angle 35^{o}. From the figure it is seen that the transverse waves are comprised of waves with an angle $\theta < 35^{o}$ while the divergent system is comprised of waves with $\theta > 35^{o}$. Also angle AOB is the Kelvin wave angle of approximately 19^{o}.

At the 11^{th} International Towing Tank Conference the components of resistance were discussed and the following diagrammatic break-down of total resistance resulted: (overleaf)

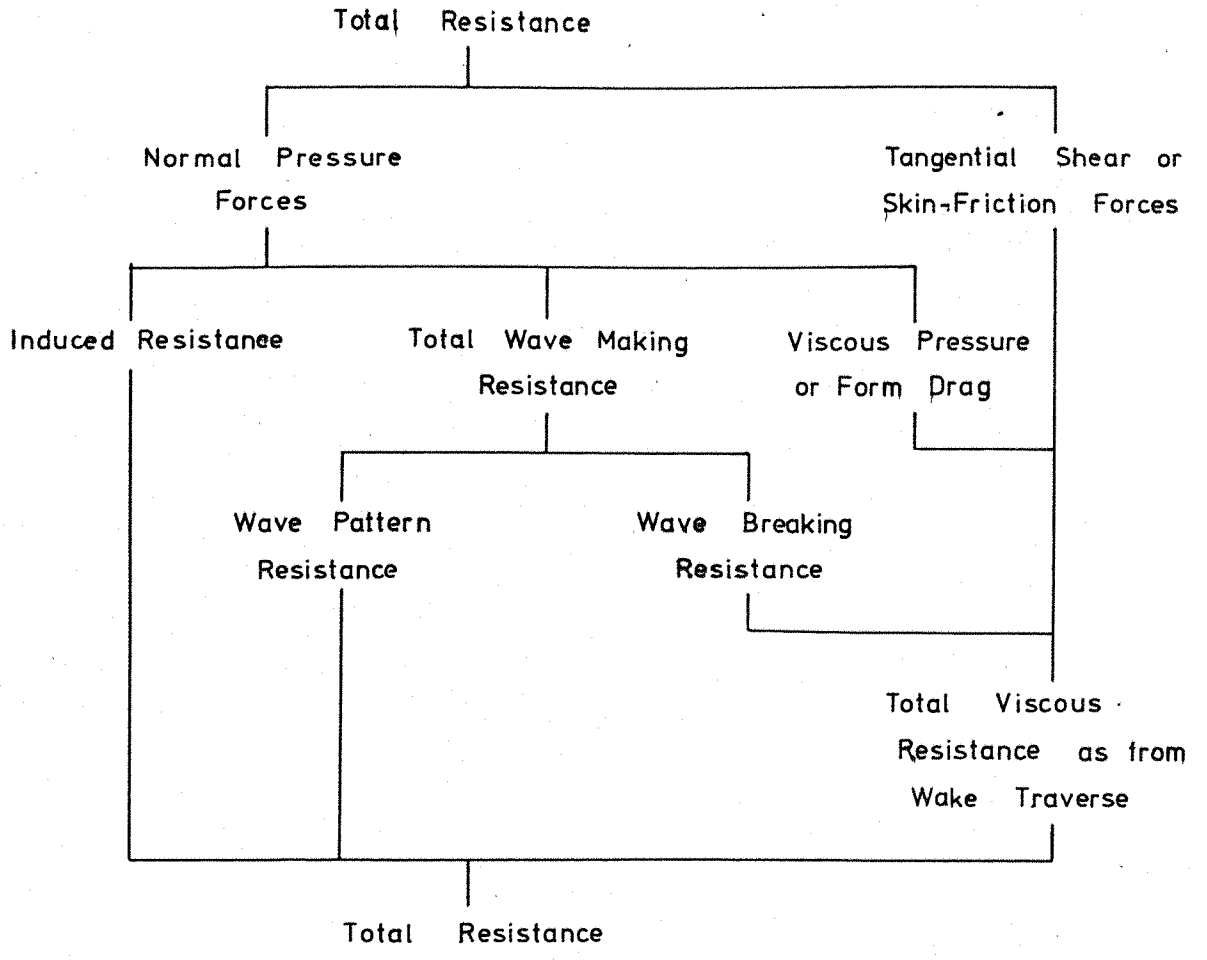

The actual forces acting directly on the hull itself are clearly the normal pressure and the tangential shear forces or skin friction which when integrated over the hull will result in the total resistance. However, actual direct measurement of these two quantities is obviously not convenient on any arbitrary model, so other components of resistance are sought by measurement, away from the hull, of the effect of the hull upon the surrounding water.

It is necessary to define the components measured such that they have a clear physical meaning and can be measured. Three components of resistance emerge:

1. The wave resistance: the force necessary to maintain the energy of the wave pattern, and can be calculated from measurements within the wave pattern. It is not the total wave making resistance of the

hull since that includes the energy dissipated into the wake through wave breaking.

2. The viscous resistance: that resistance associated with creating vorticity and turbulence, and can be measured by making a wake traverse astern of the model. Clearly this component will include the skin-friction resistance and the form drag or viscous pressure resistance due to boundary layer thickness and separation effects. Also included is the wave breaking resistance mentioned above.

3. The induced resistance: that resistance caused by the generation of trailing vortices. When the hull is not creating a net sideforce this component will in general be negligible. However, with the production of sideforce, and the inherent trailing vortices, the induced resistance will become significant. Unfortunately, at present there is no convenient way of measuring this component. It should be noted that ambiguity can arise if the induced resistance is defined as the difference between the total resistance at yaw and the total resistance at zero sideforce when it might well include some wave and viscous resistance.

Thus the total resistance can be subdivided:

$$R_T = R_W + R_V + R_I$$

It has in the past been experimental practice, when wishing to scale up measurements on ship models, to assume that the wave resistance is equal to the total resistance minus an estimation for viscous resistance based on the skin friction of a flat plate times some suitable form factor, calculated at low Froude number. However, various techniques for measuring the wave resistance have been developed and these can be divided into two main categories.

In the first instance measurements of the wave pattern are made and the wave resistance is calculated from the expression for the energy of the measured wave pattern. This method can be further subdivided into

two basic means of measurement.

Firstly the longitudinal cut method, as used in this present work and by Gadd and Hogben (ref. 2), in which measurements of the wave pattern are made by towing the model past fixed wave probes and thus obtaining longitudinal wave traces. Secondly the transverse cut method used by Eggers (ref. 1), in which measurements are made across the wave pattern at two fixed distances behind the model. An advantage of this second method is that the measuring apparatus is carried with the model thus avoiding the necessity of having separate shore-mounted wave probes.

All these methods are in fact approximate, since they rely on the application of linearised theory to the real disturbance, although in general they will be sufficiently accurate outside the wake and the vicinity of the model.

The second means of measuring the wave pattern resistance is by making measurements within the wave pattern that lead directly to an estimation of the resistance without actually establishing an expression for the wave pattern itself. Ward (ref. 12) calculates the wave pattern resistance from measurements of forces exerted by the passing wave pattern on a long circular cylinder held vertically in the water surface. This second approach does not provide as much information about the wave pattern as the first but its chief advantage is that it does not use any Fourier analysis, a technique used in all cases of the first instance, and which can lead to analysis problems, as found in the present work.

Work on wave pattern resistance at Southampton University was started in 1971 in a project by Wynne (ref. 14). He used the longitudinal cut method to study symmetric wave patterns and so all the basic equipment necessary for this method was already available. This equipment has been modified during the course of the present work and a more sophisticated

means of analysis adopted for calculating both the symmetric and anti-symmetric components of wave resistance found in an assymmetric wave pattern. For all experiments a 1/6th scale model of the 5.5 metre yacht 'Antiope' was used, although the purpose of this present work was not so much to measure the wave pattern resistance of 'Antiope', but rather to develope a reliable means of measuring symmetric and asymmetric wave patterns and hence the corresponding resistance in the towing tank.

The results from symmetric wave patterns obtained from the upright model are considered good from comparison of wave resistance with the total measured resistance and the high quality of fit of the calculated wave patterns to the measured wave patterns. However, when the model is yawed, thus producing asymmetric wave patterns, the results obtained deteriorate. The analysis of the symmetric component is still good but the antisymmetric component of resistance cannot be considered reliable.

2. THEORY

2.1 Components of Total Resistance from Consideration of Momentum

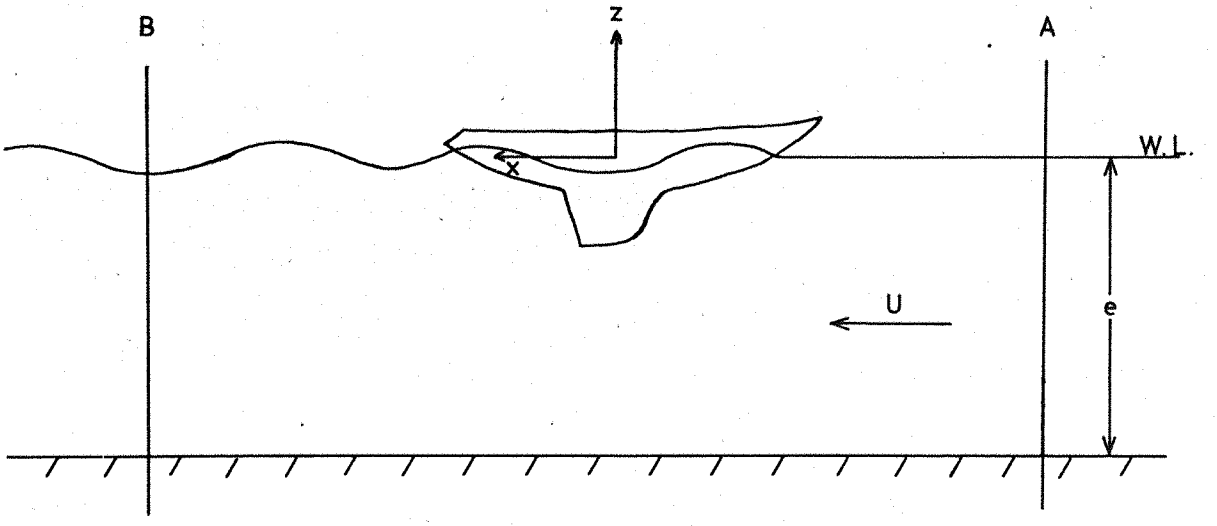

DIAGRAM OF THE MODEL IN THE TANK

Consider a model moving with constant velocity U in a towing tank of breadth b and depth e. Let axes x, y, z, having origin in the surface at the model centre, move with the model and denote longitudinal, transverse and vertical distances respectively, and u, v, w be the corresponding velocity perturbations. It is assumed that the flow about the model and within the wake and wave pattern is steady relative to the coordinate axes x, y, z. This assumption may not be strictly true if the model is free to trim and thus possibly suffer from small pitching oscillations.

Let A and B be two planes perpendicular to the x axis and such that A is in undisturbed water upstream of the model and B is a similar distance downstream of the model. Consider the control volume defined by the planes A and B, the walls and floor of the tank, the free surface and the wetted surface of the model. If it is assumed that the frictional forces at the walls and floor of the tank and also at the free surface are

negligible then the net force in the x direction acting upon the control volume is

(the integral of pressure over A) F_A

$-$ (the integral of pressure over B) F_B

$-$ (the total resistance of the model) R_T

and this must equal the change in the flux of momentum in the x direction through the control volume,

(flux of momentum // x through A) M_A

$-$ (flux of momentum // x through B) M_B.

Now suppose $\zeta(x, y)$ is the surface displacement or wave height at $(x, y, 0)$, then at A, $\zeta = 0$ and $u = v = w = 0$ and so by continuity since there is no flow through the tank walls and the surface is of constant shape, the net flow into the control volume at A must equal that flowing out at B

$$Ube = \int_{-b/2}^{b/2} \int_{-e}^{\zeta_B} (U + u)\, dzdy \tag{1}$$

Momentum flux across A is

$$M_A = \rho U^2 be = \rho U \int_{-b/2}^{b/2} \int_{-e}^{\zeta_B} (U + u) dzdy \tag{2}$$

Momentum flux across B is

$$M_B = \rho \int_{-b/2}^{b/2} \int_{-e}^{\zeta_B} (U + u)^2\, dzdy \tag{3}$$

Now from Bernoulli's principle if pressures are measured relative to atmospheric pressure the total head at A can be equated to the total head at B

$$\frac{P_A}{\rho} + \tfrac{1}{2}U^2 + gz = \frac{P_B}{\rho} + \tfrac{1}{2}((U + u)^2 + v^2 + w^2) + gz + \frac{\Delta p}{\rho} \tag{4}$$

where Δp is the viscous pressure loss and will therefore be zero outside the wake. Also on the surface at A, $P_A = 0$ and $z = 0$, so the total head is $\frac{1}{2}U^2$.

Hence the pressure force on A is

$$F_A = \int_{-b/2}^{b/2} \int_{-e}^{0} P_A \, dzdy = \tfrac{1}{2}\rho g b e^2 \qquad (5)$$

and the pressure force on B is

$$F_B = \int_{-b/2}^{b/2} \int_{-e}^{\zeta_B} P_B \, dzdy$$

$$= -\int_{-b/2}^{b/2} \int_{-e}^{\zeta_B} \{\rho g z + \Delta p + \tfrac{1}{2}\rho(2Uu + u^2 + v^2 + w^2)\} dzdy$$

$$= \tfrac{1}{2}\rho g b e^2 - \tfrac{1}{2}\rho g \int_{-b/2}^{b/2} \zeta_B^{\,2} \, dy$$

$$- \int_{-b/2}^{b/2} \int_{-e}^{\zeta_B} \Delta p \, dzdy - \tfrac{1}{2}\rho \int_{-b/2}^{b/2} \int_{-e}^{\zeta_B} (2Uu + u^2 + v^2 + w^2) dzdy \qquad (6)$$

Now from above

$$R_T = F_A - F_B + M_A - M_B$$

or

$$R_T = \tfrac{1}{2}\rho g \int_{-b/2}^{b/2} \zeta_B^{\,2} \, dy + \int_{-b/2}^{b/2} \int_{-e}^{\zeta_B} \Delta p \, dzdy + \tfrac{1}{2}\rho \int_{-b/2}^{b/2} \int_{-e}^{\zeta_B} (v^2 + w^2 - u^2) dzdy \qquad (7)$$

It is clear that the first term contributes to wave resistance while the second term is viscous resistance. Containing velocity perturbations the third term will contribute to wave pattern resistance, viscous resistance within the wake and also induced resistance due to trailing vortices.

Now define $\bar{u}$ such that

$$\frac{P_B}{\rho} + \tfrac{1}{2}((U + \bar{u})^2 + v^2 + w^2) + gz = \tfrac{1}{2}U^2$$

i.e., $$\tfrac{1}{2}(U + \bar{u})^2 = \tfrac{1}{2}(U + u)^2 + \frac{\Delta p}{\rho}$$

and $\bar{u}$ will differ from u only within the wake. Hence, equation (7) becomes

$$R_T = \tfrac{1}{2}\rho g \int_{-b/2}^{b/2} \zeta_B^{\,2}\, dy + \tfrac{1}{2}\rho \int_{-b/2}^{b/2} \int_{-e}^{\zeta_B} (v^2 + w^2 - \bar{u}^2)\, dz dy$$

$$+ \iint_{\text{wake}} \{\Delta p + \tfrac{1}{2}\rho(\bar{u}^2 - u^2)\}\, dz dy$$

and the last term can be identified as the total viscous resistance and will be zero outside the wake.

The second term must now be divided into induced resistance and some wave pattern resistance. From the theory of gravity waves, given the wave pattern $\zeta(x, y)$, the associated orbital velocities u_1, v_1, w_1 can be calculated. Thus components of resistance can be defined:

Wave pattern resistance

$$R_w = \tfrac{1}{2}\rho g \int_{-b/2}^{b/2} \zeta_B^{\,2}\, dy + \tfrac{1}{2}\rho \int_{-b/2}^{b/2} \int_{-e}^{\zeta_B} (v_1^{\,2} + w_1^{\,2} - u_1^{\,2})\, dz dy \qquad (8)$$

Viscous resistance

$$R_v = \iint_{\text{wake}} [\, \Delta p + \tfrac{1}{2}\rho(\bar{u}^2 - u^2) \,]\, dz dy \qquad (9)$$

Induced resistance

$$R_I = \tfrac{1}{2}\rho \int_{-b/2}^{b/2} \int_{-e}^{\zeta_B} (v^2 + w^2 - \bar{u}^2 - v_1^{\,2} - w_1^{\,2} + u_1^{\,2})\, dz dy \qquad (10)$$

and

$$\underline{R_T = R_w + R_v + R_I}. \qquad (11)$$

2.2 Wave Resistance Using Weighted Mean Square Method

The following method of calculating the wave pattern resistance was given by Gadd and Hogben (ref. 2) in one of their early papers on wave pattern resistance. The wave pattern of a model in a towing tank is comprised of waves moving at various angles θ to the direction of motion of the model.

Consider first the case of transverse waves moving with the model so $\theta = 0$.

Taking the mean of equation (γ) in the x direction

$$\bar{R}_w = \tfrac{1}{2}\rho g \int_{-b/2}^{b/2} \overline{\zeta_B^2}\, dy + \tfrac{1}{2}\rho \int_{-b/2}^{b/2} \int_{-e}^{\zeta_B} \overline{(v_1^2 + w_1^2 - u_1^2)}\, dz dy$$

Now $\bar{R}_w = R_w$, the motion being steady and $v_1 = 0$ since the waves being considered are transverse and hence have no transverse motion. In deep water waves the particles move round in circles; hence $\overline{w_1^2 - u_1^2} = 0$. Thus

$$R_w = \tfrac{1}{2}\rho g \int_{-b/2}^{b/2} \overline{\zeta_B^2}\, dy \qquad (12)$$

Now midway between a crest and a trough $\zeta = 0$ and also $u_1^2 = v_1^2 = 0$ in equation (γ) but w_1^2 is a maximum, therefore

$$R_w = \tfrac{1}{2}\rho \int_{-b/2}^{b/2} \int_{-e}^{\zeta_B} w_{1\,max}^2\, dz dy$$

$$= \tfrac{1}{2}\rho g \int_{-b/2}^{b/2} \overline{\zeta_B^2}\, dy \qquad (13)$$

In an oblique wave train where $\theta \neq 0$ equation (13) will still be valid and the average value of $(v_1^2 - u_1^2)$ is $(\sin^2\theta - \cos^2\theta)\overline{w_1^2}$ since the resultant of u_1 and v_1 is the horizontal component of particle motion.

Whence for an oblique wave train of angle θ

$$R_w = \tfrac{1}{2}\rho g \int_{-b/2}^{b/2} \overline{\zeta_B^2}\, dy + \tfrac{1}{2}\rho \int_{-b/2}^{b/2} \int_{-e}^{\zeta_B} 2\overline{w_1^2}\,(1 - \cos^2\theta)\, dz dy$$

$$= \tfrac{1}{2}\rho g \int_{-b/2}^{b/2} \overline{\zeta_B^2}\, dy + \tfrac{1}{2}\rho \int_{-b/2}^{b/2} \int_{-e}^{\zeta_B} w_{1_{max}}^2\,(1 - \cos^2\theta) dz dy$$

since w_1 is sinusoidal and so $w_{1_{max}}^2 = 2\overline{w_1^2}$.

Hence from equation (13)

$$R_w = \tfrac{1}{2}\rho g(2 - \cos^2\theta) \int_{-b/2}^{b/2} \overline{\zeta^2}\, dy \qquad (14)$$

for an oblique wave train of angle θ .

The wave resistance for a complete pattern is derived by choosing an effective average value for Cos θ in equation (14). Gadd & Hogben also describe a so-called Fourier strip method of analysing a series of longitudinal profiles and Hogben later developed a least square fitting technique known as the 'Matrix' method applicable to more general arrays and used in the automated system described in reference 6.

2.3 Fourier Expansion of the Wave Pattern

From work by Kelvin and Havelock it is seen that the wave pattern behind a ship is composed of wave trains moving at various angles θ to the direction of motion of the model.

Consider waves of angle θ, wavelength λ and wave velocity c contained in the wave pattern of a model moving along the centre-line of a tank of breadth b with velocity U.

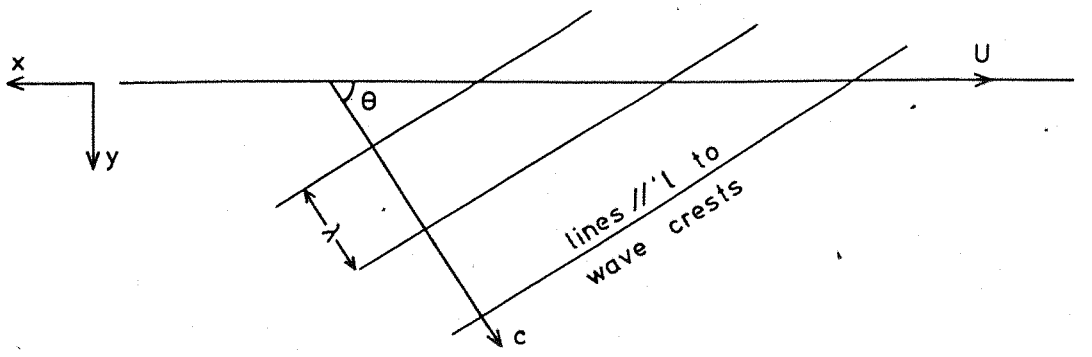

A TYPICAL WAVE TRAIN

There are three conditions which must be satisfied:

(a) The laws for gravity waves are obeyed.

(b) The wave pattern moves with the model.

(c) There is no flow through the tank walls.

Now $x \cos\theta - y \sin\theta$ = constant along lines parallel to the waves. Hence the equation for the wave elevation is

$$\zeta' = A \cos(x \cos\theta - y \sin\theta + \varepsilon)\frac{2\pi}{\lambda} \qquad (15)$$

where A and ε are constants.

From condition (a) $\frac{2\pi}{\lambda} = \frac{g}{c^2}$

and from (b) $c = U \cos\theta$.

Therefore

$$\frac{2\pi}{\lambda} = \frac{g}{U^2 \cos^2\theta} = \gamma \quad \text{(say)} \qquad (16)$$

Whence expanding (15)

$$\zeta' = A \cos[\gamma(x \cos\theta + \varepsilon)].\cos[\gamma y \sin\theta] + A \sin[\gamma(x \cos\theta + \varepsilon)].\sin[\gamma y \sin\theta] \qquad (17)$$

Now consider the wave train of angle $-\theta$ which will not necessarily be equal in magnitude or phase since the wave pattern may not be symmetric,

$$\zeta'^{-} = B \cos[\gamma (x \cos\theta + \delta)] . \cos[\gamma y \sin\theta]$$
$$- B \sin[\gamma (x \cos\theta + \delta)] . \sin[\gamma y \sin\theta] \qquad (18)$$

Now summing (17) and (18) and expanding

$$\zeta = \zeta' + \zeta'^{-}$$
$$= [\xi \cos(\gamma x \cos\theta) + \eta \sin(\gamma x \cos\theta)] \cos(\gamma y \sin\theta)$$
$$+ [\mu \cos(\gamma x \cos\theta) + \nu \sin(\gamma x \cos\theta)] \sin(\gamma y \sin\theta) \qquad (19)$$

where constants A, B, ε and δ have been absorbed in the coefficients ξ, η, μ, ν.

It is immediately seen that the first term is symmetric about the centre-line $y = 0$ while the second is antisymmetric about $y = 0$.

To satisfy condition (c) it is sufficient to apply the condition for reflection at the walls

$$\frac{d\zeta}{dy} = 0 \quad \text{at} \quad y = \pm \frac{b}{2} \quad \forall \; x.$$

Whence for the symmetric part

$$\sin(\gamma \frac{b}{2} \sin\theta) = 0$$

$$\frac{\gamma b}{2} \sin\theta = (n - 1)\pi$$

or

$$\gamma \sin\theta = \frac{2(n-1)\pi}{b} \qquad n \text{ integer} \geq 1 \qquad (20)$$

and for the antisymmetric part

$$\cos(\gamma \frac{b}{2} \sin\theta) = 0$$

$$\frac{\gamma b}{2} \sin\theta = \frac{(2m-1)}{2}\pi$$

or

$$\gamma \sin\theta = \frac{(2m-1)\pi}{b} \qquad m \text{ integer} \geq 1 \qquad (21)$$

(Note: Only positive values of m and n are taken since negative values lead to negative values of θ which are included from equation (18).)

Hence it is seen that for a model moving in a tank of breadth b

with velocity U the resulting wave pattern is composed of a discrete set of symmetric and antisymmetric waves given by equations (20), (21) and (16).

Thus for the whole wave pattern

$$\zeta = \zeta_{\text{symmetric}} + \zeta_{\text{antisymmetric}}$$

$$= \sum_{n=1}^{\infty} \left[\xi_n \cos(\omega_n x) + \eta_n \sin(\omega_n x)\right] \cos \frac{2(n-1)\pi y}{b}$$

$$+ \sum_{m=1}^{\infty} \left[\mu_m \cos(\Gamma_m x) + \nu_m \sin(\Gamma_m x)\right] \sin \frac{(2m-1)\pi y}{b} \qquad (22)$$

where $\omega_n = \gamma_n \cos \theta_n$

$\Gamma_m = \gamma_m \cos \theta_m$

and $\gamma_n \sin \theta_n = \frac{2(n-1)\pi}{b}$

$$\gamma_n = \frac{g}{U^2 \cos^2 \theta_n} = \frac{g}{2U^2}\left[1 + \sqrt{1 + 4\left(\frac{2(n-1)\pi U^2}{bg}\right)^2}\right]$$

and

$$\gamma_m \sin \theta_m = \frac{(2m-1)\pi}{b}$$

$$\gamma_m = \frac{g}{U^2 \cos^2 \theta_m} = \frac{g}{2U^2}\left[1 + \sqrt{1 + 4\left(\frac{(2m-1)\pi U^2}{bg}\right)^2}\right]$$

and ξ_n, η_n, μ_m, ν_m are constant coefficients.

2.4 The Wave Resistance From the Wave Pattern

The wave resistance for an oblique wave train as an integral of the mean wave height squared has been calculated (equation (14)),

$$R_w = \tfrac{1}{2}\rho g(2 - \cos^2\theta) \int_{-b/2}^{b/2} \overline{\zeta^2}\, dy$$

and the wave pattern is expressed in equation (22).

To arrive at an expression for the wave resistance in terms of the coefficients in the wave pattern expansion it is convenient to consider a tank of width $b' = 2b$ and with a centre-line such that $y' = y - \frac{b}{2}$.

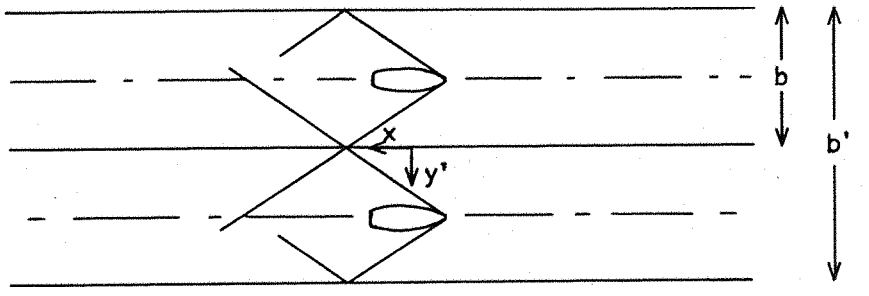

THE SYMMETRIC WAVE PATTERN IN THE DOUBLE TANK

The wave pattern now related to a tank of breadth b' represents the pattern obtained from two oppositely asymmetric models moving in tanks of breadth b with one coincident wall, as shown. The resulting wave pattern will be symmetric.

$$\zeta = \sum_{n=1}^{\infty} [\xi_n \cos(\gamma_n x \cos\theta_n) + \eta_n \sin(\gamma_n x \cos\theta_n)].\cos\frac{4(n-1)\pi(y' + \frac{b}{2})}{b'}$$

$$+ \sum_{m=1}^{\infty} [\mu_m \cos(\gamma_m x \cos\theta_m) + \nu_m \sin(\gamma_m x \cos\theta_m)].\sin\frac{2(2m-1)\pi(y' + \frac{b}{2})}{b'}$$

$$= \sum_{n=1}^{\infty} [\xi_n \cos(\gamma_n x \cos\theta_n) + \eta_n \sin(\gamma_n x \cos\theta_n)].\cos(\frac{4(n-1)\pi y'}{b'} + (n-1)\pi)$$

$$+ \sum_{m=1}^{\infty} [\mu_m \cos(\gamma_m x \cos\theta_m) + \nu_m \sin(\gamma_m x \cos\theta_m)].\sin(\frac{2(2m-1)\pi y'}{b'} + m\pi - \frac{\pi}{2})$$

$$= \sum_{r=1}^{\infty} [\alpha_r \cos(\gamma_r x \cos\theta_r) + \beta_r \sin(\gamma_r x \cos\theta_r)] \cos\frac{2(r-1)\pi y'}{b'} \qquad (23)$$

where if r is odd $\alpha_r = \pm \xi \frac{r+1}{2}$, $\beta_r = \pm \eta \frac{r+1}{2}$ $\left\{ \begin{array}{l} \frac{r+1}{2} \text{ even} \Rightarrow + \\ \frac{r+1}{2} \text{ odd} \Rightarrow - \end{array} \right.$

and if r is even $\alpha_r = \pm \mu \frac{r}{2}$, $\beta_r = \pm \nu \frac{r}{2}$ $\left\{ \begin{array}{l} \frac{r}{2} \text{ even} \Rightarrow + \\ \frac{r}{2} \text{ odd} \Rightarrow - \end{array} \right.$

and

$$\gamma_r = \frac{g}{U^2 \cos^2\theta_r}$$

$$= \frac{g}{2U^2} \left[1 + \sqrt{1 + 4\left(\frac{2(r-1)\pi U^2}{b'g}\right)^2}\right].$$

The total wave pattern resistance R_w' will be the sum of the wave resistances of each of the harmonics of the wave pattern.

$$R_w' = \tfrac{1}{2}\rho g \sum_{r=1}^{\infty} (2 - \cos^2\theta_r) \int_{-b'/2}^{b'/2} \overline{\zeta_r^2}\, dy'.$$

Now when $r = 1$, $\overline{\zeta_1^2} = \tfrac{1}{2}(\alpha_1^2 + \beta_1^2)$ since $\theta_1 = 0$

and so $\tfrac{1}{2}\rho g(2 - \cos^2\theta_1) \int_{-b'/2}^{b'/2} \overline{\zeta_1^2}\, dy' = \tfrac{1}{4}\rho g b'(\alpha_1^2 + \beta_1^2)$,

and when $r \geq 1$, $\overline{\zeta_r^2} = \tfrac{1}{2}(\alpha_r^2 + \beta_r^2)\cos^2 \frac{2(r-1)\pi y'}{b'}$

and $\tfrac{1}{2}\rho g(2 - \cos^2\theta_r) \int_{-b'/2}^{b'/2} \tfrac{1}{2}(\alpha_r^2 + \beta_r^2).\cos^2 \frac{2(r-1)\pi y'}{b'}\, dy' =$

$$= \tfrac{1}{4}\rho g b'(1 - \tfrac{1}{2}\cos^2\theta_r)(\alpha_r^2 + \beta_r^2).$$

Thus

$$R_w' = \tfrac{1}{4}\rho g b'(\alpha_1^2 + \beta_1^2) + \tfrac{1}{4}\rho g b' \sum_{r=2}^{\infty} (1 - \tfrac{1}{2}\cos^2\theta_r)(\alpha_r^2 + \beta_r^2). \qquad (24)$$

Now the actual wave pattern resistance $R_w = \tfrac{1}{2}R_w'$; thus halving equation (24) and substituting $b' = 2b$,

$$R_w = \tfrac{1}{4}\rho g b(\alpha_1^2 + \beta_1^2) + \tfrac{1}{4}\rho g b \sum_{r=2}^{\infty} (1 - \tfrac{1}{2}\cos^2\theta_r)(\alpha_r^2 + \beta_r^2)$$

$$= \tfrac{1}{4}\rho g b\{ \sum_{n=1}^{\infty}{}' (1 - \tfrac{1}{2}\cos^2\theta_n).(\xi_n^2 + \eta_n^2)\}$$

$$+ \tfrac{1}{4}\rho g b \{ \sum_{m=1}^{\infty} (1 - \tfrac{1}{2}\cos^2\theta_m).(\mu_m^2 + \nu_m^2)\} \qquad (25)$$

where the notation $\sum_{n=1}^{\infty}{}'$ $\Rightarrow$ the term in n = 1 is doubled.

2.5 Analysis of Measurements

The wave elevation ζ is measured at four positions across the tank y_1, y_2, y_3 and y_4 for K values of x from h to Kh in increments of h, such that $y_1 = -y_4$ and $y_2 = -y_3$. Now considering just one pair of y measurements, y and -y, from equation (22)

$$\zeta(y) = \zeta_s(y) + \zeta_n(y)$$

and by definition

$$\zeta_s(y) = \tfrac{1}{2}(\zeta(y) + \zeta(-y))$$

$$\zeta_a(y) = \tfrac{1}{2}(\zeta(y) - \zeta(-y)).$$

Hence the values of ζ_s and ζ_a are known at the points (x_j, y_1) and (x_j, y_2) where $1 \leq j \leq K$ and $x_j = j.h$. Consider the symmetric part

$$\zeta_s = \sum_{n=1}^{\infty} [\, \xi_n \cos(\omega_n x) + \eta_n \sin(\omega_n x)] \cos \frac{2(n-1)\pi y}{b} \qquad (26)$$

and assume that wave harmonics greater than N have negligible coefficients (see Appendix 3).

Let $\zeta_j = \zeta_s(x_j, y)$, multiply equation (26) by $\cos(\omega_r x_j)$ where $1 \leq r \leq N$, and sum over j. Whence

$$\sum_{j=1}^{K} \zeta_j \cos(\omega_r x_j)$$

$$= \sum_{j=1}^{K} \sum_{n=1}^{N} \{ [\xi_n \cos(\omega_n x_j)\cos(\omega_r x_j) + \eta_n \sin(\omega_n x_j)\cos(\omega_r x_j)] \cdot \cos \frac{2(n-1)\pi y}{b} \}$$

$$= r \sum_{n=1}^{N} \{ \cos \frac{2(n-1)\pi y}{b} \cdot \sum_{j=1}^{K} [\xi_n \tfrac{1}{2}(\cos(\omega_n + \omega_r)hj + \cos(\omega_n - \omega_r)hj) + \eta_n \tfrac{1}{2}(\sin(\omega_n + \omega_r)hj + \sin(\omega_n - \omega_r)hj)] \}$$

$$+ \sum_{j=1}^{K} \cos \frac{2(r-1)\pi y}{b} \{ \xi_r \tfrac{1}{2}(\cos(2\omega_r hj) + 1) + \eta_r \tfrac{1}{2} . \sin(2\omega_r hj) \}$$

$$= r \sum_{n=1}^{N} \cos \frac{2(n-1)\pi y}{b} \cdot [\xi_n \tfrac{1}{2} . (\frac{\cos \tfrac{1}{2}(\omega_n + \omega_r)h(K+1) . \sin \tfrac{1}{2}(\omega_n + \omega_r)hK}{\sin \tfrac{1}{2}(\omega_n + \omega_r)h}$$

$$+ \frac{\cos \tfrac{1}{2}(\omega_n - \omega_r)h(K+1) \sin \tfrac{1}{2}(\omega_n - \omega_r)hK}{\sin \tfrac{1}{2}(\omega_n - \omega_r)h})$$

$$+ \eta_n \tfrac{1}{2} (\frac{\sin \tfrac{1}{2}(\omega_n + \omega_r)h(K+1) \sin \tfrac{1}{2}(\omega_n + \omega_r)hK}{\sin \tfrac{1}{2}(\omega_n + \omega_r)h}$$

$$+ \frac{\sin \tfrac{1}{2}(\omega_n - \omega_r)h(K+1) \sin \tfrac{1}{2}(\omega_n - \omega_r)hK}{\sin \tfrac{1}{2}(\omega_n - \omega_r)h})]$$

$$+ \cos \frac{2(r-1)\pi y}{b} [\xi_r \tfrac{1}{2}(K + \frac{\cos \omega_r h(K+1) \sin \omega_r hK}{\sin \omega_r h})$$

$$+ \eta_r \tfrac{1}{2} . \frac{\sin \omega_r h(K+1) \sin \omega_r hK}{\sin \omega_r h}] \qquad (27)$$

where the notation $r \sum_{n=1}^{N}$ $\Rightarrow$ the sum omits the r^{th} term.

Now multiply by $\sin(\omega_r x_j)$ and sum over j,

$$\sum_{j=1}^{K} \zeta_j \sin(\omega_r x_j)$$

$$= \sum_{j=1}^{K} \sum_{n=1}^{N} \{[\xi_n \cos(\omega_n h\, j).\sin(\omega_r h\, j) + \eta_n \sin(\omega_n h\, j)\sin(\omega_r h j)].\cos \frac{2(n-1)\pi y}{b}\}$$

$$= r \sum_{n=1}^{N} \{ \cos \frac{2(n-1)\pi y}{b} \cdot \sum_{j=1}^{K} [\xi_n \tfrac{1}{2}(\sin(\omega_n + \omega_r)h\, j - \sin(\omega_n - \omega_r)h\, j)$$

$$- \eta_n \tfrac{1}{2}(\cos(\omega_n + \omega_r)hj - \cos(\omega_n - \omega_r)hj)]\}$$

$$+ \sum_{j=1}^{K} \cos \frac{2(r-1)\pi y}{b} \{\xi_r \tfrac{1}{2} \sin(2\omega_r h\, j) + \tfrac{1}{2}\eta_r(1 - \cos(2\omega_r h\, j))\}$$

$$= r \sum_{n=1}^{N} \cos \frac{2(n-1)\pi y}{b} [\xi_n \tfrac{1}{2}(\frac{\sin \tfrac{1}{2}(\omega_n + \omega_r)h(K+1).\sin \tfrac{1}{2}(\omega_n + \omega_r)hK}{\sin \tfrac{1}{2}(\omega_n + \omega_r)h}$$

$$- \frac{\sin \tfrac{1}{2}(\omega_n - \omega_r)h(K+1).\sin \tfrac{1}{2}(\omega_n - \omega_r)hK}{\sin \tfrac{1}{2}(\omega_n - \omega_r)h}$$

$$- \eta_n \tfrac{1}{2}(\frac{\cos \tfrac{1}{2}(\omega_n + \omega_r)h(K+1).\sin \tfrac{1}{2}(\omega_n + \omega_r)hK}{\sin \tfrac{1}{2}(\omega_n + \omega_r)h}$$

$$- \frac{\cos \tfrac{1}{2}(\omega_n - \omega_r)h(K+1).\sin \tfrac{1}{2}(\omega_n - \omega_r)hK}{\sin \tfrac{1}{2}(\omega_n - \omega_r)h})]$$

$$+ \cos \frac{2(r-1)\pi y}{b} [\xi_r \tfrac{1}{2}. \frac{\sin \omega_r h(K+1).\sin \omega_r hK}{\sin \omega_r h}$$

$$+ \eta_r \tfrac{1}{2}.(K - \frac{\cos \omega_r h(K+1).\sin \omega_r hK}{\sin \omega_r h})] \qquad (28)$$

(Note: the summation relations used above are given in Appendix 1.)

Thus a set of 2N simultaneous equations in ξ_n and η_n, $1 \leq n \leq N$ is formed

$$\underline{A}\,\underline{p} = \underline{q} \qquad (29)$$

where $p_i = \xi_i \qquad 1 \leq i \leq N$

$\eta_{i-N} \qquad N + 1 \leq i \leq 2N.$

Similarly for the antisymmetric part it is assumed that harmonics greater than M have negligible coefficients

$$\zeta_a = \sum_{m=1}^{M} \left[\mu_m \cos(\Gamma_m x) + \nu_m \sin(\Gamma_m x)\right] \sin \frac{(2m-1)\pi y}{b} \qquad (30)$$

If $\zeta_j = \zeta_n(x_j, y)$ multiply equation (30) by $\cos(\Gamma_r x_j)$ where $1 \leqslant r \leqslant M$ and sum over j. Whence

$$\sum_{j=1}^{K} \zeta_j \cos(\Gamma_r x_j)$$

$$= \sum_{j=1}^{K} \sum_{m=1}^{M} \{\left[\mu_m \cos(\Gamma_m x_j).\cos(\Gamma_r x_j) + \nu_m \sin(\Gamma_m x_j).\cos(\Gamma_r x_j)\right].\sin \frac{2(m-1)\pi y}{b}\}$$

and as above

$$= r \sum_{m=1}^{M} \sin \frac{(2m-1)\pi y}{b} \Big[\mu_m{}^{\frac{1}{2}}.\Big(\frac{\cos \frac{1}{2}(\Gamma_m + \Gamma_r)h(K+1).\sin \frac{1}{2}(\Gamma_m + \Gamma_r)hK}{\sin \frac{1}{2}(\Gamma_m + \Gamma_r)h}$$

$$+ \frac{\cos \frac{1}{2}(\Gamma_m - \Gamma_r)h(K+1).\sin \frac{1}{2}(\Gamma_m - \Gamma_r)hK}{\sin \frac{1}{2}(\Gamma_m - \Gamma_r)h}\Big)$$

$$+ \nu_m{}^{\frac{1}{2}}.\Big(\frac{\sin \frac{1}{2}(\Gamma_m + \Gamma_r)h(K+1).\sin \frac{1}{2}(\Gamma_m + \Gamma_r)hK}{\sin \frac{1}{2}(\Gamma_m + \Gamma_r)h}$$

$$+ \frac{\sin \frac{1}{2}(\Gamma_m - \Gamma_r)h(K+1).\sin \frac{1}{2}(\Gamma_m - \Gamma_r)hK}{\sin \frac{1}{2}(\Gamma_m - \Gamma_r)h}\Big)\Big]$$

$$+ \sin \frac{(2r-1)\pi y}{b} \Big[\mu_r{}^{\frac{1}{2}}\Big(K + \frac{\cos \Gamma_r h(K+1).\sin \Gamma_r hK}{\sin \Gamma_r h}\Big)$$

$$+ \nu_r{}^{\frac{1}{2}}.\frac{\sin \Gamma_r h(K+1).\sin \Gamma_r hK}{\sin \Gamma_r h}\Big] \qquad (31)$$

Now multiply by $\sin(\Gamma_r x_j)$ and sum over j:

$$\sum_{j=1}^{K} \zeta_j \sin(\Gamma_r x_j)$$

$$= \sum_{j=1}^{K} \sum_{m=1}^{M} \{[\mu_m \cos(\Gamma_m hj)\sin(\Gamma_r hj) + \nu_m \sin(\Gamma_m hj)\sin(\Gamma_r hj)].\sin\frac{(2m-1)\pi y}{b}\}$$

$$= r \sum_{m=1}^{M} \sin\frac{(2m-1)\pi y}{b} \left[\mu_m \tfrac{1}{2}\left(\frac{\sin \tfrac{1}{2}(\Gamma_m + \Gamma_r)h(K+1).\sin \tfrac{1}{2}(\Gamma_m + \Gamma_r)hK}{\sin \tfrac{1}{2}(\Gamma_m + \Gamma_r)h}\right.\right.$$

$$\left. - \frac{\sin \tfrac{1}{2}(\Gamma_m - \Gamma_r)h(K+1).\sin \tfrac{1}{2}(\Gamma_m - \Gamma_r)hK}{\sin \tfrac{1}{2}(\Gamma_m - \Gamma_r)h}\right)$$

$$- \nu_m \tfrac{1}{2}.\left(\frac{\cos \tfrac{1}{2}(\Gamma_m + \Gamma_r)h(K+1).\sin \tfrac{1}{2}(\Gamma_m + \Gamma_r)hK}{\sin \tfrac{1}{2}(\Gamma_m + \Gamma_r)h}\right.$$

$$\left. - \frac{\cos \tfrac{1}{2}(\Gamma_m - \Gamma_r)h(K+1).\sin \tfrac{1}{2}(\Gamma_m - \Gamma_r)hK}{\sin \tfrac{1}{2}(\Gamma_m - \Gamma_r)h}\right) \Big]$$

$$+ \sin\frac{(2r-1)\pi y}{b} \left[\mu_r \tfrac{1}{2}.\ \frac{\sin \Gamma_r h(K+1).\sin \Gamma_r hK}{\sin \Gamma_r h}\right.$$

$$\left. + \nu_r \tfrac{1}{2}\left(K - \frac{\cos \Gamma_r h(K+1).\sin \Gamma_r hK}{\sin \Gamma_r h}\right)\right] \qquad (32)$$

Thus a set of 2M simultaneous equations in η_m and ν_m, $1 \leq m \leq M$ is formed as above,

$$\underline{\underline{B}}\ \underline{p} = \underline{q}$$

where $p_i = \mu_i \qquad 1 \leq i \leq M$

$\nu_{i-M} \qquad M+1 \leq i \leq 2M.$

It is now necessary to solve these two sets of simultaneous equations. In practice if y_1 and y_2 are suitably chosen (see section 3.3) it is possible, for each equation, to select a value of y which will maximise the factor $\cos\frac{2(r-1)\pi y}{b}$ or $\sin\frac{(2r-1)\pi y}{b}$ and hence the coefficients of ξ_r, η_r, μ_r and ν_r in the r^{th} equations respectively.

Thus matrices $\underline{\underline{A}}$ and $\underline{\underline{B}}$ are formed with strong diagonal elements

suitable for the application of the Gauss-Seidel method of solving simultaneous equations (see ref. 11 and Appendix 2).

The computer program written for the above analysis of results is discussed in Appendix 4.

3. APPARATUS

3.1 The Towing Tank

The Southampton University towing tank was used for all experimental work carried out. The tank has a breadth b of 2.45m and depth e of 1.22m and the length over which the towed model moves at the constant set velocity is 14.2m. Since the working length of the tank is so small it was necessary to position the wave probes carefully so as to optimise the length of the recorded wave trace.

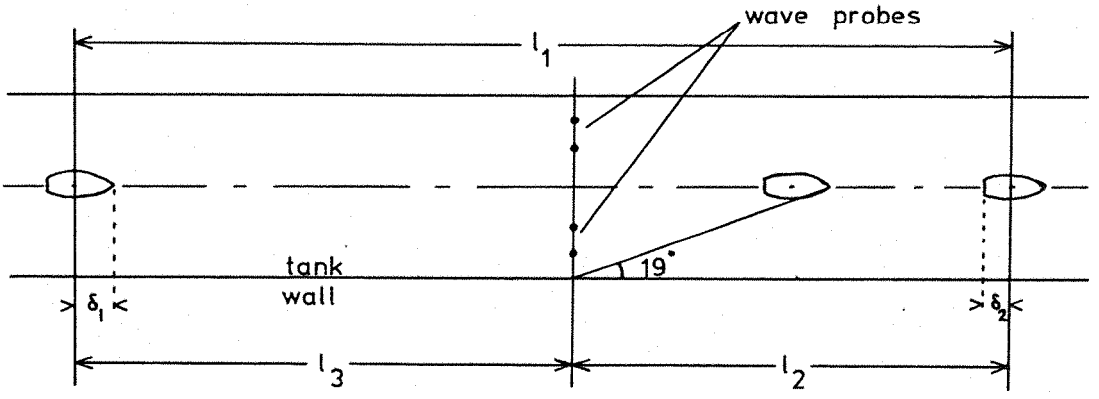

LONGITUDINAL WAVE PROBE POSITIONS

Suppose the model moves with constant velocity U between A and B, and the wave pattern as a whole also moves with the model at velocity U. However, since the group velocity of a set of waves with individual velocities U is $\frac{1}{2}U$ (ref. 10) the end of the wave pattern will move with velocity $\frac{1}{2}U$. Hence, if time $t = 0$ when the model is at A, the end of the wave pattern will reach the probes at time $t = 2(\ell_3 - \delta_1)/U$.

Also the time at which the waves due to deceleration reach the probe from B is

$$t = \frac{2(\ell_2 - \delta_2)}{U} + \frac{\ell_1}{U}.$$

Now for optimum positioning of the probes these two events will be concurrent; hence

$$2(\ell_3 - \delta_1) = 2(\ell_2 - \delta_2) + \ell_1$$

or $$4\ell_2 = \ell_1 - 2\delta_1 + 2\delta_2$$

and if $$\delta_1 \simeq \delta_2$$

then $$\ell_2 = \tfrac{1}{4}\ell_1$$

and the time at the end of the maximum length trace recordable is

$$t = \frac{2(\frac{3}{4}\ell_1 - \delta_1)}{U} \simeq \frac{3}{2}\frac{\ell_1}{U}.$$

If recording is started when the model passes the probes at time $\frac{\ell_3}{U} = \frac{3}{4}\frac{\ell_1}{U}$ then the length of the trace will be

$$\frac{3}{2}\ell_1 - \tfrac{3}{4}\ell_1 = \tfrac{3}{4}\ell_1.$$

Now substituting in dimensions of the tank it is found that

$$\ell_2 = 3.55\text{m}$$

and the length of trace ≃ 10m.

3.2 The Wave Probes

Four capacitance wave probes were used for measuring the wave elevation. This is an established method of measurement and is well developed within the Ship Division at N.P.L. Each probe consists of a polyurethane coated wire strung vertically through the water surface. By the use of four 'grey boxes' the capacitance between the wire and the water, using the polyurethane as dielectric, can be made proportional to the wave elevation about the wire, and hence, with further electronics, outputs can be obtained whose voltage is proportional to the wave elevation at the wire and thus suitable for recording. Details of the probe design and electronics are given in Appendix 5.

3.3 Lateral Spacing of Wave Probes

As mentioned above in section 2.5 it is necessary to position the wave probes laterally across the tank so that a probe may be chosen whose value of y is such that for each harmonic in the symmetric case the term $\cos \frac{2(n-1)\pi y}{b} \neq 0$ and for each harmonic in the antisymmetric case $\sin \frac{(2n-1)\pi y}{b} \neq 0$. In practice it is desirable that the probes are positioned such that the least possible values of the sine and cosine are reasonably large and the aim of the following is to establish positions where this is the case.

Considering first the symmetric case:

if $\cos \frac{2(n-1)\pi y}{b} \neq 0 \qquad \forall \quad n > 0$

a sufficient condition for this is that $\frac{2(n-1)\pi y}{b}$ is not an integral value of π whence $\frac{2(n-1)\pi y}{b} = m\pi + \frac{r}{s}\pi$ (say)

such that

$$-r_o \leqslant r \leqslant r_o$$

where

$$\frac{r_o}{s} < \tfrac{1}{2} \quad \text{and} \quad m, r, s \quad \text{are integers,}$$

and

$$\frac{y}{b} = \frac{ms + r}{2s(n-1)}.$$

Now if for each n $\exists$ m and r such that

$$m.s + r = k.(n-1) \quad \text{for some } k$$

then

$$\frac{y}{b} = \frac{k}{2s}.$$

Hence, it is sufficient to show that $ms + r$ can generate all integers, or that

$$\ldots(m-1)s + r_o, \quad ms - r_o, \ldots \quad ms, \quad ms + 1 \ldots ms + r_o \ldots$$

generates all integers,

which is true if $(m-1)s + r_o + 1 \geqslant ms - r_o$

or $s \leqslant 2r_o + 1,$

but an initial condition is $\frac{r_o}{s} < \frac{1}{2}$

whence $s = 2r_o + 1.$

Thus, s is odd and k is any integer.

In the antisymmetric case, following a similar argument:

$$\sin\frac{(2n - 1)\pi y}{b} \neq 0 \qquad \forall \quad n$$

then

$$\frac{(2n - 1)\pi y}{b} = m\pi + \frac{\pi}{2} + \frac{r}{s}\pi$$

such that $-r_o \leq r \leq r_o$

where $\frac{r_o}{s} < \frac{1}{2}$

and m, r, s are integer

is a sufficient condition.

Therefore,

$$\frac{y}{b} = \frac{(2m + 1)s + 2r}{(2n - 1).2s}.$$

Now if s is odd, then $(2m + 1)s + 2r$ can generate all <u>odd</u> integers if

$$(2m - 1)s + 2r_o + 2 \geq (2m + 1)s - 2r_o$$

or $2r_o + 1 \geq s$

but $r_o/s < \frac{1}{2}$

Therefore,

$$s = 2r_o + 1 \qquad \text{as before.}$$

Hence m and r can be chosen such that

$$(2m + 1)s + 2r = k(2n - 1) \qquad \forall \quad n$$

where k is odd.

So for optimum positioning of the probes

$$\frac{y}{b} = \frac{k}{2s} \qquad \text{where k is odd} \tag{33}$$

$$-r_o \leq r \leq r_o \qquad \text{as above}$$

$$\text{and} \quad s = 2r_o + 1.$$

Now clearly $\frac{y}{b} < \frac{1}{2}$ for the probes to be within the tank. Also it is necessary to mount the probes sufficiently far away from the tank centre-line and walls to avoid interference from the model and wake and wall effects.

If $r_o = 1$, $s = 3$, then $\frac{y}{b} = \frac{1}{6}$ which is too close to the centre-line.

If $r_o = 2$, $s = 5$, then $\frac{y}{b} = \frac{1}{10}, \frac{3}{10}$ and $\frac{y}{b} = \frac{3}{10}$ is a suitable position, giving cosine and sine values of ± 1, ± 0.81 and ± 0.31.

If $r_o = 3$, $s = 7$, then $\frac{y}{b} = \frac{5}{14}$ is suitable, giving cosine and sine values of ± 1, ± 0.9, ± 0.62 and ± 0.22.

Hence, if the probes are positioned at

$$\frac{y}{b} = \pm \frac{3}{10} \text{ and } \pm \frac{5}{14}$$

the minimum possible cosine and sine value will be 0.31 if the probe giving the maximum value is chosen, and in general it will be larger than this. In the analysis program the trace with the maximum value of the sine or cosine is chosen for each individual harmonic, on the assumption that the larger the diagonal elements in the matrix of equation (29), the less sensitive the analysis is to noise.

3.4 The Model

Much towing tank work has been carried out on the 5.5 metre yacht 'Antiope' and also on the full scale yacht in order to obtain some correlation between various towing tank results (Ref. 4).

For this reason and because of the availability of the model, a one-sixth scale fibreglass model of 'Antiope' was used for all wave pattern measurements. In accordance with other tests the model was given a fixed static trim and allowed to trim freely when being towed. Turbulence studs were fitted at approximately 1/5 waterline length and on the leading edge of the keel. The model displacement was 11.85 kg and L.W.L. = 1.15m. In order to be within the wave making speed range the model was towed in various aspects at speeds from 0.92 m/s to 1.48 m/s which correspond to full scale speeds of 4.4 knots and 7 knots.

4. EXPERIMENTAL PROCEDURE

In order to obtain data of the wave pattern suitable for the above analysis it is necessary to record the output from the wave probes (i.e., the wave elevations) as the model and wave pattern pass the probes. The resulting four traces must then be digitised and punched on to paper tape in a mode suitable for acceptance by the analysis program. Initially the wave pattern was recorded on magnetic tape and then digitised on an analogue computer. This method was found very unsatisfactory for this particular work so it was abandoned in favour of a more manual digitisation process.

The outputs from the four probes were recorded simultaneously on a u/v recorder and the resulting wave traces were digitised by hand, using a trace reader which was able to punch the data obtained directly on to paper tape. A trigger which put a pulse on to the wave trace as the model centre passed the probes was incorporated for reference purposes. Digitisation started at one model's length aft of the model in order to be beyond the bow waves and clear of the local wave disturbances around the model, so the maximum length of usable trace was 8.2m. Due to zero shifting and changes in wave magnitude with speed, it was necessary to calibrate the wave probes before every other run. However, since the probes are linear it was sufficient for calibration of the trace reader to record only two positions, mean zero and a wave elevation of 2.54 cm, which was convenient due to the wave probe construction. The four wave traces were sampled simultaneously every tenth of a second in real time, the reason for this being given in Appendix 6.

Although this method is found to be much more reliable in digitising the actual part of the wave pattern required, it is a time consuming method

of obtaining results since one run in the tank takes up to half an hour, due to settling time, and one wave trace also takes about half an hour to digitise. It is therefore recommended that if this method of wave pattern analysis is to be pursued, a digital voltmeter or analogue computer is connected direct to the wave probe amplifier which could then produce digitised wave traces immediately, ready for analysis.

5. PRESENTATION OF RESULTS

The results are presented in three main sections:

5.1 Results Concerning the Credibility of the Analysis Method, Figs. 1 to 12

Included in this section is a table of the quality of fit parameter Λ at the various speeds and aspects tested (Fig. 1). The quality of fit is defined for the symmetric component of the wave pattern

$$\Lambda = \tfrac{1}{2}\left(\frac{\text{r.m.s. of symmetric residuals on trace at } y_1}{\text{r.m.s. of symmetric wave heights } \zeta_s(y_1)} + \frac{\text{r.m.s. of symmetric residuals on trace at } y_2}{\text{r.m.s. of symmetric wave heights } \zeta_s(y_2)}\right)$$

where at the point (x, y)

the residual = (measured wave height - estimated wave height)

and similarly for the quality of fit of the antisymmetric component.

Figures 5 to 8 are the wave spectra results of tests carried out with changed wave probe positions and are included with the original results for comparison. In these plots the wave resistance is plotted against the wave harmonic number rather than the harmonic angle, for clarity in establishing harmonics with 'spikes'. As in all plots of wave resistance spectra the resistance due to each wave harmonic δR_w is non-dimensionalised by dividing by the total resistance of the component of which it is a part. Hence for symmetric wave resistance spectra it is $\delta R_w/R_{ws}$ and antisymmetric spectra $\delta R_w/R_{wa}$. This is done so that the relative concentration of energy within spectra at different speeds can be compared more easily.

5.2 Symmetric and Antisymmetric Wave Resistance Spectra, Figs. 13 to 30

In the plots of wave resistance spectra, symmetric and antisymmetric, the non-dimensional wave harmonic resistance $\delta R_w/R_w$ as above is plotted against wave angle θ.

It should be noted that the spectra are composed of discrete points which are not part of a continuous spectrum of wave energy. The lines joining these points are only drawn for reasons of clarity and are not supposed to represent any form of continuous spectrum.

5.3 The Wave Resistance as a Whole, Figs. 31 to 42

In the plots of wave resistance components and total wave resistance against aspect for the speeds tested (Figs. 31 to 39) the actual calculated values of wave resistance in newtons are plotted rather than any with the correction to the antisymmetric resistance suggested in section 6.3.

The coefficients of resistance in Figs. 41 and 42 are derived using the underwater side profile area of the model when static as the area factor.

6. DISCUSSION

6.1 The Method of Analysis

The method of wave pattern analysis used in this work is basically a refinement of the method originally used by Wynne (ref. 14) in his work on the wave pattern of a symmetrically towed yacht model. Wynne used the Fourier integral rather than the Fourier summation to establish simultaneous equations for the coefficients in the wave pattern expansion

$$\underline{\underline{A}}\,\underline{p} = \underline{q} \qquad \text{see equation (29)}$$

He then assumed the off diagonal elements to be small and obtained the solution for $\underline{p}$ by the equations

$$p_i = q_i/A_{ii} \qquad 1 \leq i \leq 2N$$

In the present work, as is shown in Chapter 2, a more accurate solution is sought by solving the simultaneous equations as a whole using the Gauss-Seidel method.

The problems in solution which are immediately encountered and which are the only apparently significant problems in this analysis, are the magnitudes of the diagonal elements of the matrix, and their size relative to the off diagonal elements. For convergence, when using the Gauss-Seidel method of solution, it is necessary that the on diagonal elements are large compared with the off diagonal elements (ref. 11) and also it is desirable that the sum of the moduli of the off diagonal elements in any row is less than that diagonal element, although this condition is not strictly necessary. It is possible to increase their relative size by increasing the length of the wave trace used or by varying the sampling rate. However, as shown in section 3.1, the length of the wave trace is at a maximum for the tank used and the sampling rate of 10 samples per second is about optimum from the arguments put forward in Appendix 6.

During early experiments this problem became acute due to the large number of wave harmonics being analysed (35 in each component in the first instance) thus causing the sum of the moduli of the off diagonal elements to be large. However, from study of wave resistance spectra and harmonic wave angles an empirical formula for the maximum wave harmonic number significant in the symmetric component was obtained

$$N = bg(1.39 - 0.595U) + 1 \qquad (34)$$

(Appendix 3)

which reduced considerably the number of wave harmonics being analysed and thus increased the chance of convergence in the Gauss-Seidel solution. This was also taken as the maximum wave number necessary for the antisymmetric case, since it seems unlikely that the maximum wave angle appearing in the antisymmetric spectra should be any different from that in the symmetric spectra.

The problem of the relative magnitudes of the diagonal elements appears to be more serious, although theoretically the varying magnitudes should have no effect upon the solution. Upon studying the wave resistance spectra over the whole range of speeds it seemed an odd coincidence that peaks, often representing more than half the total wave resistance, should occur always at the same harmonic number. These 'spikes' are particularly noticeable in the antisymmetric component of resistance. If now the plots of the magnitude of the diagonal elements in the symmetric and antisymmetric matrices (Fig. 3) are compared with the wave spectra, then it is seen that almost invariably where there occurs a small diagonal element then there also occurs a corresponding 'spike' in the wave spectrum.

Now the magnitudes of the diagonal elements are determined by the positions of the wave probes (see section 3.3) so it was therefore decided to conduct an experiment with one of the pairs of wave probes in a different lateral position. Appealing to equation (33) and putting $r_o = 4$ the following positions for the probes were obtained

$$\frac{y}{b} = \pm\frac{3}{10} \text{ and } \pm\frac{7}{18}$$

and the magnitudes of the diagonal elements of the resulting matrices are shown in Fig. 4. There are of course still low diagonal elements but since these now occur on other harmonic numbers it is possible to establish whether the 'spikes' are a genuine feature of the spectra or just a consequence of the low diagonals. The results of this experiment are discussed in section 6.3.

As mentioned above the analysis used is a refinement upon the method used by Wynne and by comparison with results obtained using Wynne's method on the same wave trace data, it does produce a better fit. However, a further refinement was considered.

Since for each wave harmonic only one of the two wave traces is used to derive the corresponding equations in equation (29) depending on the maximum cosine or sine function with y, it was thought that a method of least squares fit covering all the sampled points might produce a better result. The method already used is in fact a least squares fit for each harmonic on the appropriate wave trace. However when the matrix of the set of simultaneous equations derived from a least squares fit over all the points was calculated, it was found that instead of evening out the relative magnitudes of the diagonal elements and increasing their magnitude relative to the off diagonal elements, the very opposite occurred and diagonal elements that were originally large became even larger in comparison with the smaller elements since they were effectively squared, while off diagonal elements were all increased by a factor of an on diagonal element, thus magnifying the weaknesses of the original matrices in this new one.

This method was therefore abandoned in favour of the original which, although not entirely satisfactory, particularly in the antisymmetric case, appears to be the best method of analysis for the data collected.

6.2 Theoretical Tests

During the development of the computer program used in the wave pattern analysis a few theoretical wave patterns, obtained from a source distribution, were analysed. The relations between the source strengths and distribution, wave elevation and the Fourier coefficients for the wave pattern expansion used in this work are those derived by Hogben (ref. 5).

Although the wave patterns and resistance spectra so obtained bore little resemblance to those measured in the tank, the theoretical wave traces were analysed by program to a very good degree of comparison with the original. A certain disparity did still occur at one of the low diagonal wave harmonics. It is thought that the reason for the good resolution of the theoretical pattern is due to the much higher degree of accuracy in the theoretical wave trace data, calculated by computer, than in the data obtained from the tank. This data is subject to considerable noise and error in the method of digitisation which only gives three significant figures in the range approximately $\pm$ 3.00 anyway.

Following this train of thought and considering the method of analysis, noise on the wave trace data will have an equal effect upon all the components in the vector $\underline{q}$ of equation (29). Hence the effect of noise upon the coefficients with small diagonal elements will, in the solution, be greater than on those with large diagonals.

6.3 Quality of Results

The wave resistance of the model of 'Antiope' was measured at nine speeds in the range 0.92 m/s to 1.48 m/s, corresponding Froude numbers being 0.27 to 0.44, upright at zero yaw and at 10° heel to starboard with yaw angles 2°, 4°, 6° and 8°. Apart from the tests with the different wave probe positions, three non-consecutive runs were made at each speed for every aspect, apart from the 8° yaw, when only one run was made. A few runs have

been omitted from the results due to inaccuracies in the analysis caused by faulty wave trace data.

It is seen from the plots of wave resistance against aspect (Figs. 31 to 39) that a fairly good degree of repeatability is obtained, particularly in the upright case where the average scatter is about 6% of total wave resistance. As might be expected from the analysis problems, discussed in the previous sections, the repeatability of the antisymmetric wave pattern component is on average not as good, although in some cases it is found to be very good. A measure of the noise on the wave trace data can be found in the component of antisymmetric wave resistance computed for the upright case. In all cases this is less than the scatter of the corresponding symmetric resistance and in most cases it is less than the scatter in the antisymmetric resistance at yaw, which might imply that some of the scatter is due to conditions of testing not being repeated sufficiently accurately.

Except where spurious peaks occurred in the wave resistance spectra causing the magnitude at that wave harmonic to vary considerably, thus contributing to the larger scatter encountered in the asymmetric case, the repeatability in the general shape of the spectra was found to be good, the scatter being on average 6% of harmonic resistance in the symmetric spectra and 15% in the antisymmetric case. For this reason the results obtained from only one run are plotted in Figs. 13 to 30.

Again a good indication of accuracy, particularly of the symmetric wave resistance spectra, is given by the results of the tests, mentioned in section 6.1, which were carried out with the wave probes in a different lateral position, in order to establish the credibility of the results first obtained. Two speeds $F_r = 0.315$ and 0.38 were chosen for test since their original wave spectra were fairly typical of the general pattern. The results are shown in Figs. 5 to 8.

The similarity between the symmetrical component wave spectra is most

encouraging although a slight disparity is discernible at the 10^{th} and 12^{th} harmonics in the higher speed, while there is rather less overall agreement at the lower speed. This would tend to prove the reliability of these spectra, a fact which is borne out by the quality of fit Λ, in these cases good, as it is in all symmetric cases, and the plots of the traces as measured and as fitted, Figs. 9 and 10.

In the antisymmetric case the situation changes. The 'spikes' which were so prevalent on the 2nd and 9th harmonics, particularly at the lower speed, completely give way to a peak on the 7th harmonics corresponding to the first very low diagonal element in the corresponding matrix, and not surprisingly the remaining harmonics are dissimilar because of the non-independent method of analysis. It is not surprising then to find that the quality of fit Λ is not good in these cases.

An indication of the meaning of the quality of fit Λ can be found in the plots of the wave traces as measured and as fitted given in Figs. 9 to 12.

The fairly good fit that is found with the symmetric wave patterns is immediately clear from the two examples illustrated here. However, the two examples of asymmetric wave patterns have, as previously discussed, a poorer quality of fit, the antisymmetric part of the trace at y_1 for the lower speed bearing little resemblance to the original at all.

The reason for a considerable difference in fit between one trace and the other, which happens in several instances with the antisymmetric component, although not in the case of the higher speed illustrated here, is not clear. In spite of the selection in the analysis of traces depending upon values of the sine and cosine with y, there is an equal overall distribution, among the wave harmonics, of the traces used in the analysis, so no weighting should occur. However, in the first ten harmonics of the antisymmetric component, where the magnitudes of the harmonics are likely to be greatest,

seven use the trace at y_2, which is closer to the centre line, and although this weighting is evened out in later harmonics, it is thought that this probably contributes to the better fit on the trace at y_2. In the symmetric case the weighting over the first ten harmonics is six to four in favour of the trace at y_1 but the fits at y_1 and y_2 are both still good in spite of this. Because of the trace selection dependent upon the sine and cosine values, the bad 'spikes' always occur on the trace at y_2 which in the asymmetric case illustrated in fact has a better estimated fit than the other trace although the harmonics with spurious peaks have more influence on this trace.

A table of the quality of fit Λ for all runs tested is given in Fig. 1. From this it is seen that the quality of fit for the symmetric wave pattern produced by the upright model improves with increasing speed to around 0.2 for the four highest speeds. It is thought that this may be due to the signal on the wave trace being amplified to a maximum at these speeds and thus reducing the effect of noise, while at lower speeds the recorded wave trace cannot be amplified to give a maximum recordable signal because of the need for calibration in the trace. For this reason a change in the calibration is recommended in Appendix 5. Although not as good as the quality of fit obtained by Hogben in his results of symmetrically towed models (ref. 6) where Λ is in the range 0.15 to 0.2, the quality of fit in the upright case is considered satisfactory for reliance upon the accuracy of results.

In the asymmetric results, the quality of fit of the symmetric component is seen to be similar in most cases to that of the corresponding upright case except there is a slight increase in Λ with increasing asymmetry and at the lower speeds the quality of fit is not good at the higher yaw angles. The quality of fit of the antisymmetric component of the wave pattern does not show such a good degree of accuracy as the symmetric component, which is

expected from earlier discussion. Since the author is unaware of any other results published on asymmetric wave patterns it is not possible to cite a suitable comparison of fit.

It has been suggested by the author that by halving the wave amplitude of the harmonics which cause the spurious peaks (i.e. the 2nd and 9th anti-symmetric harmonics) and thus quartering their contribution to the wave resistance spectra, their magnitude will in general be brought more into line with adjacent harmonics. This has been tried on the runs at 10° heel and 4° yaw. It was found, in general, that the fit on the trace at y_1, the trace with less weighting from these elements, improved slightly, while that at y_2 worsened, giving a net quality of fit Λ equal to the previous value, but improving slightly the balance between y_1 and y_2. The wave resistance was, of course, reduced significantly.

It is clear from the above that the analysis given here of the anti-symmetric component of wave resistance in an asymmetric wave pattern is not satisfactory. However, since the fitted wave pattern produced when the 'spikes' in the wave resistance spectra are reduced, is not greatly altered and its general amplitude is as near as with the 'spikes' to that of the original traces, it is felt that the antisymmetric wave pattern resistance so obtained will be a close approximation to the actual value and the best estimation obtainable from the data available.

6.4 The Symmetric Wave Pattern Resistance

Plots of the wave resistance spectra against wave angle obtained from the symmetric wave patterns produced by the model being towed upright are included in Figs. 13 to 21.

The theoretical prediction for the wave resistance spectrum from a

source/sink pair, a very crude approximation to a towed model, indicates a series of 'humps' decaying in magnitude with increasing wave angle θ. The rate of decay and the relative magnitude at $\theta = 0$ increase with increasing Froude number.

Both these phenomena can be seen in the plotted spectra. The peaks which occur on the 10^{th} harmonic, due to small diagonal elements in the matrix, and particularly noticeable at the two lower speeds, can, as previously suggested, probably be ignored. However, the remaining peaks which in general comprise more than one wave harmonic can be assumed genuine. At the lower speeds the bulk of the energy in the wave pattern lies in the diverging system of waves which comprises wave harmonics of angle $\theta > 35^{o}$ (section 1 and ref. 3). At the higher speeds most of the wave energy lies within the transverse system of waves, those harmonics with angle $\theta < 35^{o}$. It cannot be determined from the present results but it seems likely that at these higher speeds the second and third harmonics comprise the second 'hump' in the wave resistance spectra rather than being part of the first. It is also seen that at the Froude numbers 0.36 and 0.38 corresponding to $v/\sqrt{L} = 1.2$ and 1.27 most of the wave pattern energy is in the first harmonic ($\theta = 0^{o}$).

All these trends are apparent from visual observations of the wave patterns actually produced in the towing tank.

In Fig. 40 the total measured resistance R_T of 'Antiope' being towed upright is plotted with the symmetric wave pattern resistance R_w against speed U. Included in this figure are the resulting viscous resistance $R_v = R_T - R_w$ and for comparison the viscous resistance estimated from the 11^{th} I.T.T.C. standard formula

$$C_f = \frac{R_f}{\frac{1}{2}\rho A U^2} = \frac{0.075}{(\log_{10} \frac{R_e}{100})^2} \qquad (35)$$

where Reynold's number $R_e = \frac{U\ell}{\nu}$.

In order to obtain the length factor ℓ in Reynold's number the effective waterline length was taken as 3/5 of L.W.L.

Thus $\ell = \frac{3}{5}.1.15 = 0.69m$

kinematic viscosity $\nu = 1.14 \times 10^{-6}\ m^2/s$

and wetted surface area $A = 0.42\ m^2$.

Whence the skin friction

$$R_f = \frac{15.9 \times U^2}{(\log_{10}U \times 6.05 \times 10^3)^2} \qquad (36)$$

Now the total viscous resistance R_v is estimated at 120% of R_f, since it then produces a close approximation to total resistance at lower Froude number. Thus the estimated viscous resistance plotted is

$$R_v = 1.2R_f. \qquad (37)$$

The increasing discrepancy with speed between the estimated and measured viscous resistance which is almost negligible at the lowest plotted speed is probably attributable to non-linear effects such as wave breaking, which becomes apparent at higher speeds, boundary layer separation, variations in the wetted surface area of the hull and variations in trim. However, in general the agreement is considered good and thus provides more proof of the accuracy of the symmetric wave pattern resistance.

6.5 The Asymmetric Wave Pattern Resistance

Asymmetry in the wave pattern behind the yawed and heeled model is clearly seen on the wave traces obtained and in the tank itself. However, as previously discussed, the antisymmetric wave resistance spectra are not good and so no general trends or features can really be seen. The spectra from the symmetric components of resistance are very similar to those obtained in the equivalent upright case and the trends and features discussed earlier are found again here.

Following the suggestion put forward in section 6.3 above, to reduce the 'spikes' in the resistance spectra to a magnitude equivalent to surrounding harmonics, it is found generally that the antisymmetric resistance is reduced by one third. From consideration of plots of resistance against aspect, Figs. 31 to 39, where the plotted points are those originally calculated, it is seen that the antisymmetric wave resistance at 4° yaw comprises between 8% and 50% of total wave resistance. Thus a third of the antisymmetric resistance is just above the order of the scatter found in the total wave resistance and so is not really as dramatic a reduction as it first appears. However, the effect on the total wave resistance is enough to reduce the previously calculated increase with yaw. It therefore appears that the total wave pattern resistance of the model only increases slightly with yaw, by about 5% at 4° yaw for some speeds, while at others there is no increase with yaw.

However, from observations of the towed model it is seen that the wave-breaking at the bow increases with yaw and is apparent at all speeds. This of course dissipates wave energy into the wake and would appear in the total viscous resistance obtained from a wake survey. Thus it seems likely then that the actual wave making of the model increases faster with yaw than is measured from the wave pattern. From resistance measurements it is found that the total resistance R_T increases much faster with yaw than the wave resistance, by about 15% at 4° yaw, as is to be expected from the production of sideforce creating an inherent induced resistance R_I.

6.6 Comparison with Wind Tunnel Results

A comparison between wind tunnel results obtained by Maclaverty (ref. 8) from a double model of a 5.5 metre yacht at 10° heel and various degrees of yaw and corresponding results in the towing tank has been made by Milward (ref. 9). From Milward's plots of lift coefficient against yaw and drag coefficient against lift coefficient squared, values for the drag coefficient

in the tank minus the drag coefficient in the wind tunnel $C_{D_{tank}} - C_{D_{tunnel}}$ have been calculated for varying degrees of yaw and two Froude numbers corresponding to two used in this present work. The results are plotted with the coefficient of wave resistance,

$$C_{R_w} = \frac{R_w}{\frac{1}{2}\rho U^2 S}$$ where S is underwater plan area, in Figs. 41 and 42.

It should be noted that the points corresponding to 10° heel and 0° yaw in Milward's results have been made coincident with those of the wave resistance from the upright model in this present work, 0° heel and 0° yaw. Also, Milward points out that the tank and tunnel results were at different Reynold's numbers and when an estimated correction is made for this, the increase in $C_{D_{tank}} - C_{D_{tunnel}}$ with yaw is slightly diminished. Points representing the total wave resistance originally calculated are plotted together with a line representing the wave resistance independent of yaw as suggested by some cases above.

No reliable quantitative information can be gleaned from this comparison since Milward's results were from a different model, although of the same class, and as stated above, he was using different Reynold's numbers. The phenomenon of the tank resistance increasing more rapidly than the tunnel resistance with increasing yaw has been noted before and attributed to increasing wave pattern resistance. Now if the wave pattern resistance does not increase then the increase must be in the total viscous resistanace and the resistance due to trailing vortices. As mentioned previously, the wave breaking is seen to increase with yaw and this will of course increase the apparent viscous resistance. Other variations in viscous resistance and induced resistance are not possible to ascertain without measurements made within the wake.

In conclusion it can be said that if the wave pattern resistance does

increase with yaw, although in some cases it appears that it may not, the greater increase with yaw of resistance in the tank from that in the tunnel cannot be attributed entirely to increased wave pattern resistance.

7. CONCLUDING REMARKS

1. It has been shown in this work that the total wave pattern resistance of an asymmetric hull form can be considered as the sum of the resistance due to the symmetric and antisymmetric parts of the wave pattern

$$R_w = R_{ws} + R_{wa}.$$

2. Experimental results for the symmetric wave pattern from the upright non-yawed hull and the symmetric part of the asymmetric wave pattern are good, the percentage error being about 6% of total wave resistance.

3. The results for the antisymmetric part of the wave pattern are not so successful, there being certain wave harmonics which cause spurious peaks in the wave resistance spectra. An estimate of the antisymmetric resistance is given, but this is clearly unsatisfactory as a general technique.

4. There is, in some cases, a slight increase in the wave resistance with yaw, but it is not enough to account for the greater increase with yaw in total resistance in the towing tank over that in the wind tunnel which must therefore be accounted for by an increase in the viscous resistance or induced resistance.

5. It is recommended that, for any further work on this subject, an investigation is made into the analysis of the antisymmetric component of the wave pattern with the first object being the elimination of the spurious peaks in the wave resistance spectra.

6. In order to develop a simple, routine, wave resistance measuring technique it will be necessary to incorporate a digital voltmeter or an on-line analogue computer in the system that can produce, through a tape punch, records of the wave trace directly on paper tape ready for analysis. Alternatively, the ultimate system would connect the wave probe outputs directly,

through an on-line consul to the computer which could then analyse data as it is produced and wave resistance data could be made immediately available with each run in the tank.

REFERENCES

1. Eggers, K. — Uber die Ermittlung des Wellenwiderstandes eines Schiffsmodells durch Analyse seines Wellensystems - Schiffstechnik Vol. 9, 1962.

2. Gadd, G.E. and Hogben, N. — The resistance of wave-making bodies in the light of measurements of the surface wave pattern. N.P.L. Ship Rep. 43, 1963.

3. Havelock, T.H. — Wave patterns and wave resistance. Trans. I.N.A. Vol. 76, 1934.

4. Herreshoff, H.C. and Newman, J.N. — Full scale tank tests of the 5.5 metre yacht 'Antiope'. S.N.A.M.E. Tech. and Res. Bulletin No. 1-28, 1967.

5. Hogben, N. — A note on the relation of a wave pattern and a source distribution. N.P.L. Ship T.M. 76, 1964.

6. Hogben, N. — Automated recording and analysis of wave patterns behind towed models. Trans. R.I.N.A. Vol. 114, 1972.

7. Lamb, H. — Hydrodynamics - 6th Edition, C.U.P., 1932.

8. Maclaverty, K. — Test of a 5.5 metre yacht form with various fin sweepback angles. S.U.Y.R. Rep. no. 17, 1966.

9. Milward, A. — The induced drag of a yacht's hull. S.U.Y.R. Rep. no. 24, 1968.

10. Milne-Thomson, L.M. — Theoretical Hydrodynamics. 5th edition. Macmillan, 1968.

11. Mitchell, A.R. — Computation Methods in Partial Differential Equations. London, Wiley, 1969.

12. — Report of the Resistance Committee. Proc. 11th I.T.T.C. 1966.

13. Ward, L.W. — Direct determination of wave resistance from the wave pattern. Proc. 11th I.T.T.C., 1966.

14. Wynne, J.B. — Wave pattern measurements of a yacht form fitted with a bustle. Part III Project Report, Southampton University, 1971.

APPENDIX 1: The Relations Used in Deriving Equations (23), (24),(27) and (28) in Section 2.5

$$\sum_{j=1}^{K} \cos aj = \sum_{j=1}^{K} \tfrac{1}{2}(e^{iaj} + e^{-iaj})$$

$$= \tfrac{1}{2}\left(\frac{e^{iaK} - 1}{1 - e^{-ia}} + \frac{e^{-iaK} - 1}{1 - e^{ia}}\right)$$

(from the geometric progression $\sum_{j=1}^{K} r^{j} = \frac{r^{K} - 1}{1 - r}$)

$$= \frac{\tfrac{1}{2}(e^{iaK} - 1 - e^{ia(K+1)} + e^{ia} + e^{-iaK} - 1 - e^{-ia(K+1)} + e^{-ia})}{(1 - e^{-ia})(1 - e^{ia})}$$

$$= \frac{\cos aK + \cos a - \cos a(K + 1) - 1}{2(1 - \cos a)}$$

$$= \frac{\cos \tfrac{1}{2} a(K + 1).\sin \tfrac{1}{2}aK}{\sin \tfrac{1}{2}a}$$

and

$$\sum_{j=1}^{K} \sin aj = \sum_{j=1}^{K} \tfrac{1}{2}(e^{iaj} - e^{-iaj})$$

$$= \tfrac{1}{2}\left(\frac{e^{iaK} - 1}{1 - e^{-ia}} - \frac{e^{-iaK} - 1}{1 - e^{ia}}\right)$$

$$= \frac{\tfrac{1}{2}e^{iaK} - 1 - e^{ia(K+1)} + e^{ia} - e^{-iaK} + 1 + e^{-ia(K+1)} - e^{-ia}}{(1 - e^{-ia})(1 - e^{ia})}$$

$$= \frac{\sin aK + \sin a - \sin a\,(K + 1)}{2(1 - \cos a)}$$

$$= \frac{\sin \tfrac{1}{2}a(K + 1).\sin \tfrac{1}{2}aK}{\sin \tfrac{1}{2}a}$$

APPENDIX 2: The Gauss-Seidel Method of Solving Simultaneous Equations

To solve the simultaneous equations given by

$\underline{\underline{A}}\,\underline{x} = \underline{q}$ where A is the n x n matrix

$$\begin{pmatrix} a_{11} & a_{12} & \cdots & a_{1n} \\ a_{21} & a_{22} & & \cdot \\ \vdots & & & \\ a_{n1} & & & a_{nn} \end{pmatrix}$$

and $a_{ii} \neq 0 \qquad 1 \leqslant i \leqslant n$

assume an initial solution $(x_1^{(1)} \ \ldots \ x_n^{(1)})$ and derive a second approximation for x_1

$$x_1^{(2)} = [q_1 - (a_{12}x_2^{(1)} + \ldots a_{1n}x_n^{(1)})]/a_{11}$$

and for x_2

$$x_2^{(2)} = [q_2 - (a_{21}x_1^{(2)} + a_{23}x_3^{(1)} + \ldots a_{2n}x_n^{(1)})]/a_{22}$$

and so on for all n elements to obtain the second approximation $(x_1^{(2)} \ \ldots\ x_n^{(2)})$.

Iterations continue until sufficient convergence is attained, the general term for the r^{th} element in the i^{th} approximation being

$$x_r^{(i)} = [q_r - (a_{r1}x_1^{(i)} + \ldots a_{r,r-1}x_{r-1}^{(i)} + a_{r,r+1}x_{r+1}^{(i-1)} \ldots \ldots a_{r,n}x_n^{(i-1)})]/a_{rr}$$

A sufficient but not necessary condition for convergence is

$$|a_{rr}| > \sum_{\substack{i=1 \\ i \neq r}}^{n} |a_{r,i}| \qquad \forall\ r$$

i.e., that the matrix $\underline{\underline{A}}$ is strongly diagonal.

APPENDIX 3: Defining the Optimum Number of Wave Harmonics N

From plots of results obtained in early experiments using 35 symmetric harmonics it was found that above a certain harmonic number at each speed the value of the right hand side of the equations in (29) became very small relative to the corresponding diagonal element of the matrix. These harmonic numbers are plotted in Fig. 2 and are considered the maximum necessary for analysis and a formula for them is derived as follows:

Suppose $N = c - dU + 1$ where c and d are constants for a given tank width b.

Now it is required that

$$\theta_N = \theta_{max}$$

and

$$\theta_{max} = f(U, b)$$

Also,

$$2\cos^2\theta = 1 + \sqrt{1 + 4\left(\frac{2(n-1)\pi U^2}{bg}\right)^2}$$

or

$$\theta_{max} = \cos^{-1}\sqrt{\left\{\tfrac{1}{2}\left[1 + \sqrt{1 + 4\left(\frac{2(N-1)\pi U^2}{bg}\right)^2}\right]\right\}}$$

$$= \cos^{-1}\sqrt{\left\{\tfrac{1}{2}\left[1 + \sqrt{1 + 4\left(\frac{2(c-dU)\pi U^2}{bg}\right)^2}\right]\right\}}$$

Now the maximum wave angle in any wave pattern can only be a function of velocity U and therefore independent of b and g.

Therefore $c - dU = bg(C - DU)$

where C and D are constants

and $C = \frac{c}{bg}$, $D = \frac{d}{bg}$.

From Fig. 2 where the maximum wave harmonic numbers derived from early tests are plotted against U, it is found that when

$b = 2.45m$ and $g = 9.81\ m/s^2$

$c = 34.14$ and $d = 14.3$;

Therefore, $C = 1.39$, $D = 0.595$.

Hence,

$$N = bg(1.39 - 0.595U) + 1.$$

Since this relation was derived from information in the Froude number range 0.27 to 0.44, it should not be expected necessarily to apply to situations outside this range. However, it does apply to tanks of different breadth b when used in this speed range.

APPENDIX 4: The Computer Program

The program used for the analysis of the wave trace is written in Fortran. A complete listing of the program is not given since the fundamental parts are simply a translation of the wave pattern analysis given in the text.

Apart from the wave trace data which is on paper tape, all data is input on cards. This comprises the basic statistics of the model and tank required in the analysis, the number of runs to be analysed and the velocity, sampling rate and aspect related to each run. All other variables are then derived within the program, including the values of y at the wave probes since it was found that the accuracy of y needs to be higher in the analysis than that measureable in the tank. Having found the symmetric and antisymmetric wave heights, the simultaneous equations for the symmetric part (equation 29) are then calculated from the relations in equations (27) and (28). A subroutine is used to solve these equations by the Gauss Seidel method and is listed.

```
      SUBROUTINE GAUSS(A,Q,N,P)
      DIMENSION A(70,70),Q(N),P(N)
      AC=0.005
      IJ=0
    9 DO 10 I=1,N
      IF(Q(I),NE,0,0)IJ=1
   10 P(I)=Q(I)/A(I,I)
      IF(IJ,EQ,0)GO TO 17
      JJ=0
```

(cont/d...)

```
11  J=0
    JJ=JJ+1
    DO 15 K=1,N
    B=0,0
    DO 12 L=1,N
    IF(L,EQ,K) GO TO 12
    B=B+A(K,L)*P(L)
12  CONTINUE
    S=(Q(K)-B)/A(K,K)
14  IF(ABS((S-P(K))/(ABS(S)+ABS(P(K)))),GT,AC  ) J=1 +J
15  P(K)=S
    IF(JJ,EQ,25)GO TO 16
    IF(J,GE,1) GO TO 11
25  FORMAT(/10X,14,11H ITERATIONS, 16,17H WITH LARGE ERROR)
16  WRITE(3,25)JJ,J
17  CONTINUE
    RETURN
    END
```

Iterations continue until the change from one approximation to the next is less than 0.5% on all elements of the unknown vector. There is an upper limit of 25 iterations in case of a diverging iteration process, and also the number of iterations together with the number of non-convergent elements if any is printed out.

The antisymmetric part of the wave pattern is then calculated in a similar way using equations (31) and (32). The wave pattern as fitted is calculated simply now, knowing the coefficients in its Fourier expansion, whence the symmetric and antisymmetric residuals at the points measured are found and printed out with the measured wave heights. The resistance due to each wave harmonic and thus the total resistance is calculated from

the relations in equation (29).

Apart from the symmetric, antisymmetric and total wave resistances, the final print out for each run lists for each wave harmonic, symmetric and antisymmetric, γ, θ, δR_w, ξ, η (or μ and ν) and $\delta R_w/R_w$. Also printed are the r.m.s. residuals and wave heights on trace and the number of samples used so that any error in the input of the paper tape data can be noted.

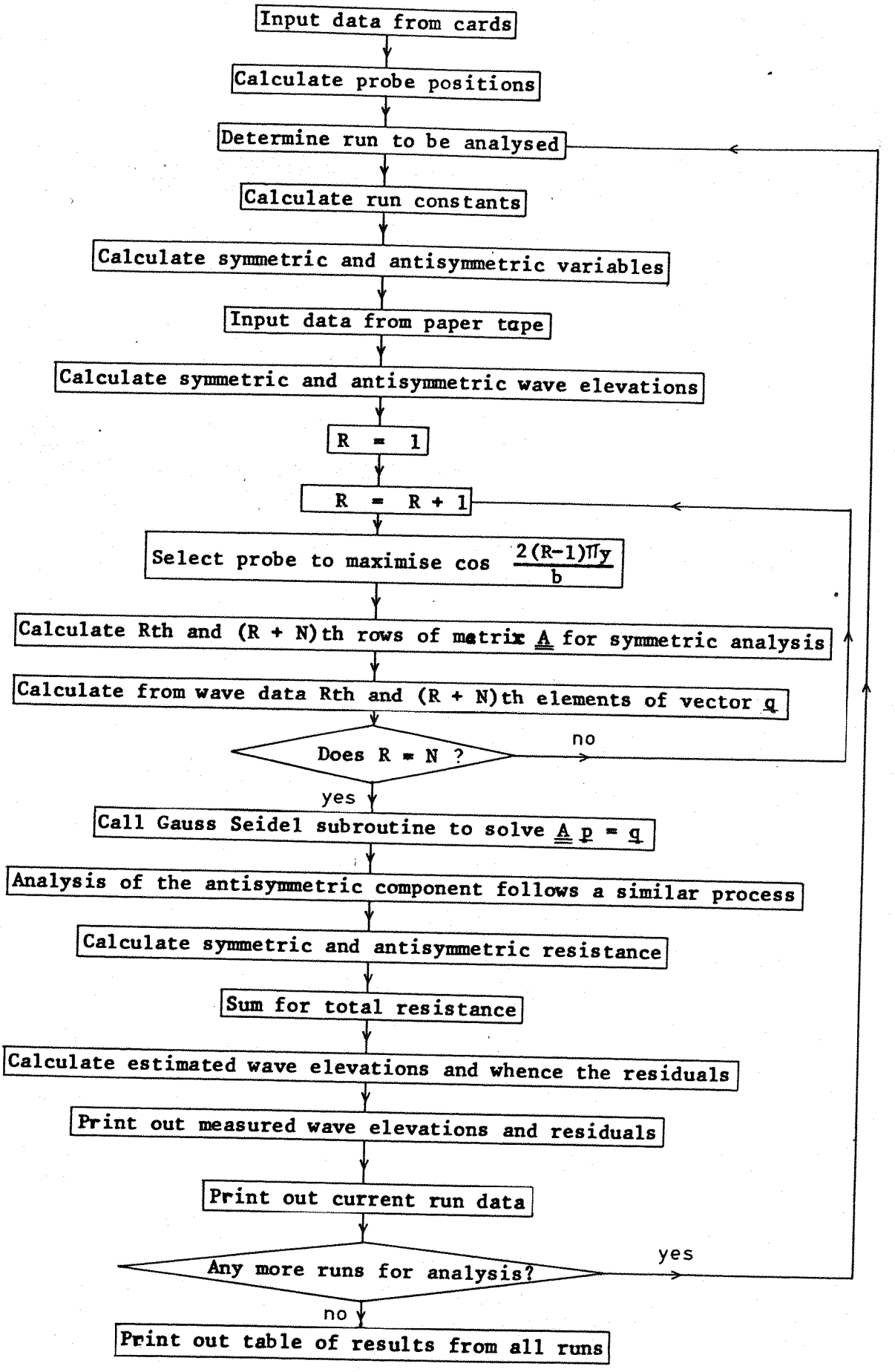

FLOW DIAGRAM

APPENDIX 5: Wave Probe Design and Electronics

The original wave probe design was considered too cumbersome and not sufficiently accurate when used dynamically. It seemed likely that the underwater support for the probe interfered with the orbital motion of the waves. Also, since the wire was looped at the bottom, there were in effect two probes, which made it difficult to determine the exact position of measurement.

The probes were therefore re-designed. The upper part of the original probes was used including the electronic unit. Use of the original electronics required using a similar length polyurethane coated wire of diameter 0.165 mm for the probe, which was convenient since then a single surface piercing strand could be used and taken to twice the original depth, thus minimising the effect of the support on the waves. For the support, 20 gauge stainless steel tube was braised into the upper section and bent appropriately for stringing the wire. The whole apparatus is secured by wing nuts into a vertical support and can thus be raised and lowered as required. A pin can be inserted in holes spaced at one inch intervals for calibration. Since the relation between wave elevation and wave probe output is linear, and from plots of output against immersion this is seen to be true, only two positions were used for calibration, zero and a wave height of one inch. A recommendation for an improved design would be the ability to calibrate in intervals of less than one inch, which would be useful when measuring waves of small amplitude at low speeds.

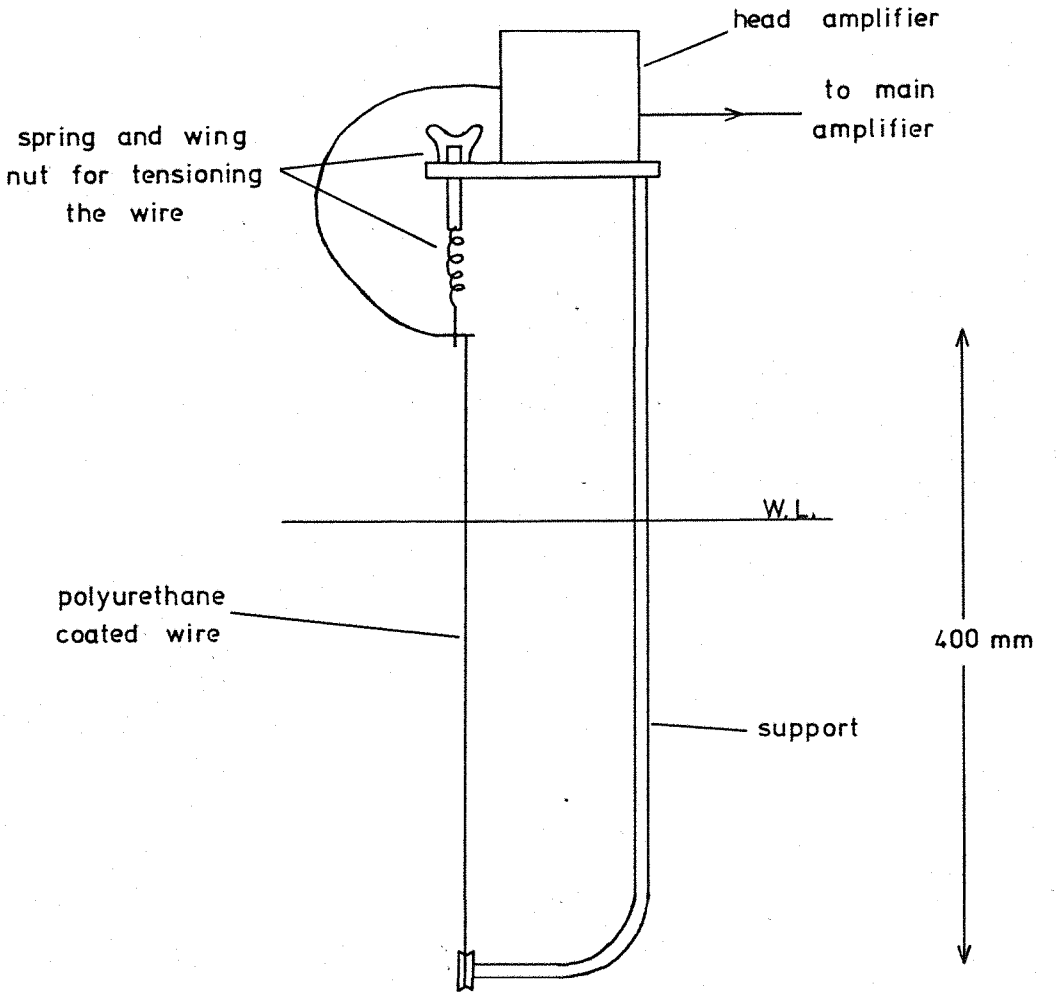

A WAVE PROBE

The electronic equipment is in two parts:

(1) the head amplifier unit mounted on each wave probe;

(2) the main amplifier unit at the control console.

(1) The head amplifier unit uses the capacitance of the wave probe assembly to determine the amount of negative feed-back to an amplifier and hence control its gain. A 50 KHz oscillator voltage fed into the unit is amplitude modulated, the depth of modulation being proportional to the depth of probe immersion. This A.M. signal is demodulated by a phase sensitive rectifier and fed to the main amplifier unit.

(2) The detected output from each probe unit is fed to one of the four amplifiers in the main amplifier unit. Provision is made for off-setting the D.C. voltage from the probe by means of a 10 term 'set zero' control on the front panel of the amplifier unit. A centre zero meter on the front panel is used in conjunction with the 'set zero' controls and this meter is switched to the outputs of each of the amplifiers in turn. The 50 kHz oscillators are of the astable multivibrator type. The output of this oscillator is integrated and fed via an amplifier and emitter to the head amplifier units.

During early experiments a great deal of noise at 100 cycles was found on all outputs and of an amplitude equivalent to the wave amplitudes. It is thought that the cause of this noise is untraceable earth loops in spite of the extensive earthing of the tank and apparatus. Filters were therefore built into each channel of the main amplifier unit but there was still appreciable noise, so the signals were passed through an external filter unit which cut out sufficient noise for the traces to be measure-able. Since the maximum frequency being measured in the wave pattern is about 5 c/s, it was necessary that the minimum frequency damped by the filters was higher than this. 20 c/s was taken as a safe limit.

APPENDIX 6: On Sampling Rate as Related to the Generation of Matrices Used in the Analysis

As discussed in the text it is necessary that the matrix $\underline{\underline{A}}$ used in equation (29), $\underline{\underline{A}}\,\underline{p} = \underline{q}$, is strongly diagonal.

Now if $\underline{\underline{A}}$ is a 2N x 2N matrix each off diagonal element except those elements A_{rn} where $r = n \pm N$ (the diagonal elements of the top right and bottom left hand quarter matrices) has denominators $\sin \frac{1}{2}(\omega_n + \omega_r)h$ and $\sin \frac{1}{2}(\omega_n - \omega_r)h$, where h is the longitudinal distance between sampling points and is therefore a measure of the sampling rate. Hence in order for these off diagonal elements not to become large it is necessary that

$$\tfrac{1}{2}(\omega_n + \omega_r)h \neq k\pi$$

and

$$\tfrac{1}{2}(\omega_n - \omega_r)h \neq k\pi \qquad n \neq r \text{ for any integer } k.$$

Also for the diagonal elements of each quarter matrix there is a denominator $\sin \omega_r h$, so it is also necessary that

$$\forall \; r \qquad \omega_r h \neq k\pi.$$

Now $\omega_r > 0 \quad \forall \; r$; hence, if $\omega_r h < \pi \quad \forall \; r$

then

$$0 < \left| \tfrac{1}{2}(\omega_n + \omega_r)h \right| < \pi$$

$$0 < \left| \tfrac{1}{2}(\omega_n - \omega_r)h \right| < \pi \qquad \forall \; n, r \text{ s.t. } n \neq r$$

Thus a sufficient condition for elements of the matrix to remain finite is

$$\omega_r h < \pi \qquad \forall \; r$$

which means that the sampling rate must be high enough to sample at least twice per wavelength in the longitudinal x-direction for all wave harmonics encountered.

Now from calculations $\omega_r < 30$, $1 \leq r \leq N$, over the whole speed range used if the number of wave harmonics $N < 25$, which gives the condition

$$h \lesssim 0.1.$$

But if $n = r \pm 1$, $|\omega_n - \omega_r| \simeq 0.5$, when r is large, and $|\sin \tfrac{1}{2}(\omega_n - \omega_r)h| \simeq 0.025$ when $h = 0.1$ and therefore $|\sin \tfrac{1}{2}(\omega_n - \omega_r)h^{-1}| \simeq 40$, and the remaining factors in this term are

$$\tfrac{1}{2} \cos\left(\frac{2(n-1)\pi y}{b}\right)$$

and the product of a cosine and sine with nearly equal arguments, thus making a total factor of the order on average of 0.1. Hence the elements adjacent to a diagonal element can be of the order of 4 when r is large and from calculations of the matrices used, the lowest diagonal element encountered is only 12 when h = 0.1m and U = 1.0 m/s.

Now the magnitude of the diagonals is proportional to the number of samples taken, K, which is proportional to the sampling rate. Hence, it turns out that increasing the sampling rate increases the elements $A_{i,i+1}$ with the diagonal elements and at the same rate. Since the digitisation was by hand, it was desirable that the sampling rate should be kept low, and so since the traces were in fact marked by the recorder every tenth of a second, the sampling rate chosen was 10 per second for all speeds, and from the above it appears that there would be not much advantage in increasing this.

FIG 1

TABLE OF THE QUALITY OF FIT Λ

	speed m/s	0·92	0·99	1·06	1·13	1·2	1·27	1·34	1·4	1·48
Upright	symmetric	0·56	0·43	0·34	0·33	0·29	0·21	0·2	0·22	0·2
10°heel 2°yaw	symmetric	0·59	0·49	0·41	0·36	0·28	0·19	0·19	0·18	0·17
	antisymmetric	0·76	0·73	0·65	0·59	0·63	0·74	0·85	0·85	0·8
10°heel 4°yaw	symmetric	0·72	0·51	0·53	0·39	0·27	0·23	0·21	0·23	0·17
	antisymmetric	0·76	0·68	0·66	0·64	0·52	0·63	0·77	0·82	0·74
10°heel 6°yaw	symmetric	0·8	0·76	0·7	0·44	0·28	0·25	0·22	0·23	0·15
	antisymmetric	0·7	0·69	0·67	0·59	0·44	0·58	0·73	0·78	0·74

FIG 2 OPTIMUM WAVE HARMONIC NUMBERS FOR S.U. TANK

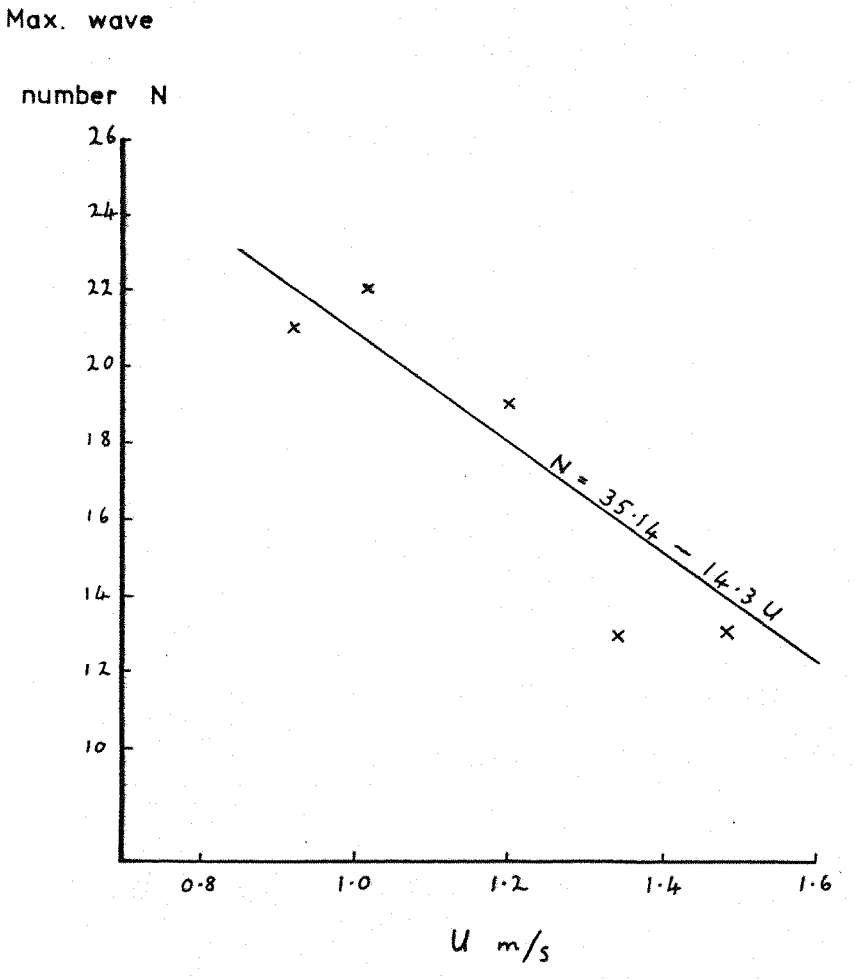

FIG 3 RELATIVE MAGNITUDES OF THE MATRIX

DIAGONAL ELEMENTS

when $\frac{y}{b} = \frac{3}{10}$ and $\frac{5}{14}$

Symmetric

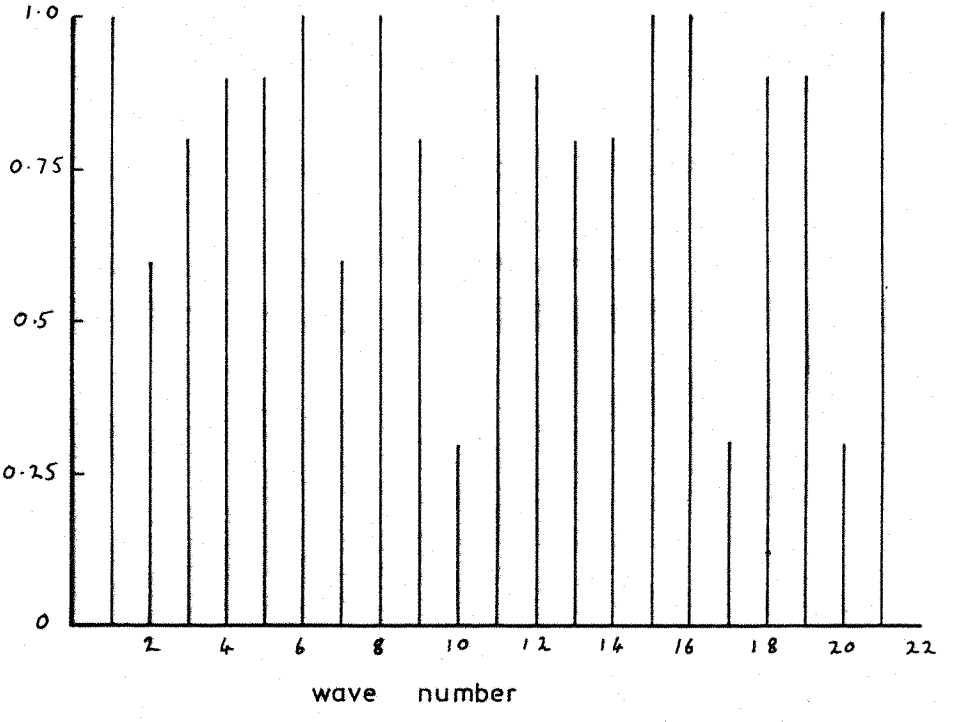

Antisymmetric

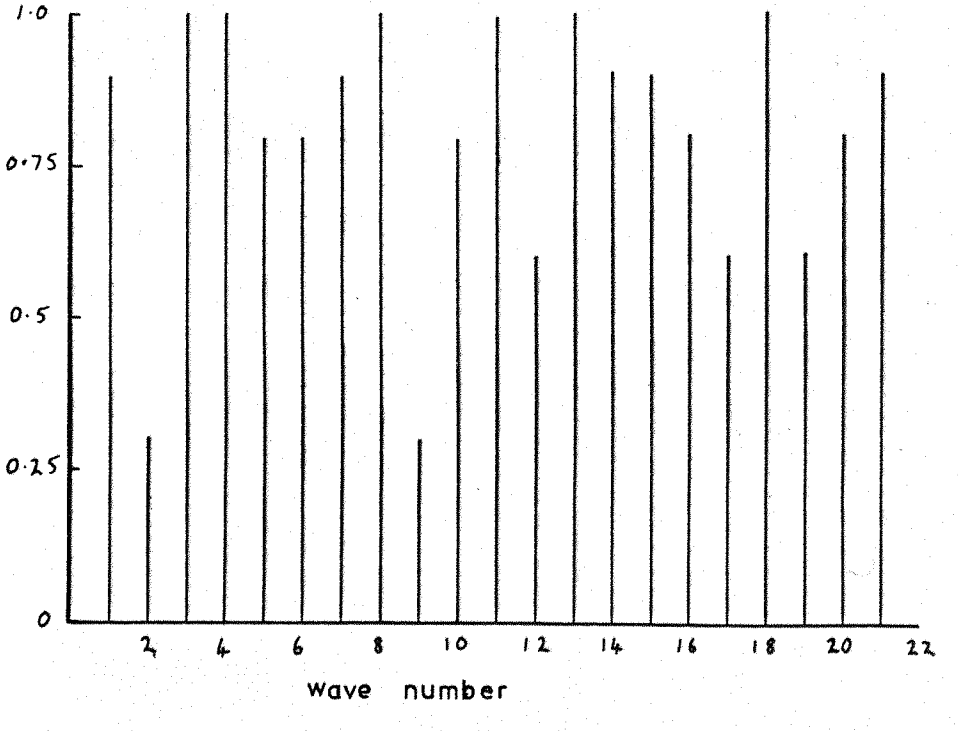

FIG 4 RELATIVE MAGNITUDES OF THE MATRIX

DIAGONAL ELEMENTS

when $\frac{y}{b} = \frac{3}{10}$ and $\frac{7}{18}$

Symmetric

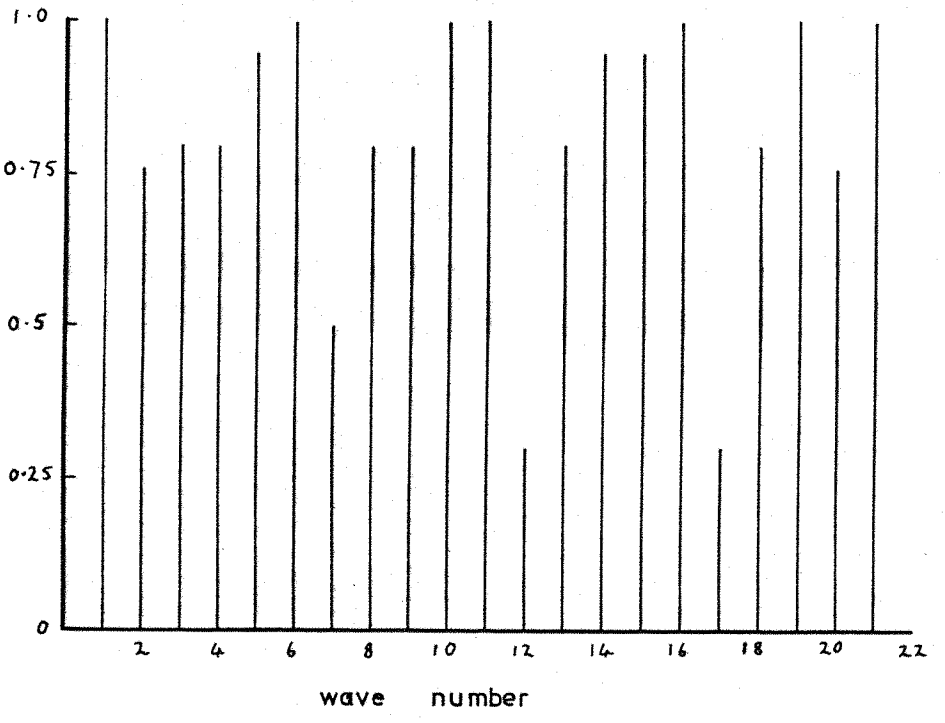

Antisymmetic

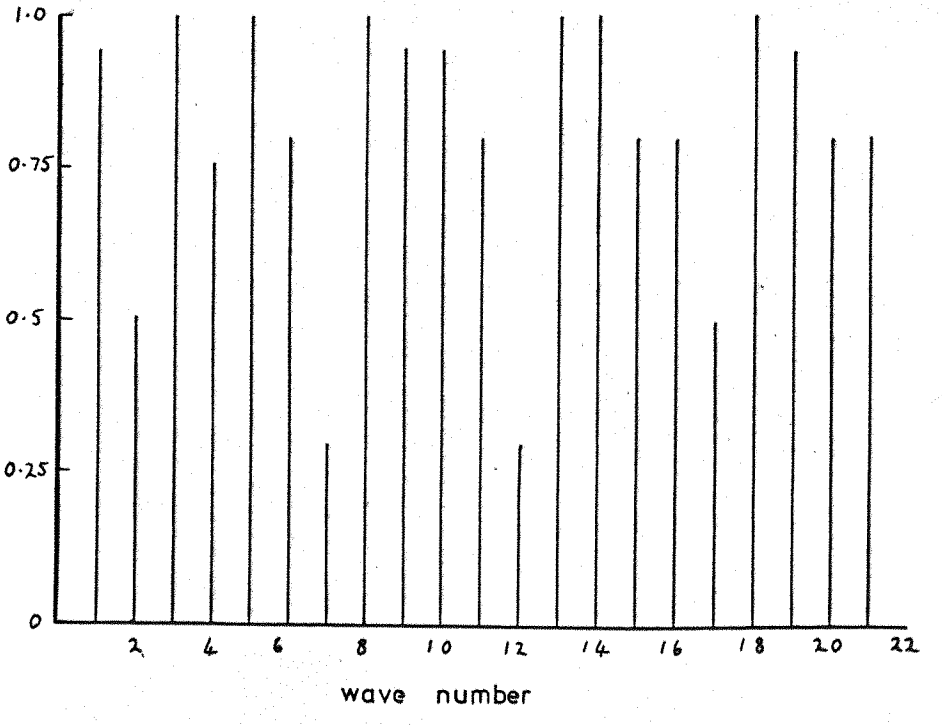

FIG 5 **COMPARISON OF SYMMETRIC WAVE RESISTANCE SPECTRA FROM DIFFERENT PROBE POSITIONS**

Upright $U = 1{\cdot}06$ m/s $F_L = 0{\cdot}315$

——⊙—— $\frac{y}{b} = \frac{3}{10} \cdot \frac{5}{14}$ $R_{ws} = 0{\cdot}095$ N $\Lambda = 0{\cdot}34$

------×------ $\frac{y}{b} = \frac{3}{10} \cdot \frac{7}{18}$ $R_{ws} = 0{\cdot}097$ N $\Lambda = 0{\cdot}35$

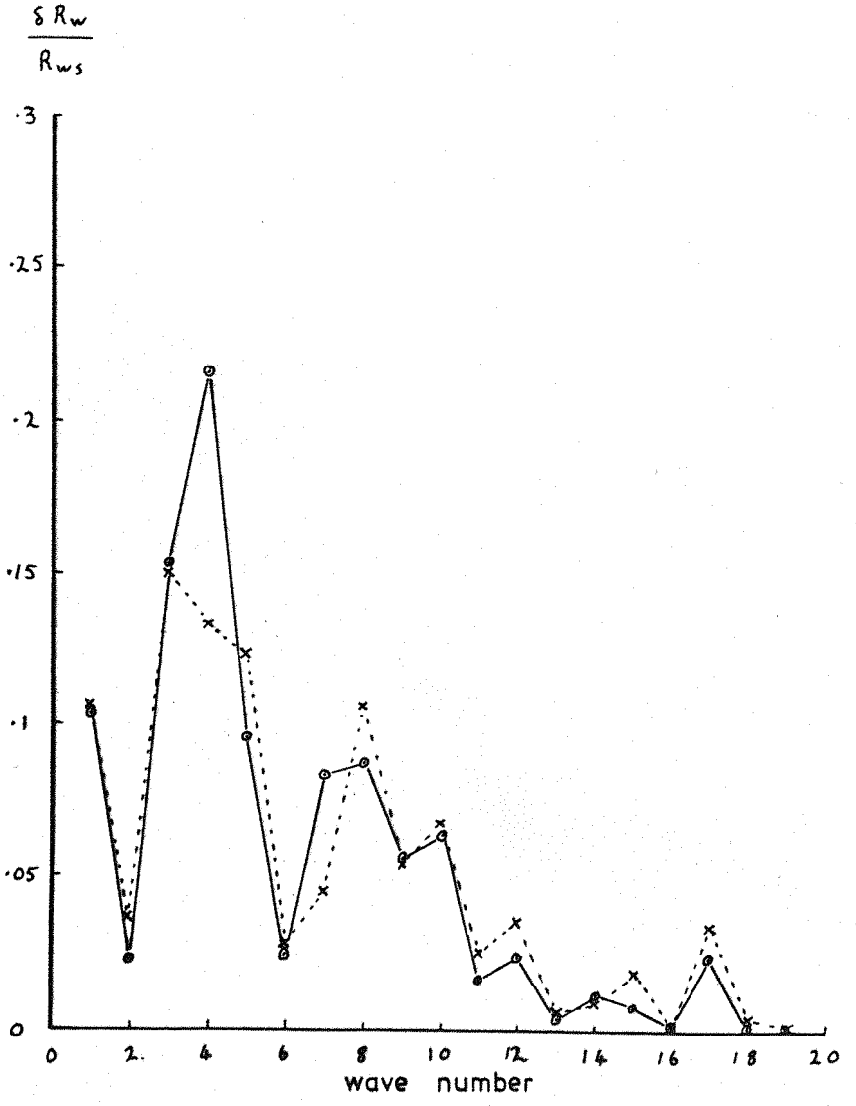

FIG 6 **COMPARISON OF SYMMETRIC WAVE RESISTANCE SPECTRA FROM DIFFERENT PROBE POSITIONS**

Upright $U = 1{\cdot}27 m/s$ $F_\nabla = 0{\cdot}38$

——o—— $\frac{y}{b} = \frac{3}{10}, \frac{5}{14}$ $R_{ws} = 0{\cdot}685$ N $\Lambda = 0{\cdot}21$

------x------ $\frac{y}{b} = \frac{3}{10}, \frac{7}{18}$ $R_{ws} = 0{\cdot}695$ N $\Lambda = 0{\cdot}26$

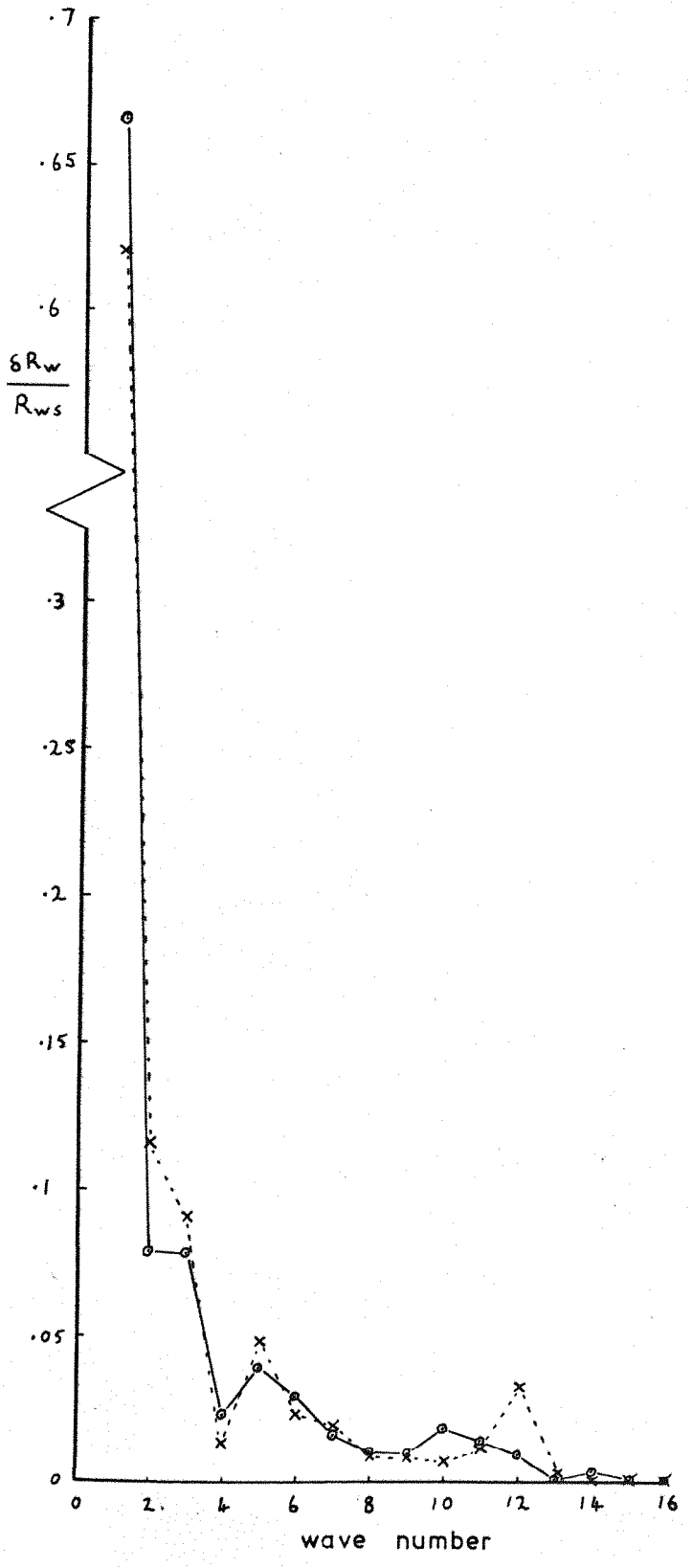

FIG 7

COMPARISON OF ANTISYMMETRIC WAVE RESISTANCE SPECTRA FROM DIFFERENT PROBE POSITIONS

10° Heel 4° yaw U = 1·06 m/s F_∇ = 0·315

——o—— $\frac{y}{b} = \frac{3}{10}, \frac{5}{14}$ R_{wa} = 0·073 N Λ = 0·66

------x------ $\frac{y}{b} = \frac{3}{10}, \frac{7}{18}$ R_{wa} = 0·032 N Λ = 0·69

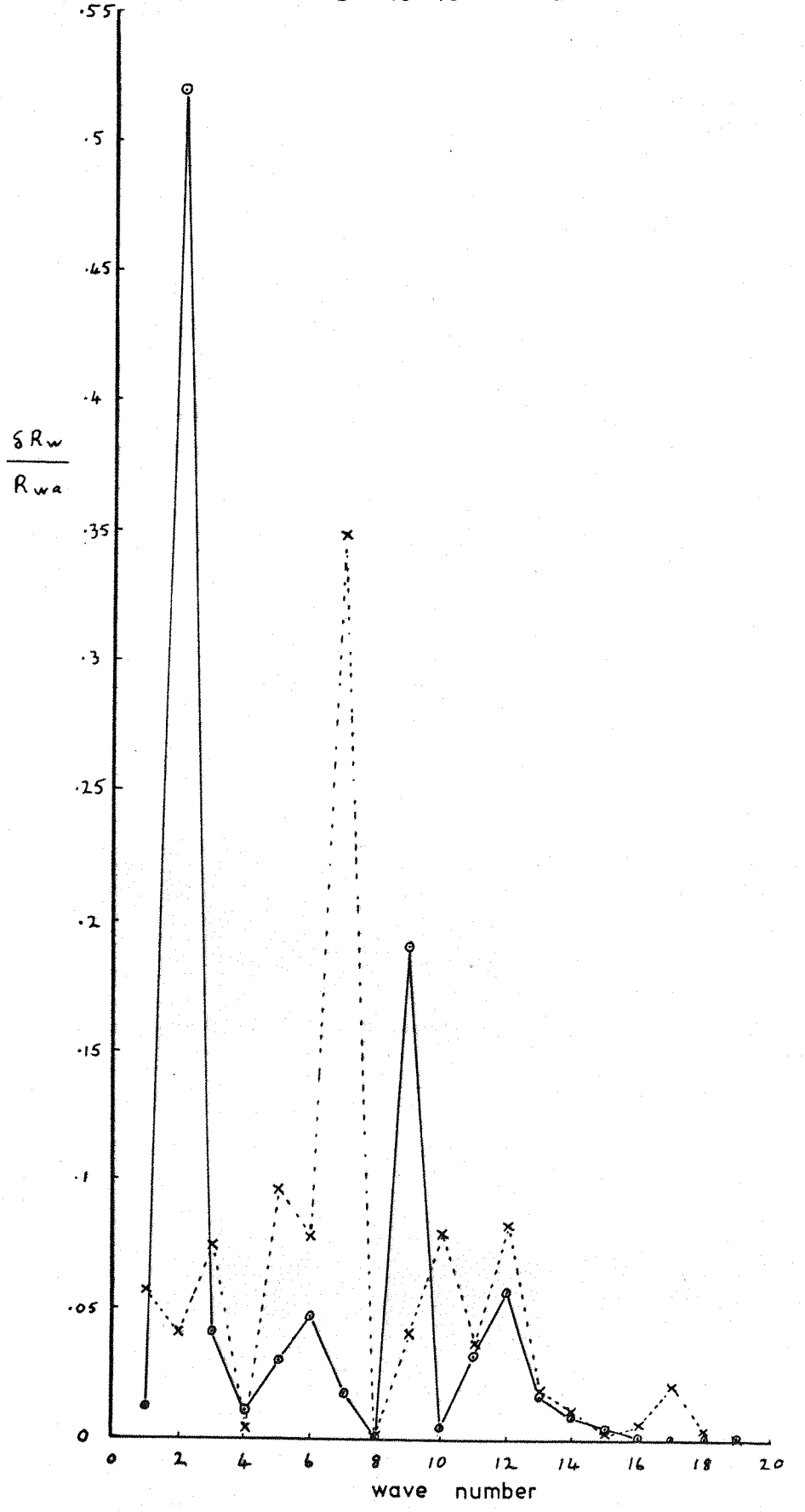

FIG 8

COMPARISON OF ANTISYMMETRIC WAVE RESISTANCE SPECTRA FROM DIFFERENT PROBE POSITIONS

10° heel 4° yaw U = 1·27 m/s F_∇ = 0·38

——o—— $\frac{y}{b} = \frac{3}{10}, \frac{5}{14}$ R_{wa} = 0·086 N Λ = 0·63

------x------ $\frac{y}{b} = \frac{3}{10}, \frac{7}{18}$ R_{wa} = 0·099 N Λ = 0·61

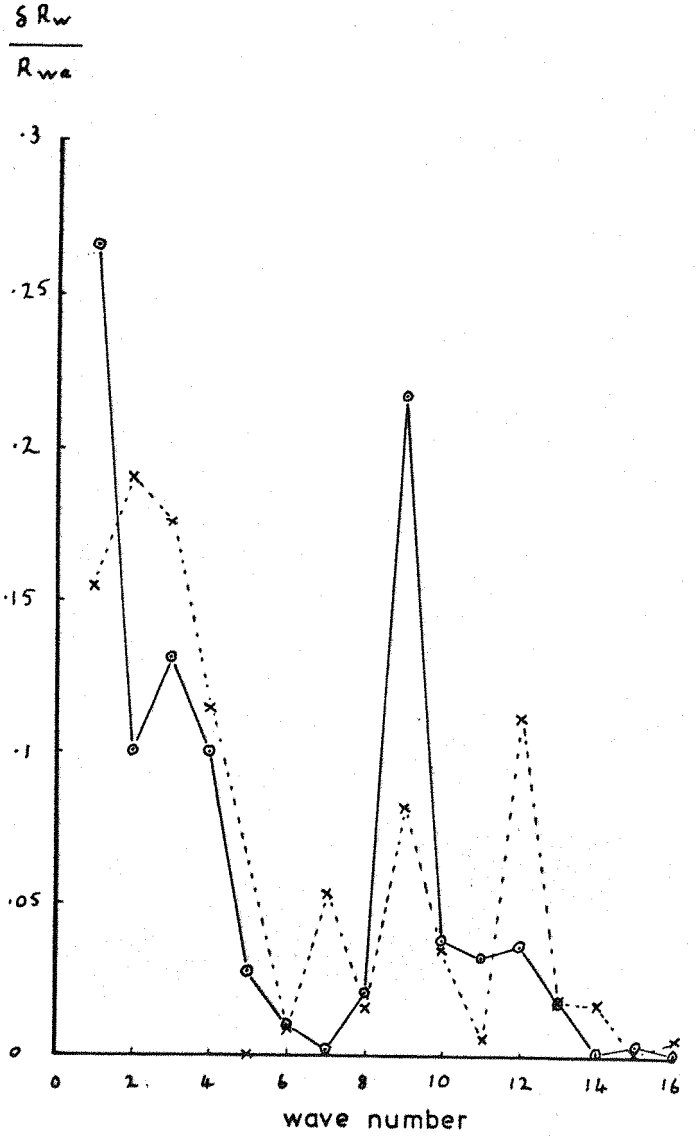

FIG 9 **PLOTS OF THE SYMMETRIC WAVE TRACES AS MEASURED AND AS FITTED**

Upright $U = 1{\cdot}06$ m/s $F_r = 0{\cdot}315$ $\Lambda = 0{\cdot}34$

× as fitted

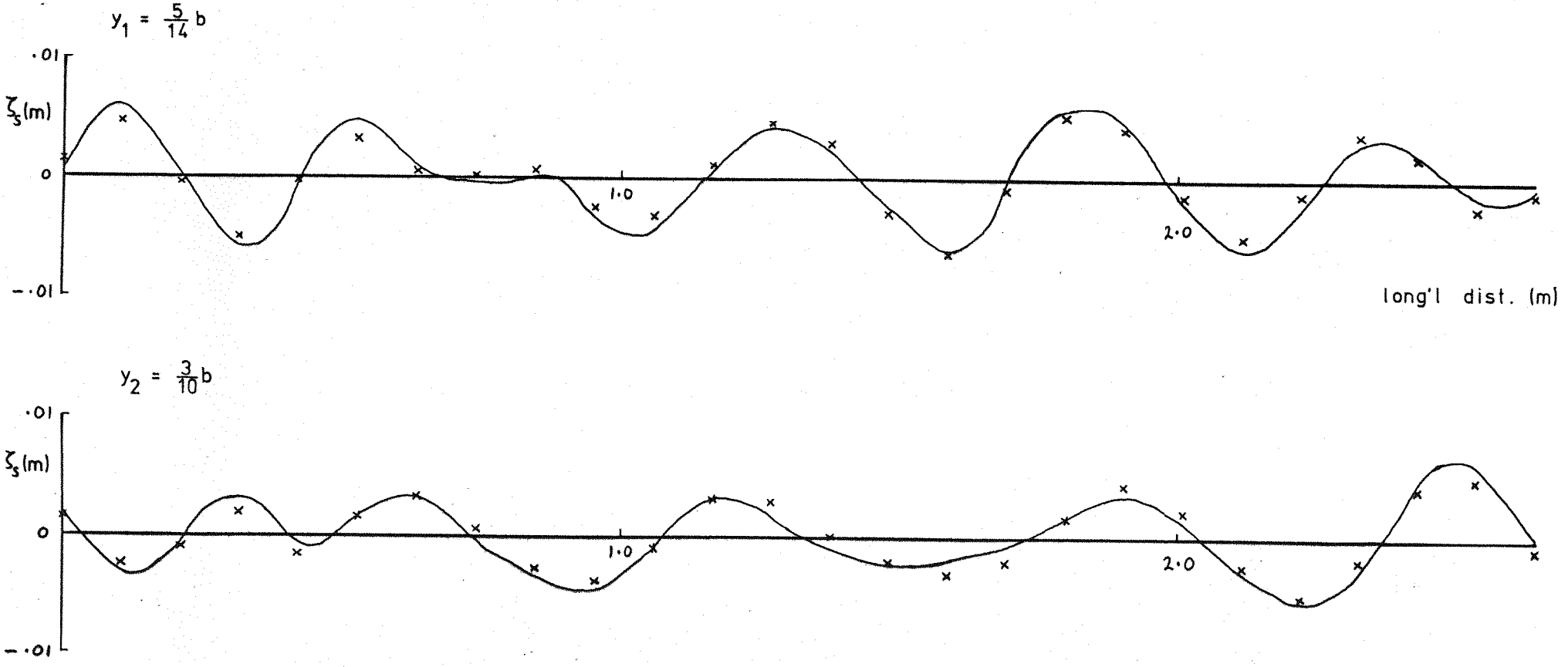

FIG 10 **PLOTS OF THE SYMMETRIC WAVE TRACES AS MEASURED AND AS FITTED**

Upright **U** = 1·27 m/s F_r = 0·38 Λ = 0·21

× as fitted

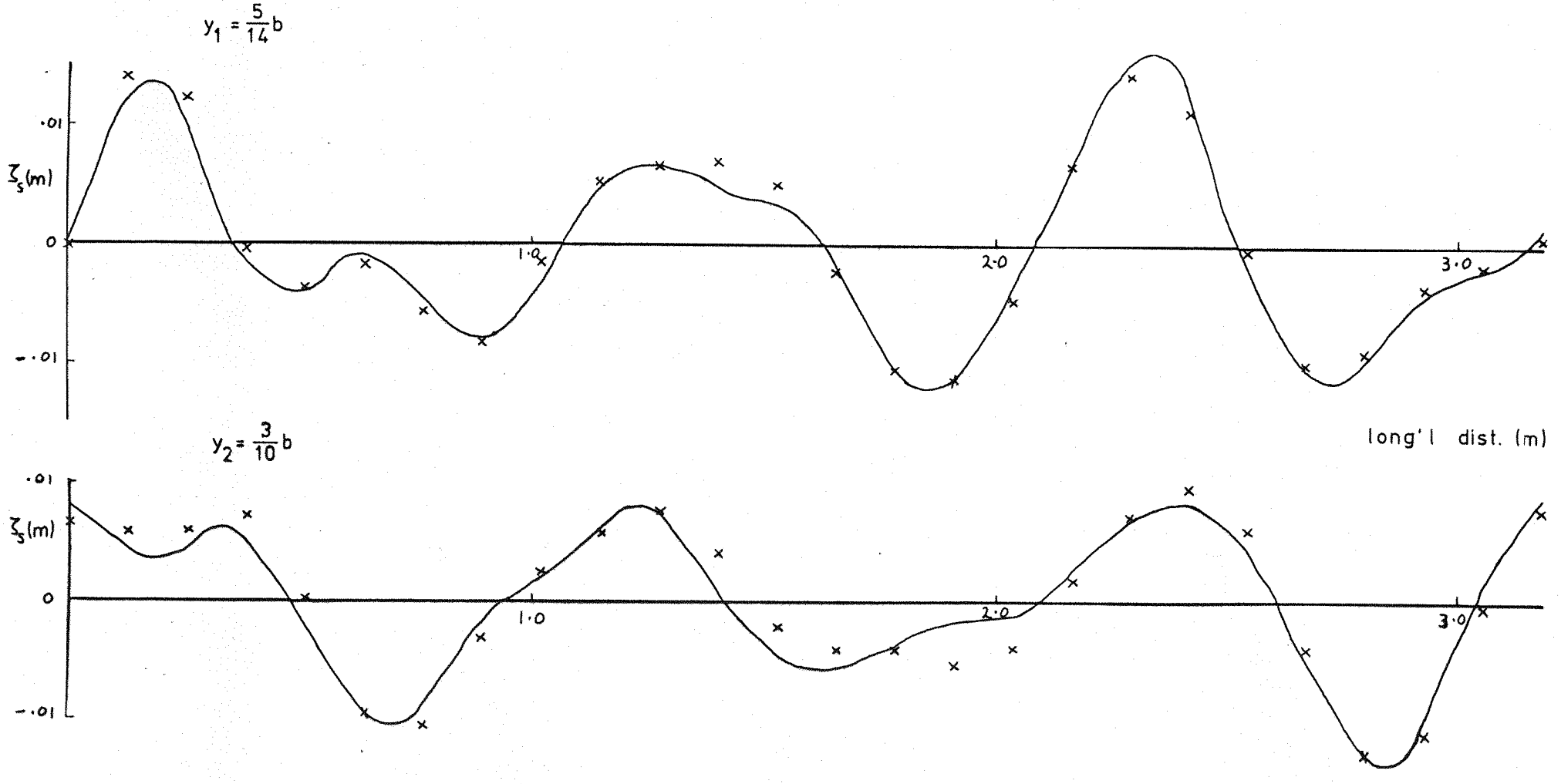

FIG 11

PLOTS OF THE ANTISYMMETRIC WAVE TRACES AS MEASURED AND AS FITTED

10° **heel** 4° **yaw** **U** = 1·06 m/s F_r = 0·315 Λ = 0·66

× as fitted

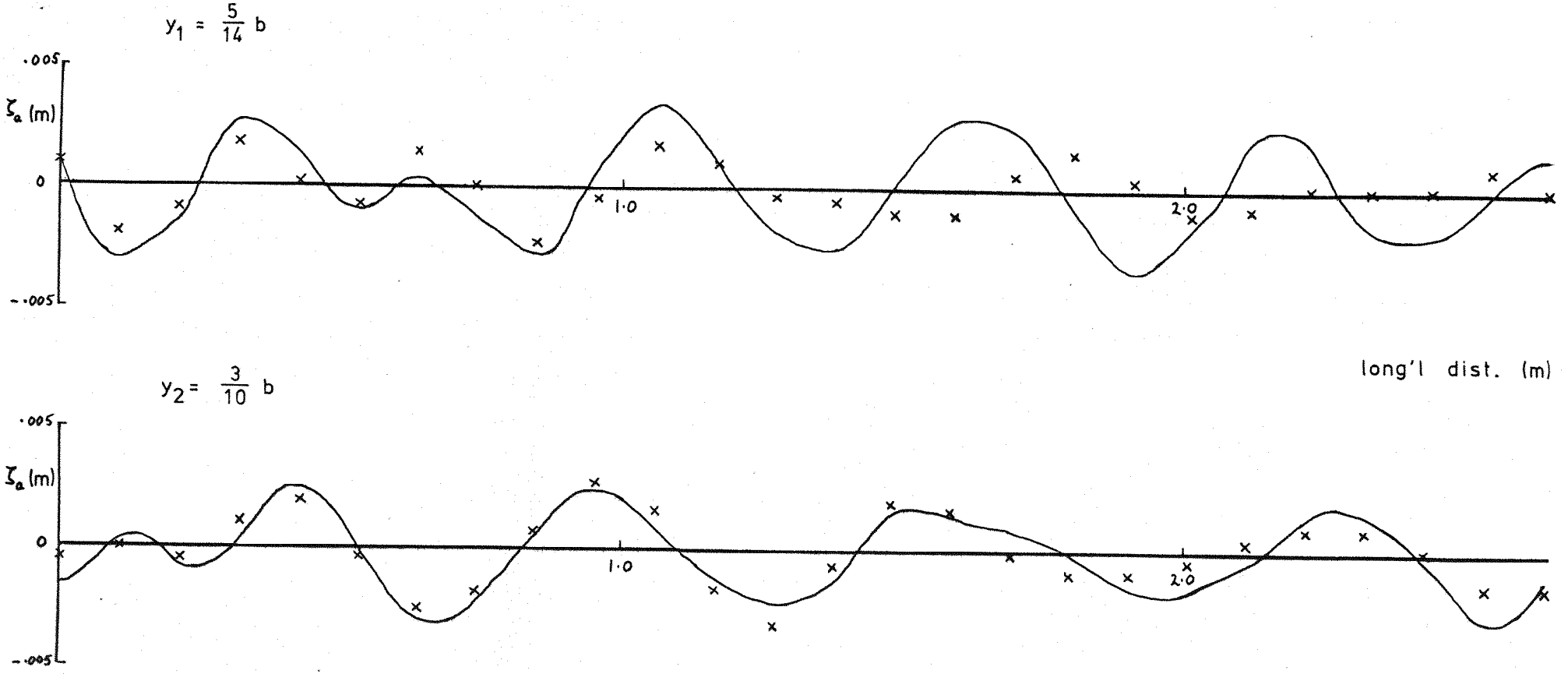

FIG 12 **PLOTS OF THE ANTISYMMETRIC WAVE TRACES AS MEASURED AND AS FITTED**

10° heel 4° yaw $U = 1{\cdot}27\,m/s$ $F_r = 0{\cdot}38$ $\Lambda = 0{\cdot}63$

× as fitted

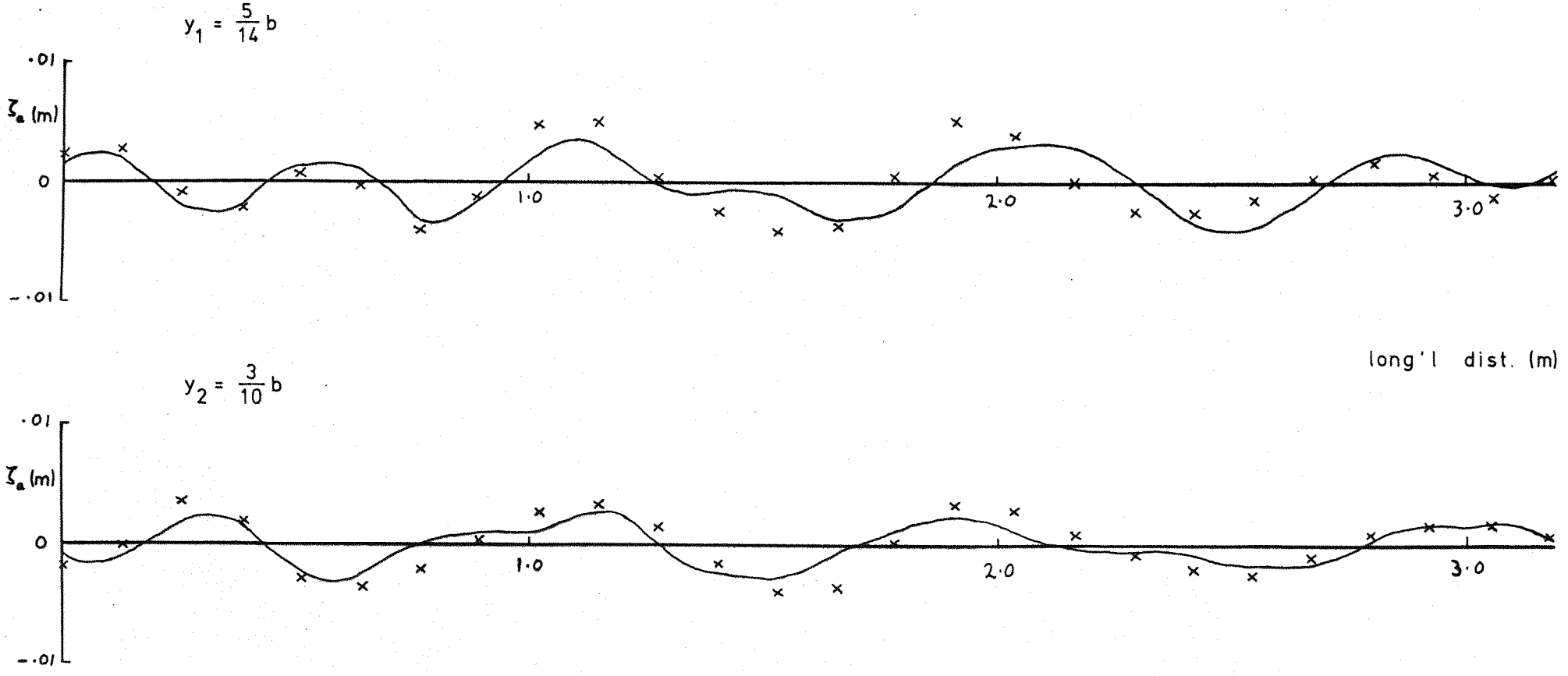

FIG 13 **WAVE RESISTANCE SPECTRUM** Upright

U = 0·92 m/s F_r = 0·27

R_{ws} = 0·035 newtons

——o—— **Symmetric Component**

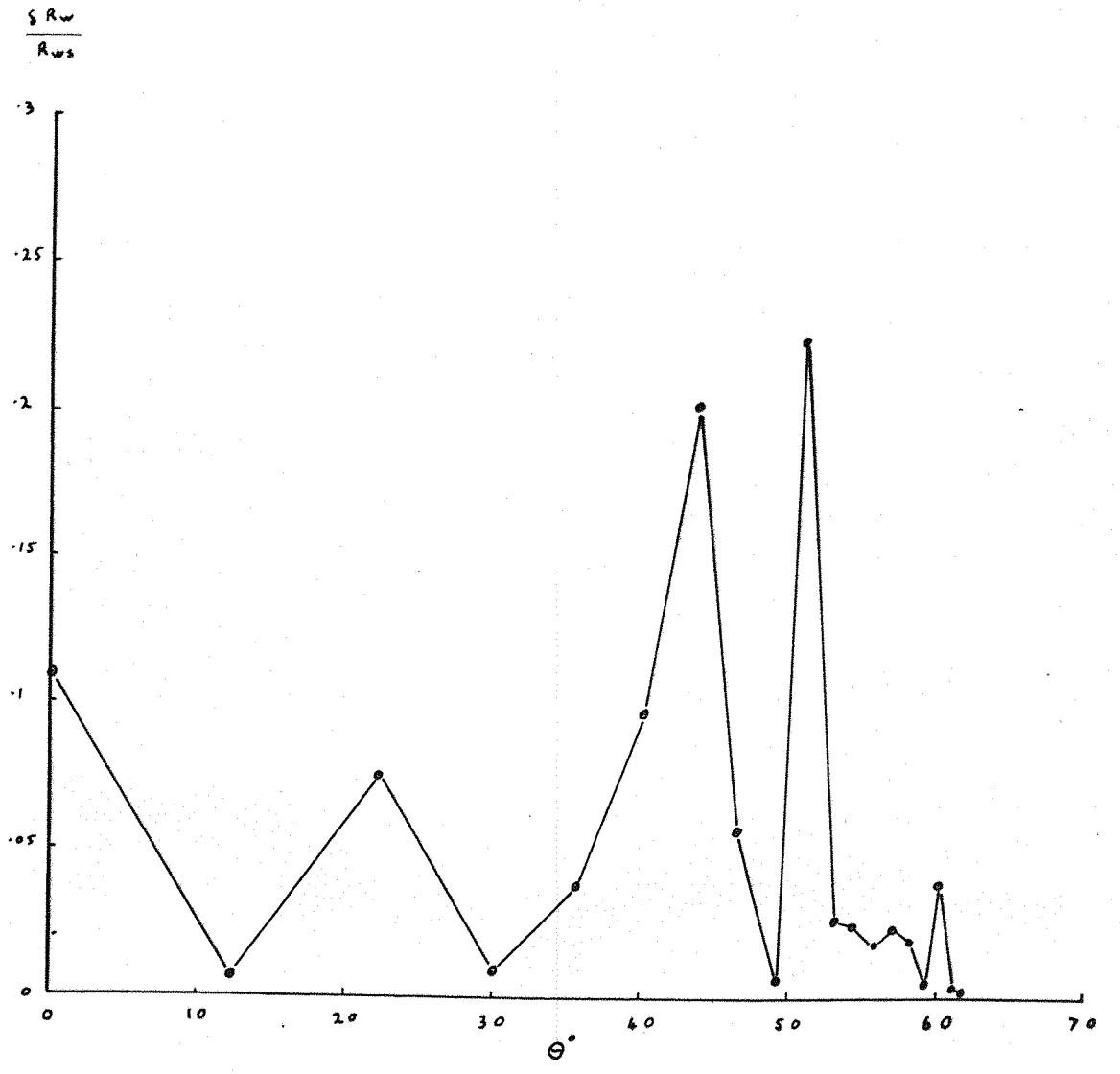

FIG 14 **WAVE RESISTANCE SPECTRUM** Upright

$U = 0.99$ m/s $F_r = 0.29$

$R_{ws} = 0.064$ newtons

——⊙—— Symmetric Component

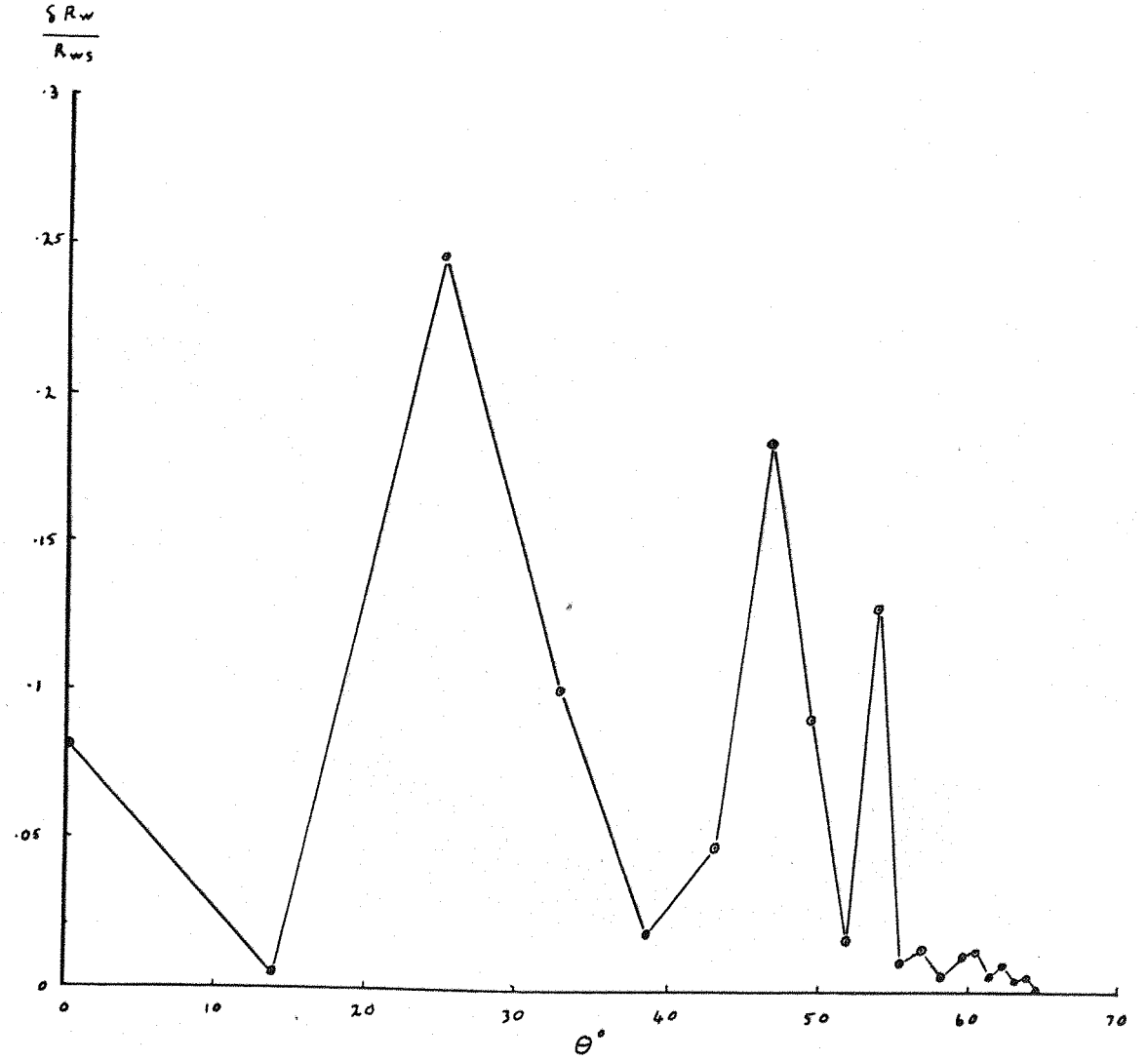

FIG 15 **WAVE RESISTANCE SPECTRUM** Upright

U = 1·06 m/s F_r = 0·315

R_{ws} = 0·095 newtons

——⊙—— Symmetric Component

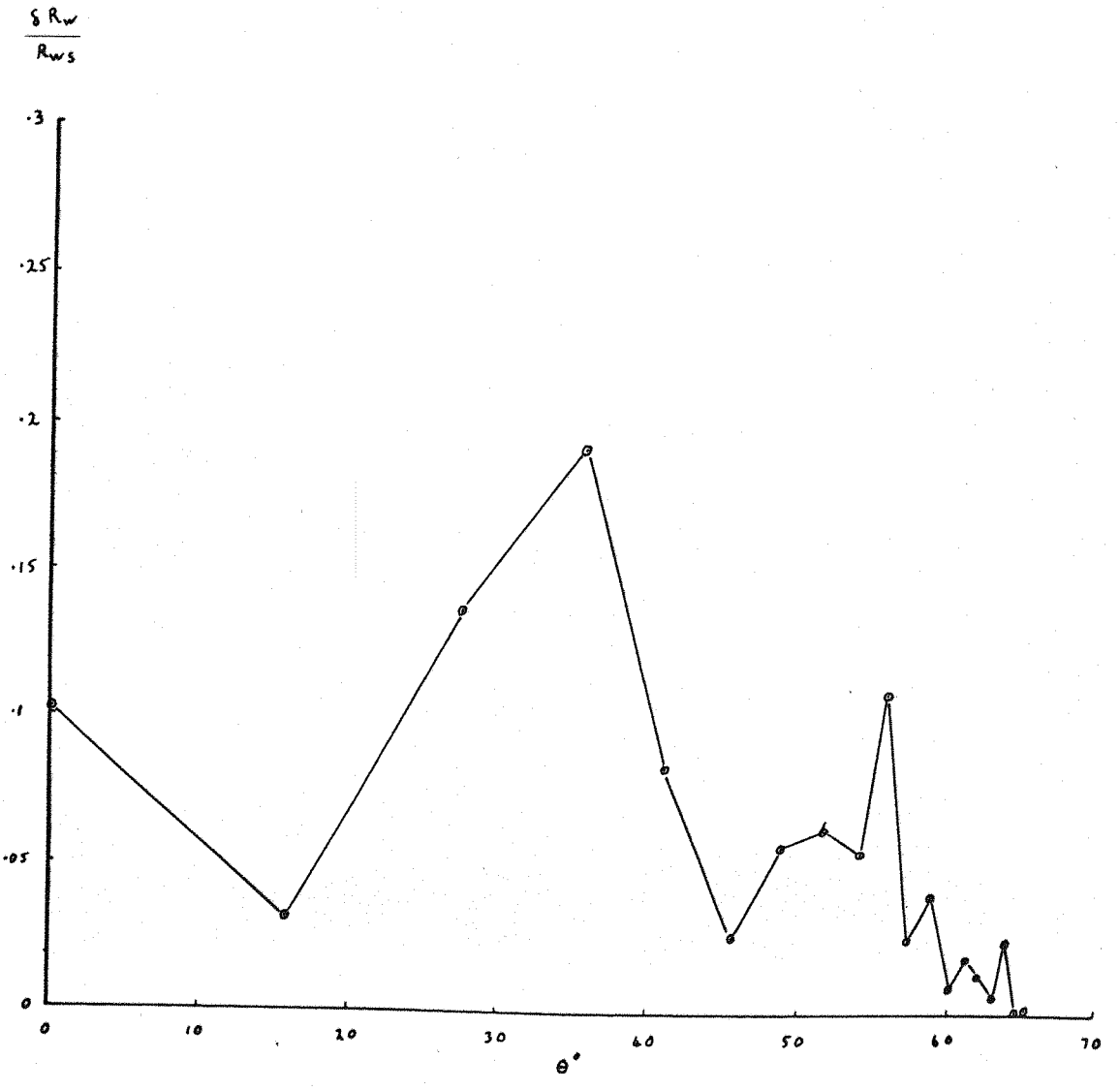

FIG 16 **WAVE RESISTANCE SPECTRUM** Upright

U = 1·13 m/s F_r = 0·34

R_{ws} = 0·171 newtons

——⊙—— Symmetric Component

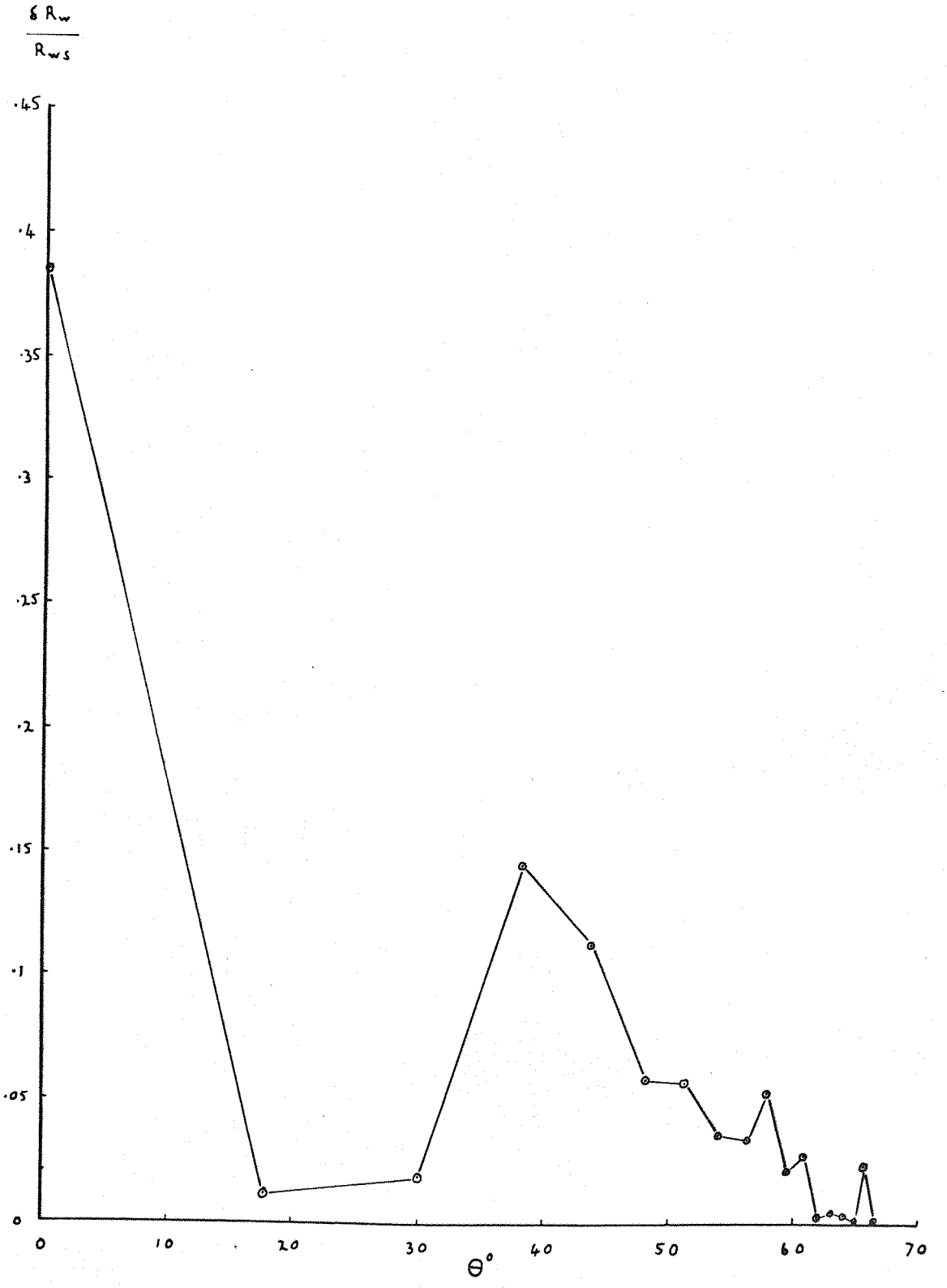

FIG 17 **WAVE RESISTANCE SPECTRUM** Upright

U = 1·2 m/s F_r = 0·36

R_{ws} = 0·357 newtons

——⊙—— Symmetric Component

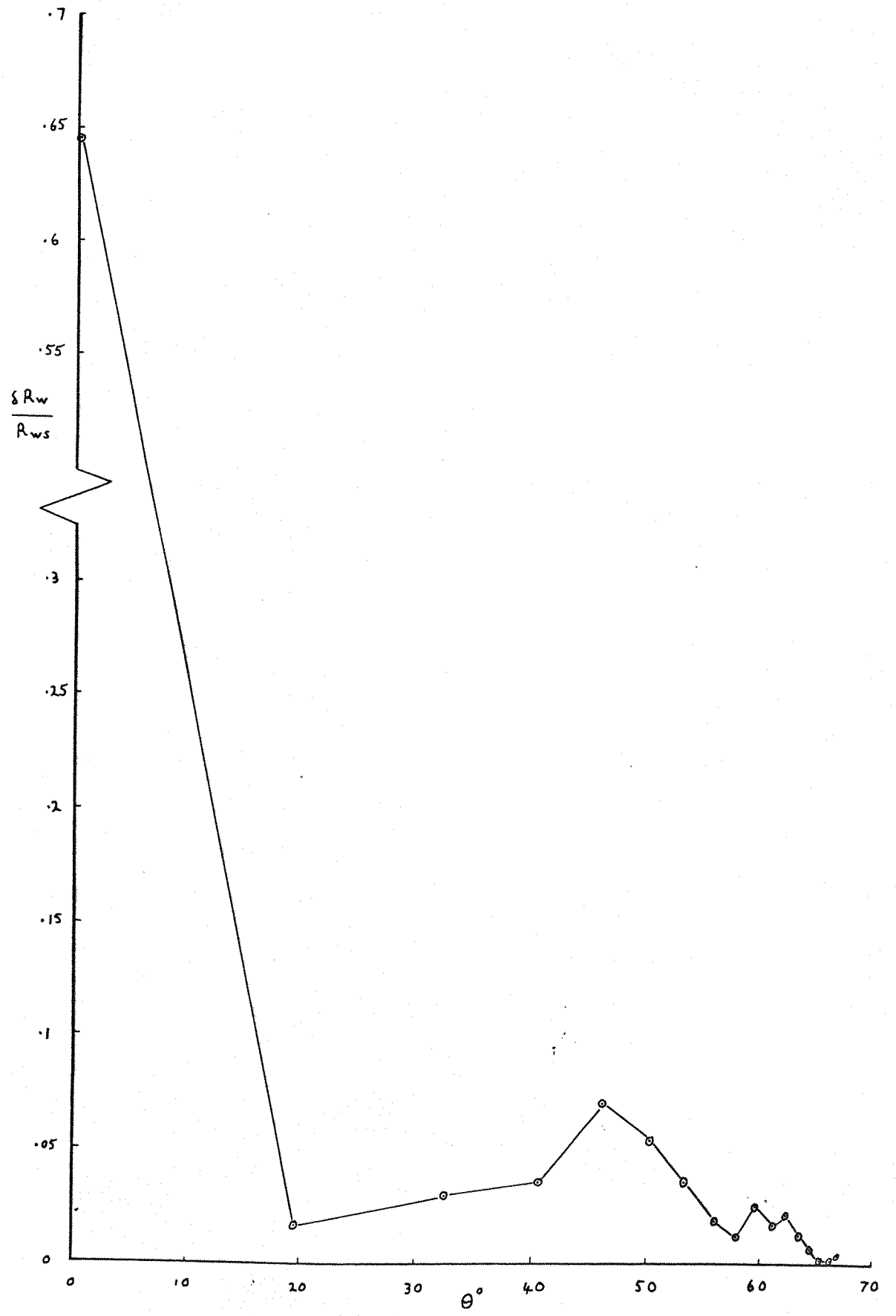

FIG 18 **WAVE RESISTANCE SPECTRUM** Upright

U = 1·27 m/s F_r = 0·38

R_{ws} = 0·685 newtons

——o—— Symmetric Component

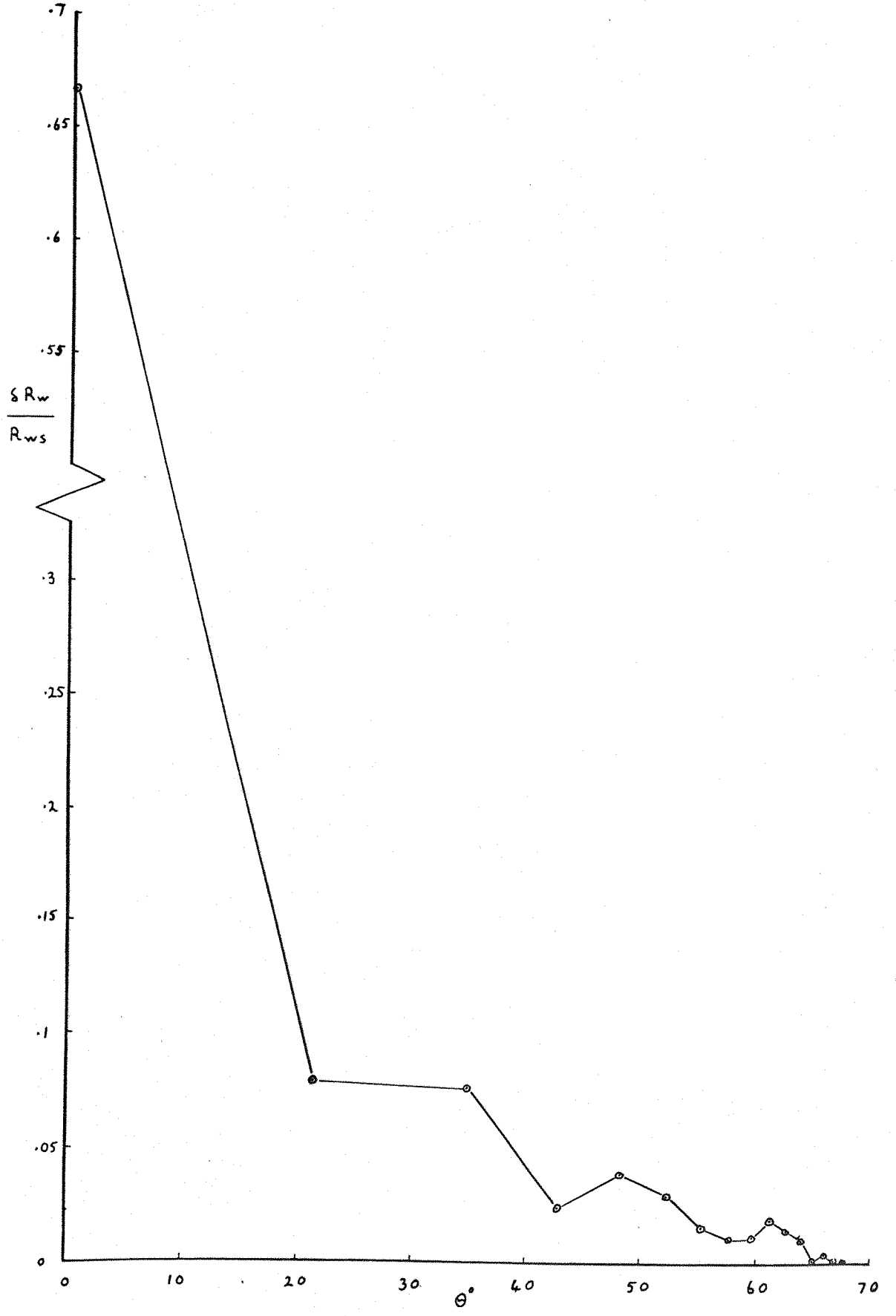

FIG 19 **WAVE RESISTANCE SPECTRUM** Upright

U = 1·34 m/s F_r = 0·4

R_{ws} = 1·305 newtons

——⊙—— Symmetric Component

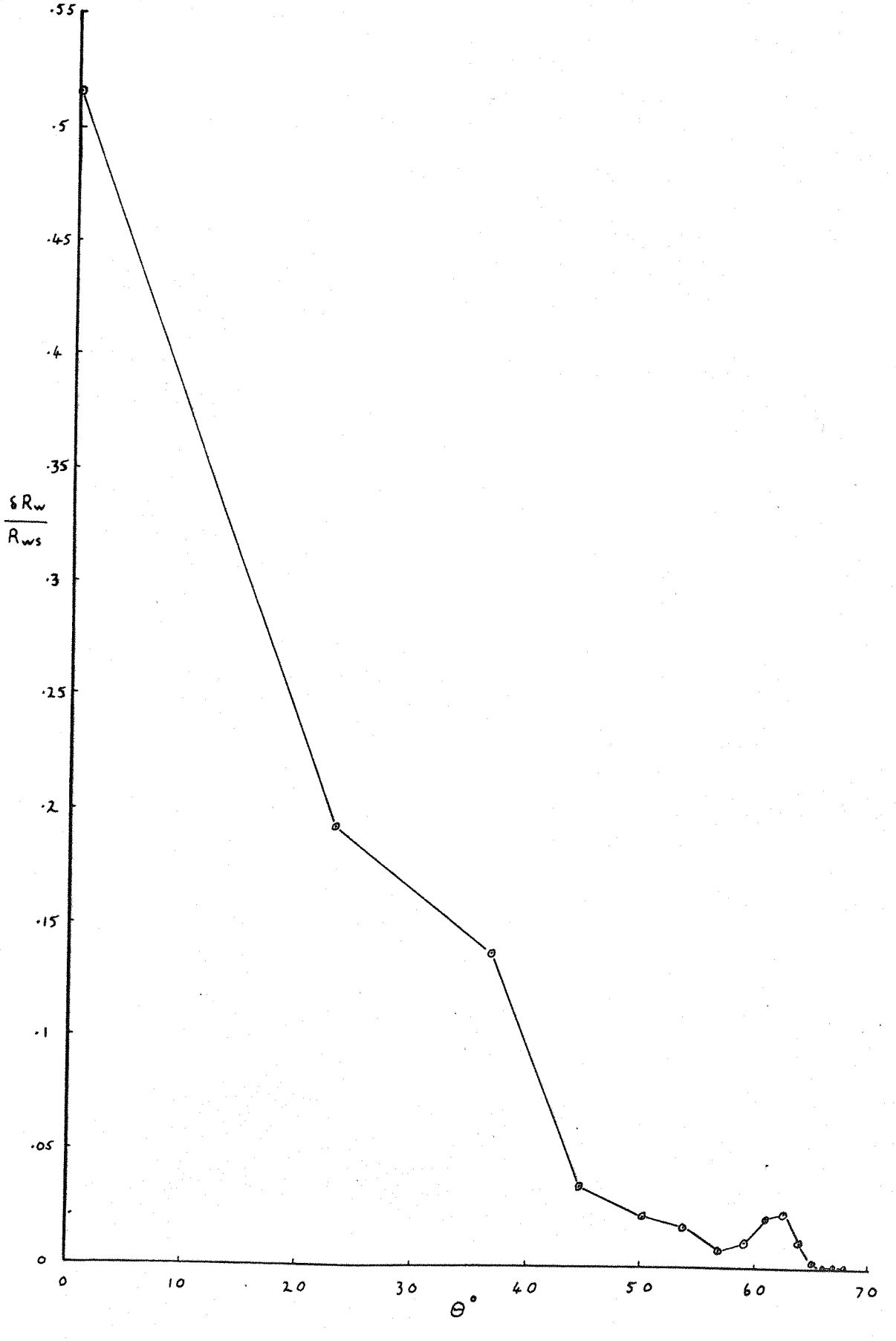

FIG 20 **WAVE RESISTANCE SPECTRUM** Upright

U = 1·4 m/s F_r = 0·42

R_{ws} = 2·209 newtons

——o—— **Symmetric Component**

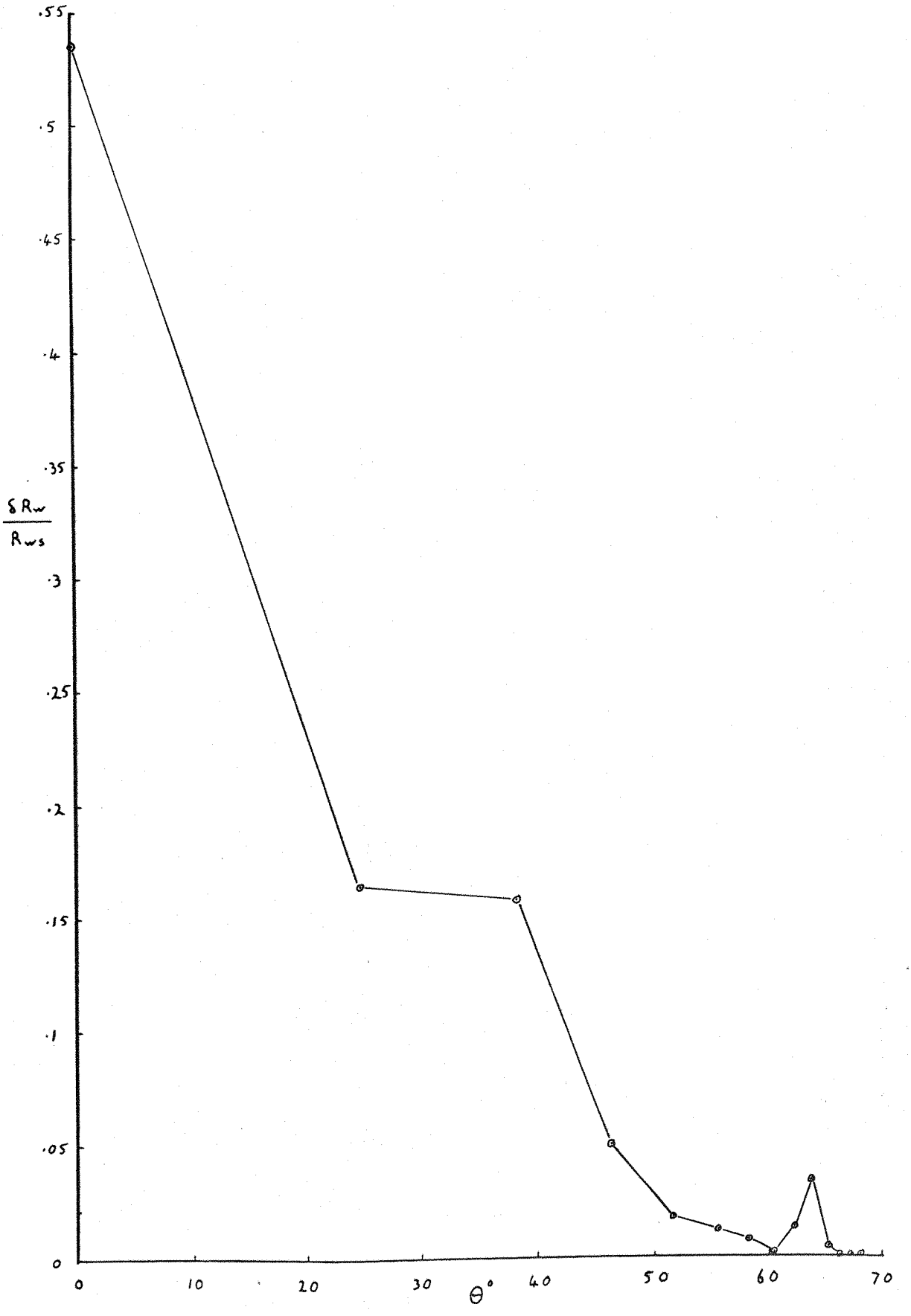

FIG 21 **WAVE RESISTANCE SPECTRUM** Upright

$U = 1.48$ m/s $F_r = 0.44$

$R_{ws} = 3.393$ newtons

—— o —— Symmetric Component

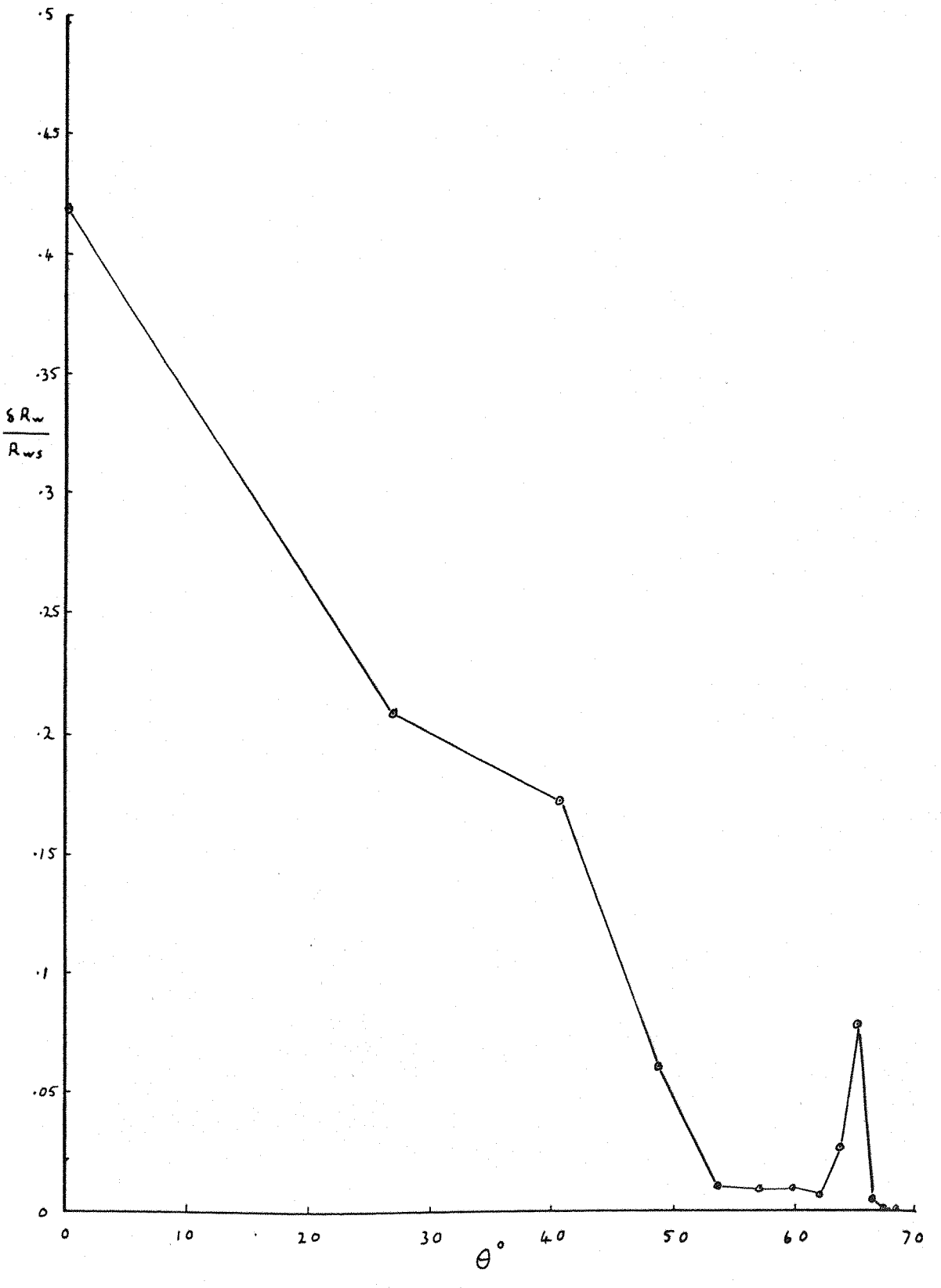

FIG 22 **WAVE RESISTANCE SPECTRUM** 10° heel 4° yaw

U = 0·92 m/s F_r = 0·27

R_{wa} = 0·011 newtons

— — × — — **Antisymmetric Component**

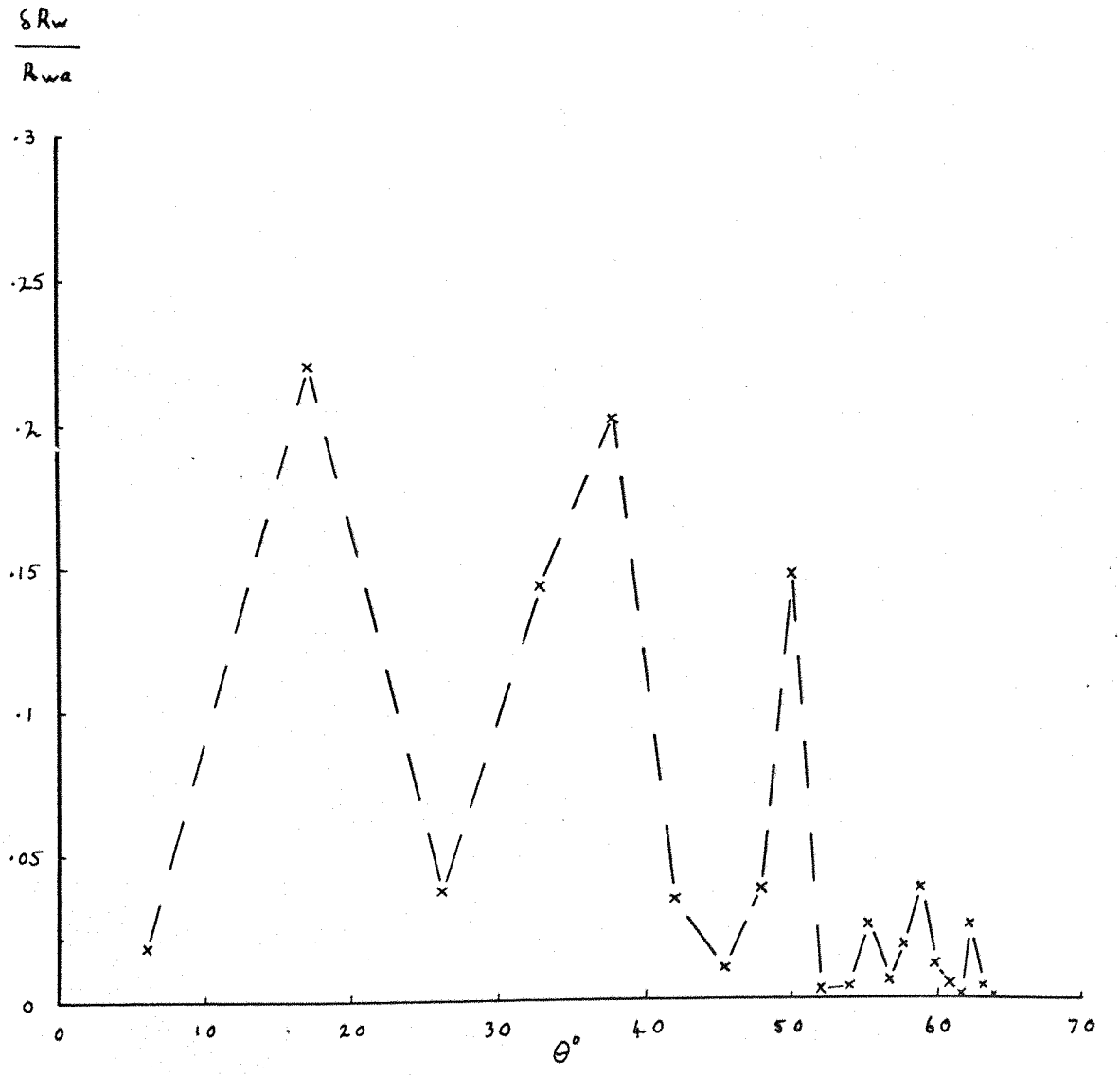

FIG 23 **WAVE RESISTANCE SPECTRA** 10° heel 2° yaw

U = 1·06 m/s F_r = 0·315

R_{ws} = 0·061 R_{wa} = 0·036 newtons

——o—— Symmetric Component

— — × — — Antisymmetric Component

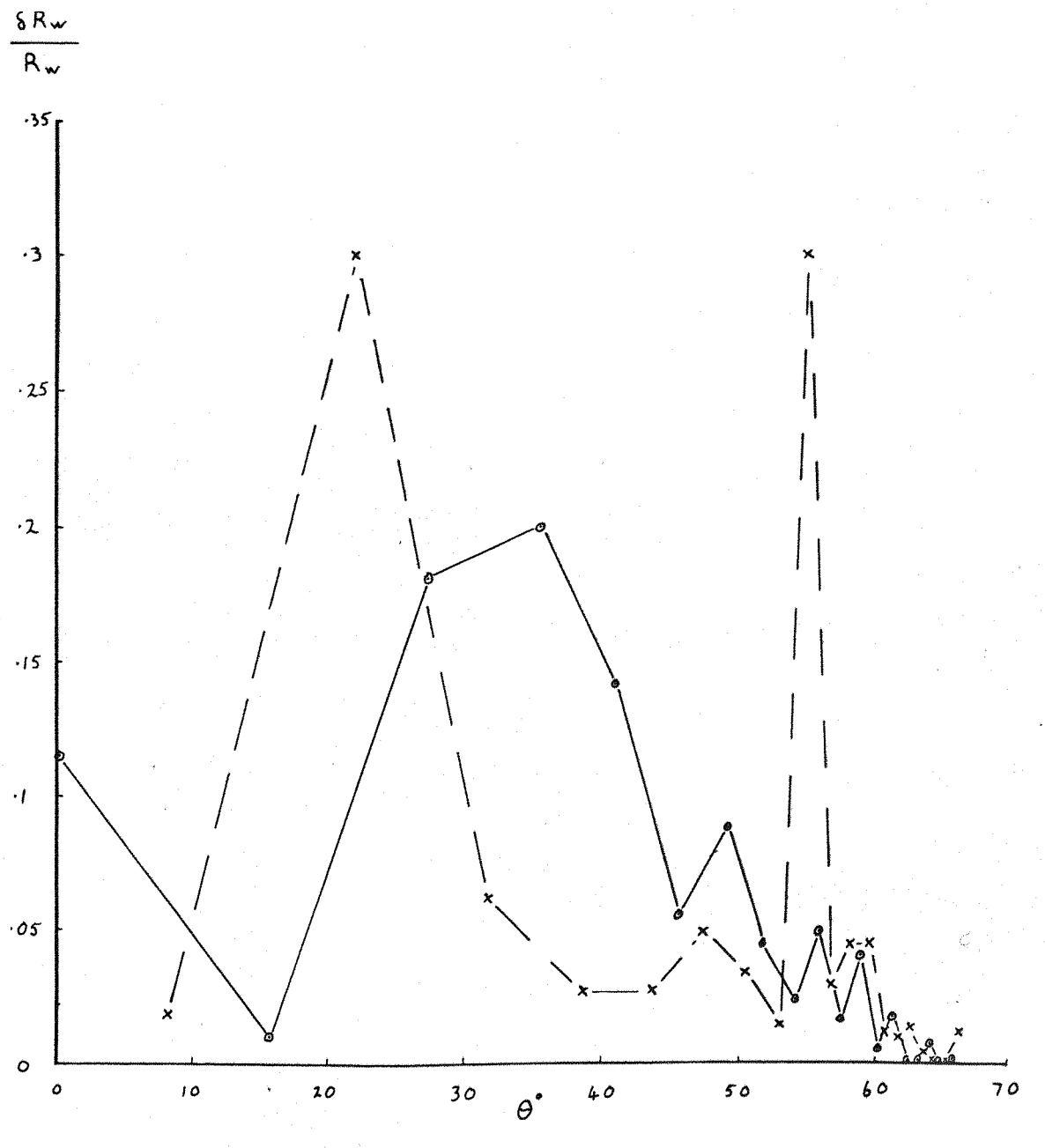

FIG 24 **WAVE RESISTANCE SPECTRA** 10° heel 4° yaw

U = 1·06 m/s F_r = 0·315

R_{ws} = 0·052 R_{wa} = 0·073 newtons

——⊙—— Symmetric Component

— —×— — Antisymmetric Component

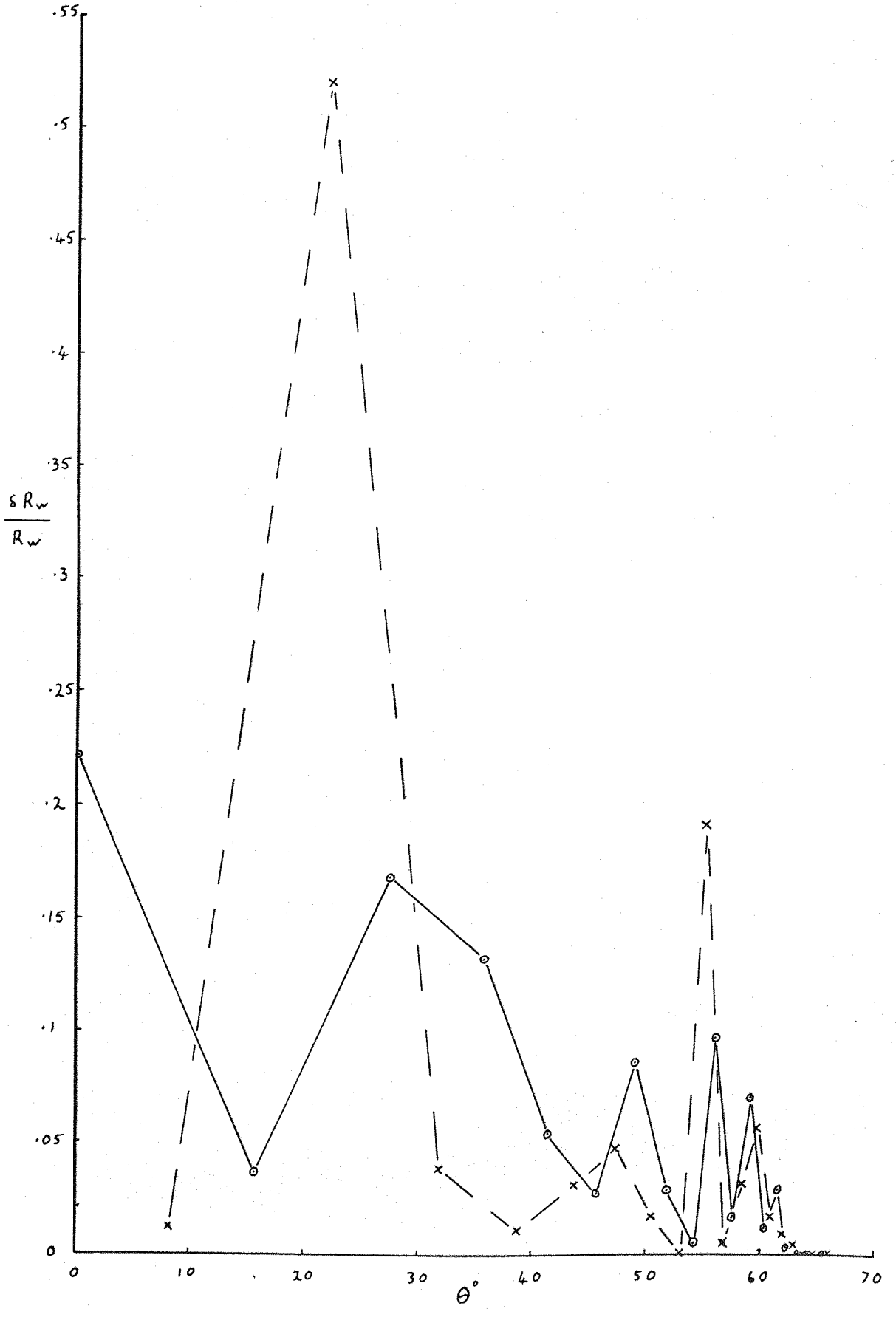

FIG 25 **WAVE RESISTANCE SPECTRA** 10° heel 6° yaw

U = 1·06 m/s F_r = 0·315

R_{ws} = 0·045 R_{wa} = 0·069 newtons

——o—— Symmetric Component

— —x— — Antisymmetric Component

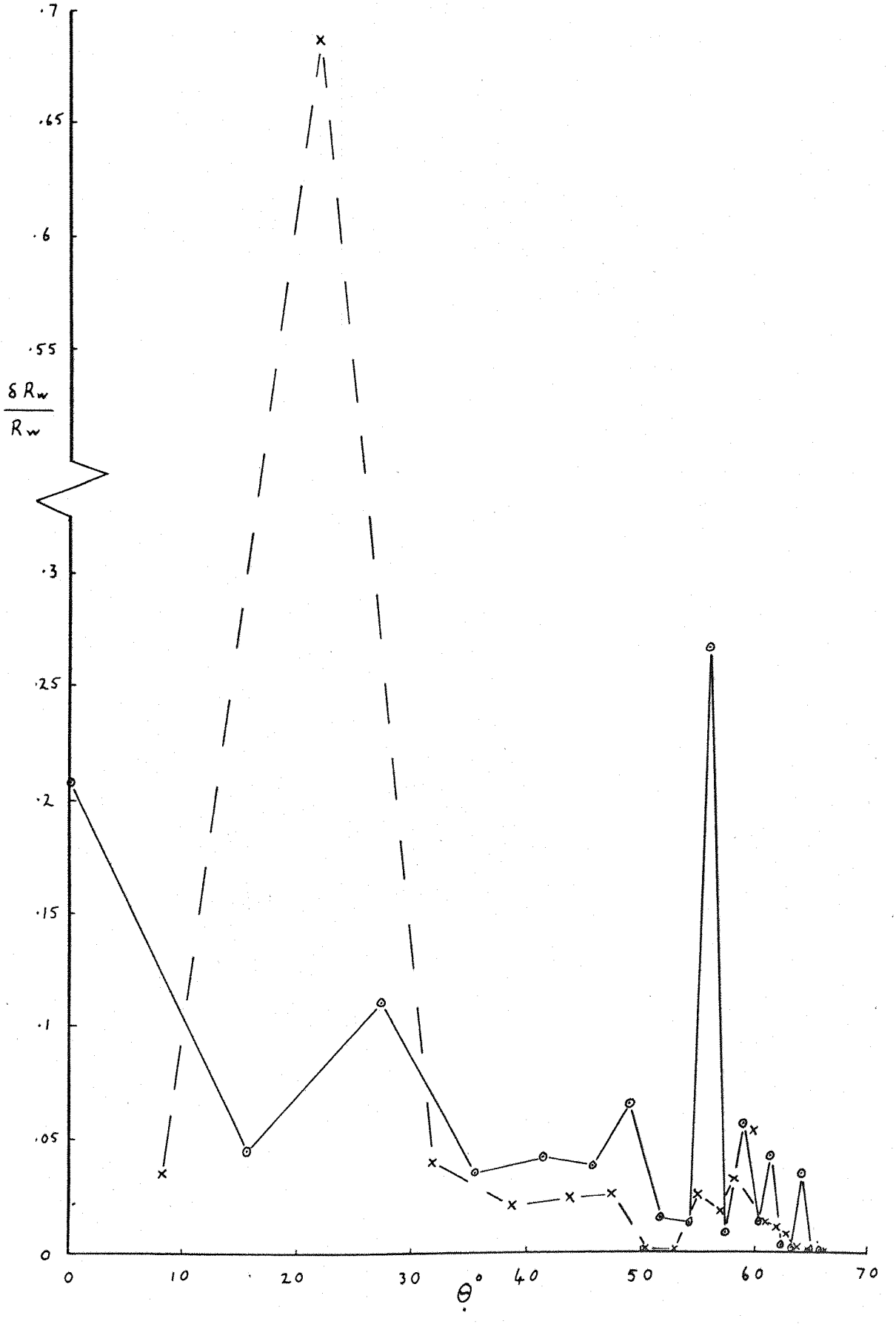

FIG 26 **WAVE RESISTANCE SPECTRUM** 10° heel 4° yaw

U = 1·2 m/s F_r = 0·36

R_{wa} = 0·071 newtons

— — × — — **Antisymmetric Component**

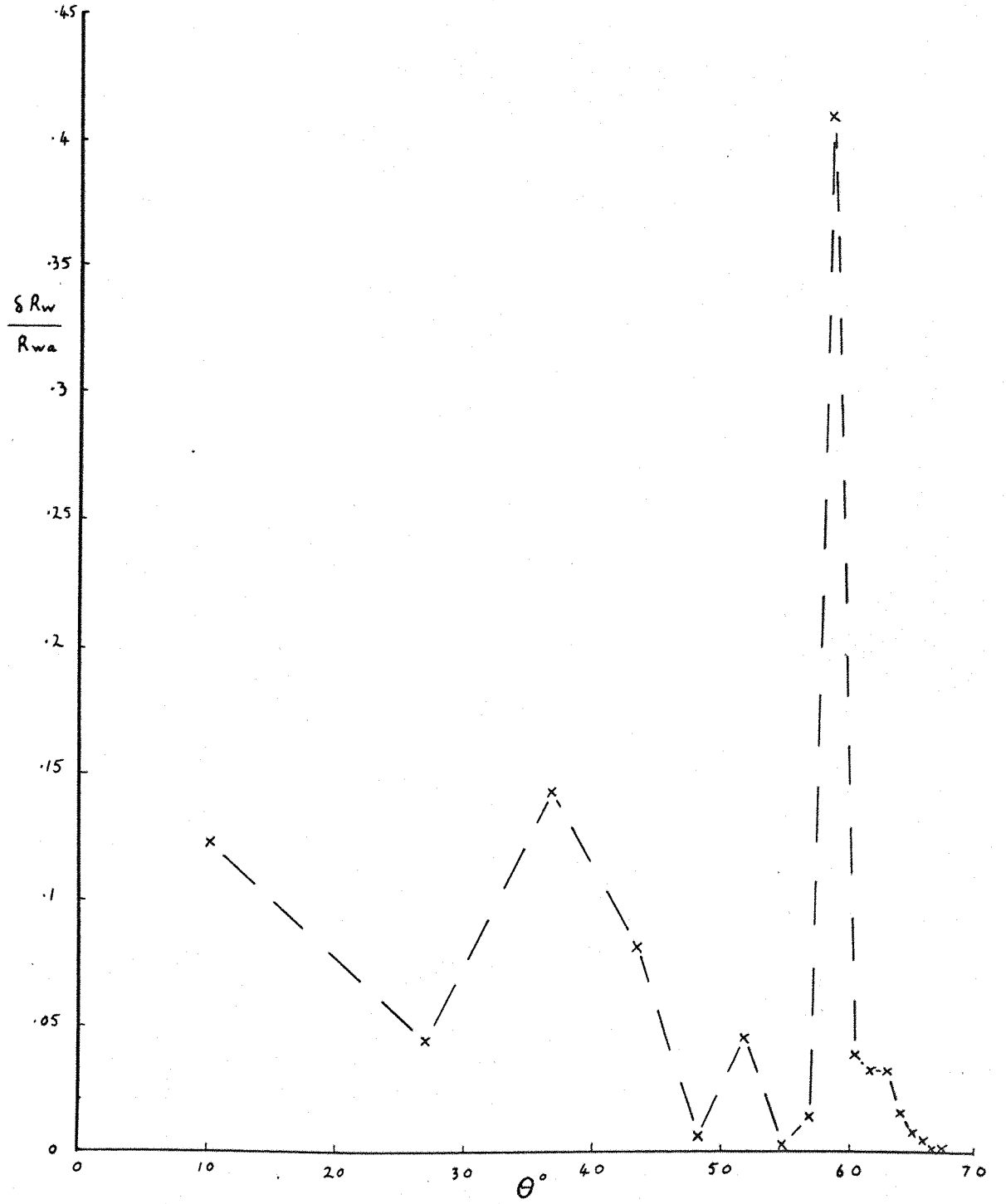

FIG 27 **WAVE RESISTANCE SPECTRA** 10° heel 2° yaw

U = 1·27 m/s F_r = 0·38

R_{ws} = 0·625 R_{wa} = 0·071 newtons

——⊙—— Symmetric Component

— —×— — Antisymmetric Component

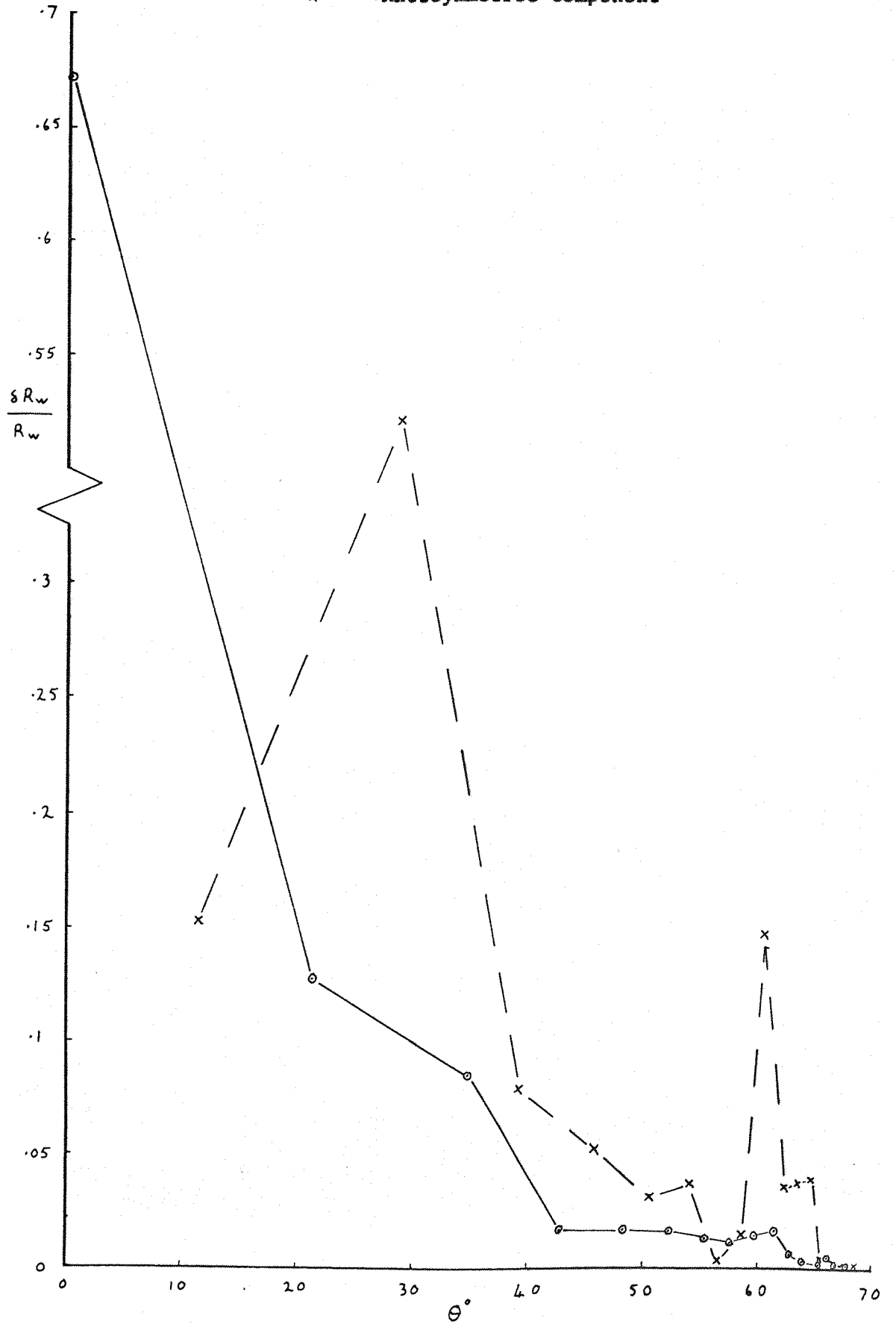

FIG 28 **WAVE RESISTANCE SPECTRA** 10° heel 4° yaw

$U = 1{\cdot}27$ m/s $F_r = 0{\cdot}38$

$R_{ws} = 0{\cdot}642$ $R_{wa} = 0{\cdot}086$ newtons

——o—— Symmetric Component

— —×— — Antisymmetric Component

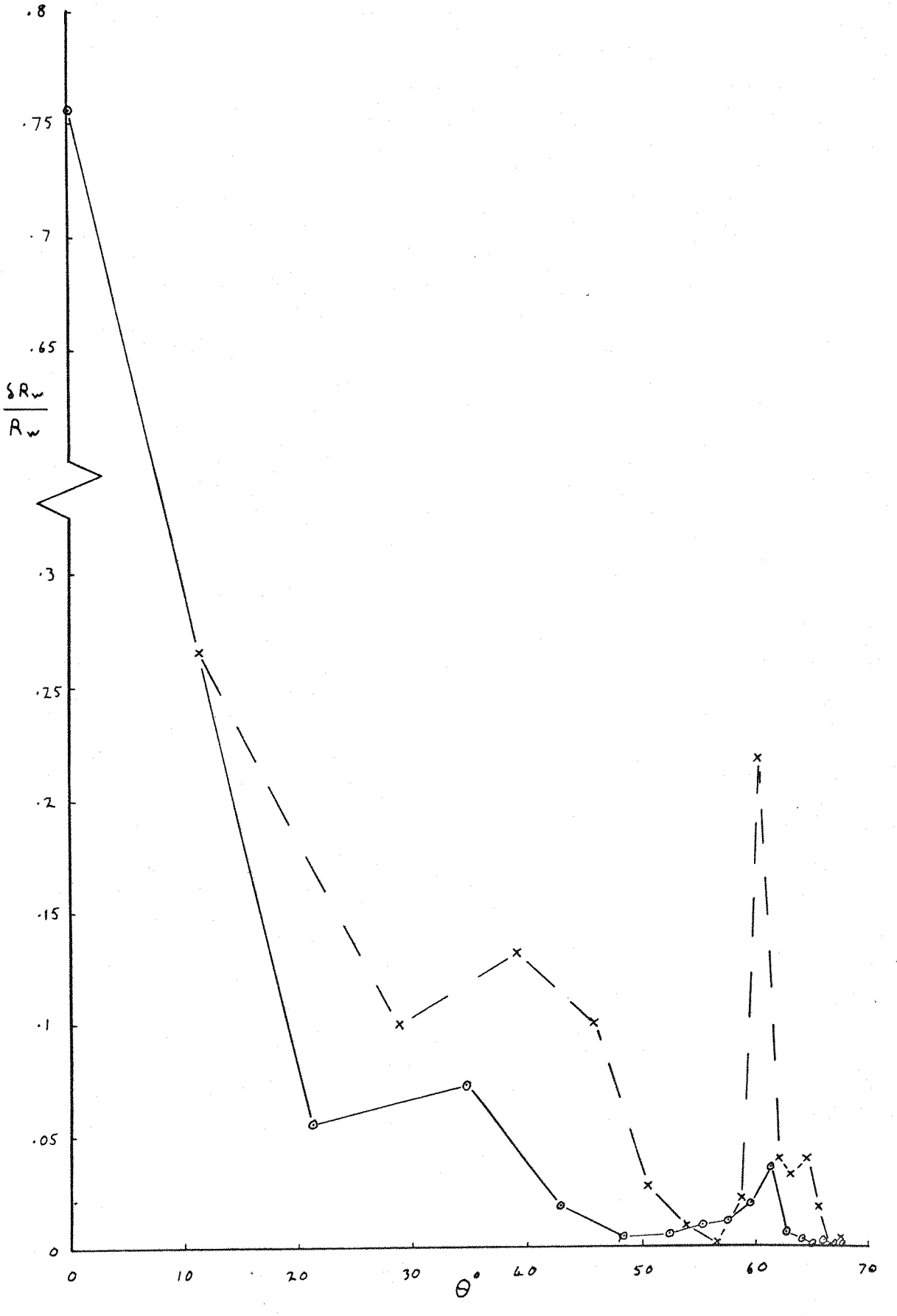

FIG 29 **WAVE RESISTANCE SPECTRA** 10° heel 6° yaw

U = 1·27 m/s F_r = 0·38

R_{ws} = 0·673 R_{wa} = 0·102 newtons

——o—— Symmetric Component

— — x — — Antisymmetric Component

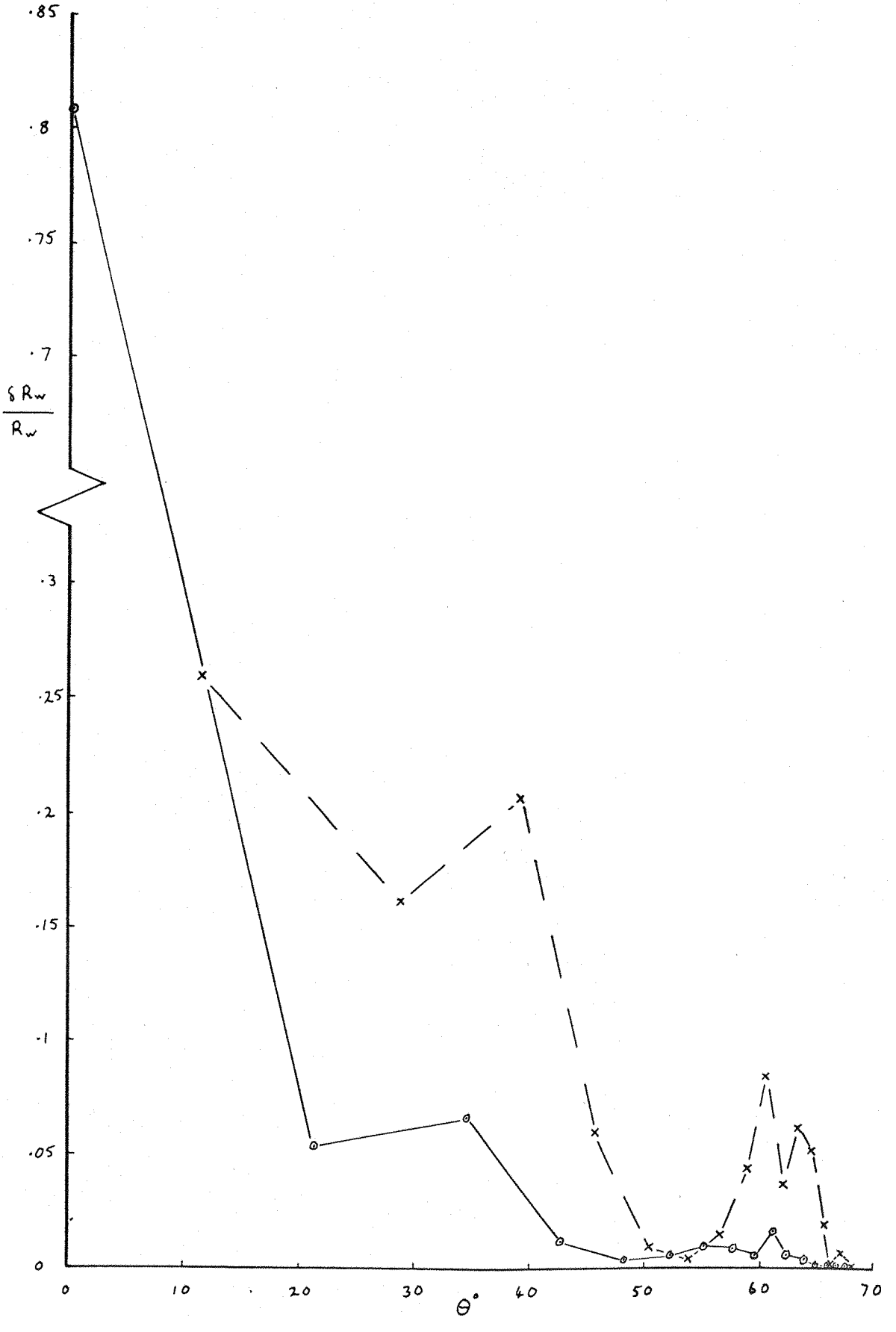

FIG 30 **WAVE RESISTANCE SPECTRUM** 10° heel 4° yaw

U = 1·48 m/s F_r = 0·44

R_{wa} = 0·302 newtons

— —x— — **Antisymmetric Component**

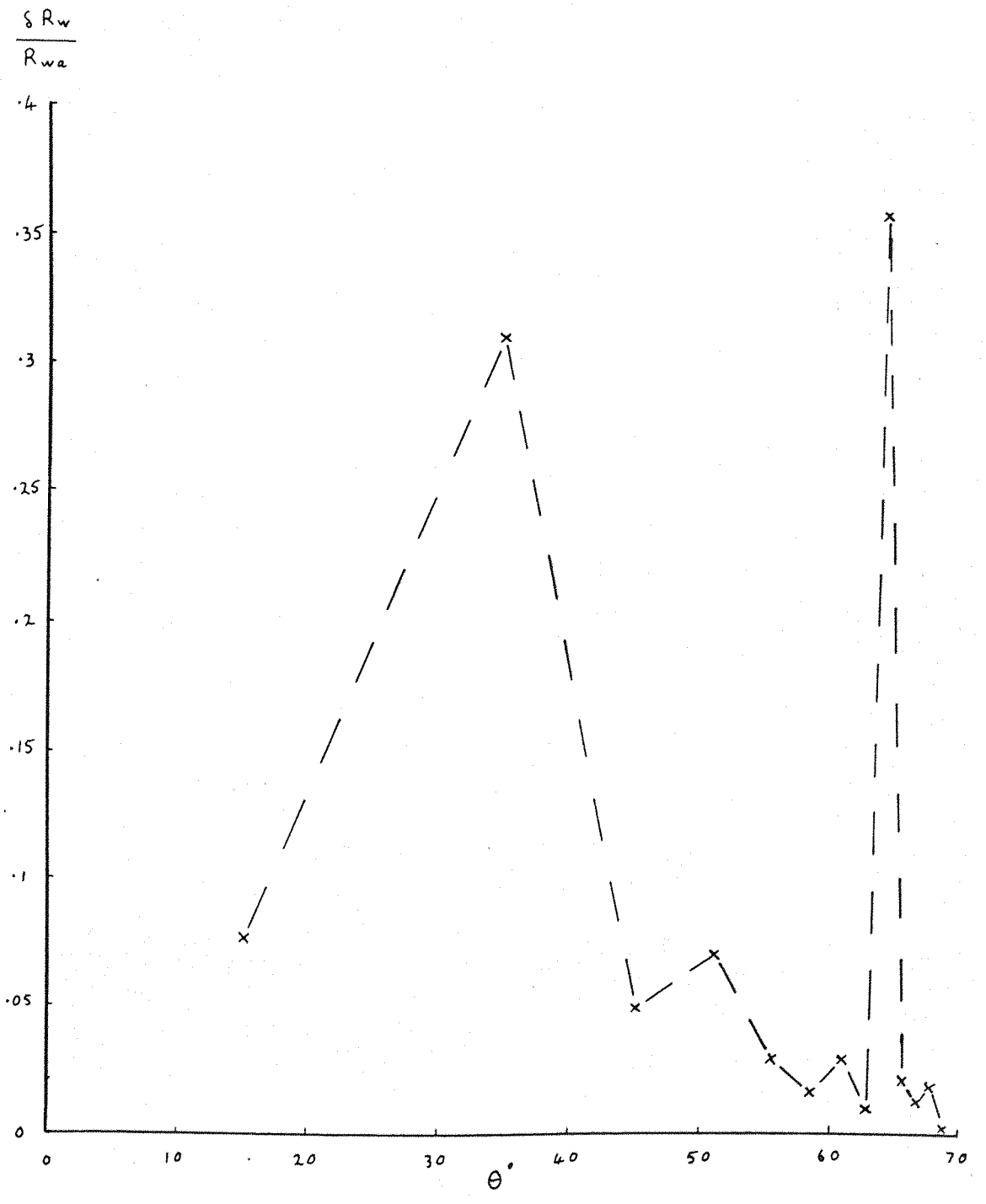

FIG 31

SYMMETRIC, ANTISYMMETRIC AND TOTAL WAVE RESISTANCE AGAINST ASPECT

U = 0·92 m/s F_r = 0·27

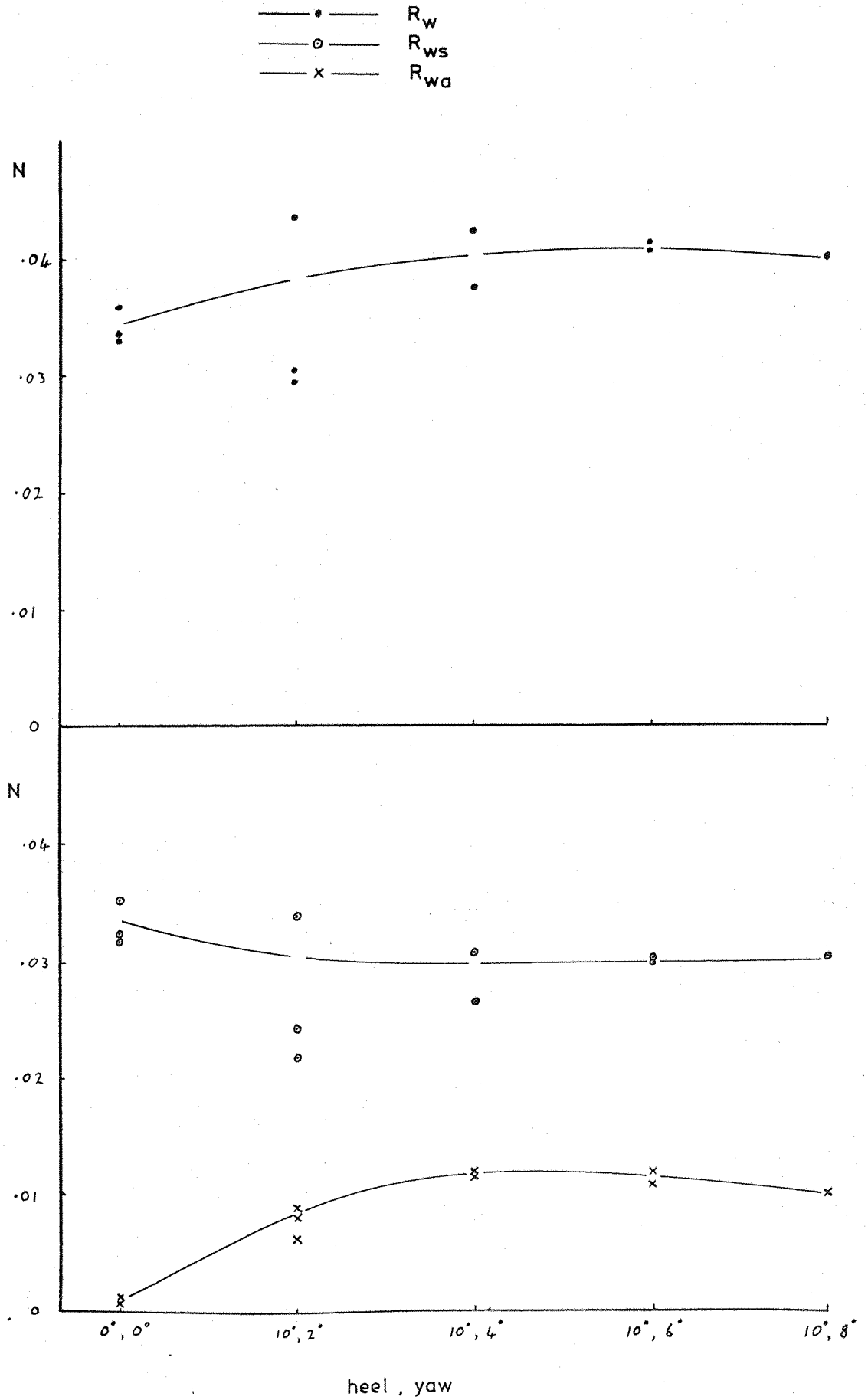

FIG 32

SYMMETRIC, ANTISYMMETRIC AND TOTAL WAVE RESISTANCE AGAINST ASPECT

U = 0·99 m/s F_r = 0·29

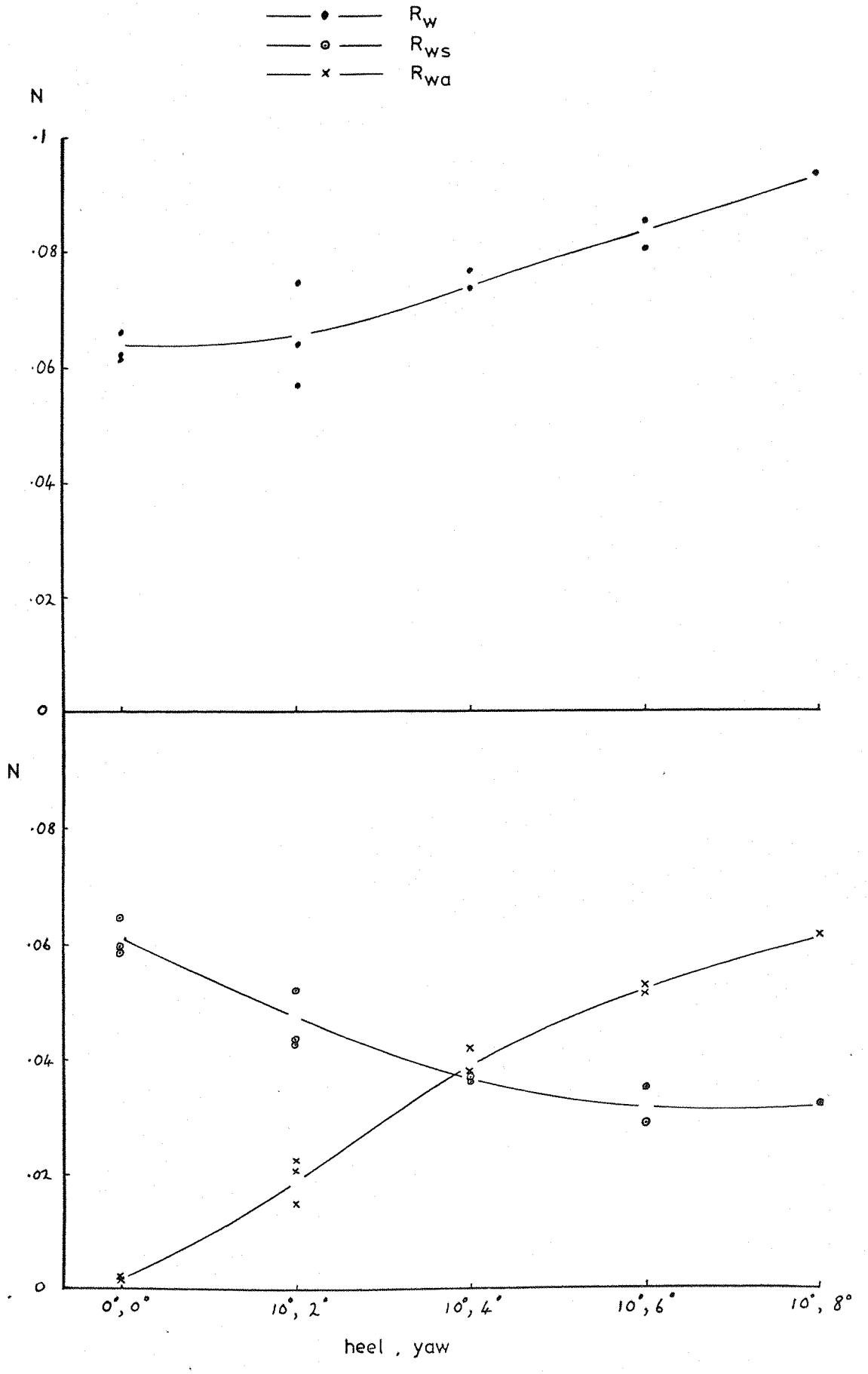

FIG 33

SYMMETRIC, ANTISYMMETRIC AND TOTAL WAVE RESISTANCE AGAINST ASPECT

U = 1·06 m/s F_r = 0·315

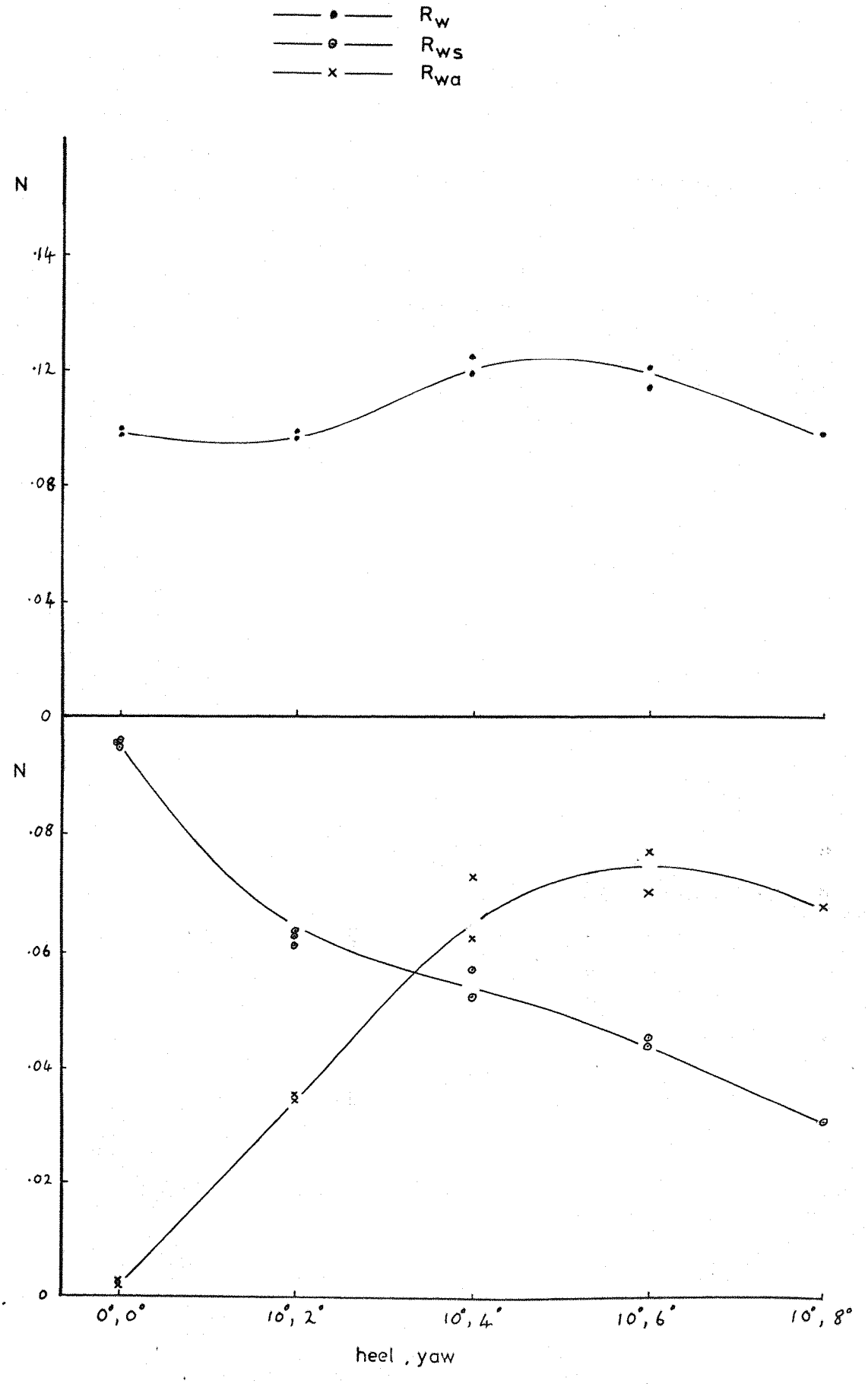

FIG 34

SYMMETRIC, ANTISYMMETRIC AND TOTAL WAVE RESISTANCE AGAINST ASPECT

U = 1·13 m/s F_r = 0·34

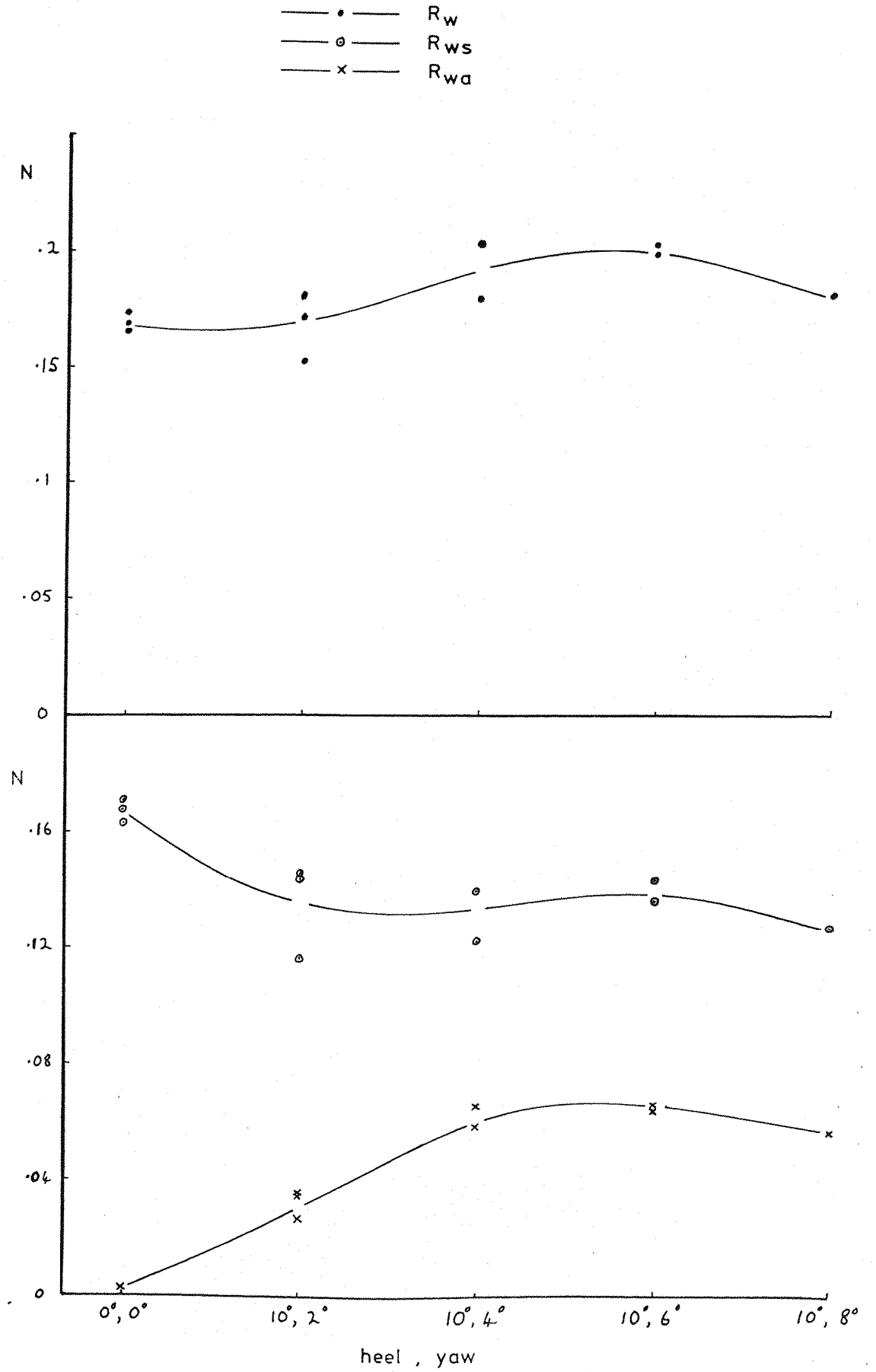

FIG 35 **SYMMETRIC, ANTISYMMETRIC AND TOTAL WAVE RESISTANCE AGAINST ASPECT**

$U = 1{\cdot}2$ m/s $\quad F_r = 0{\cdot}36$

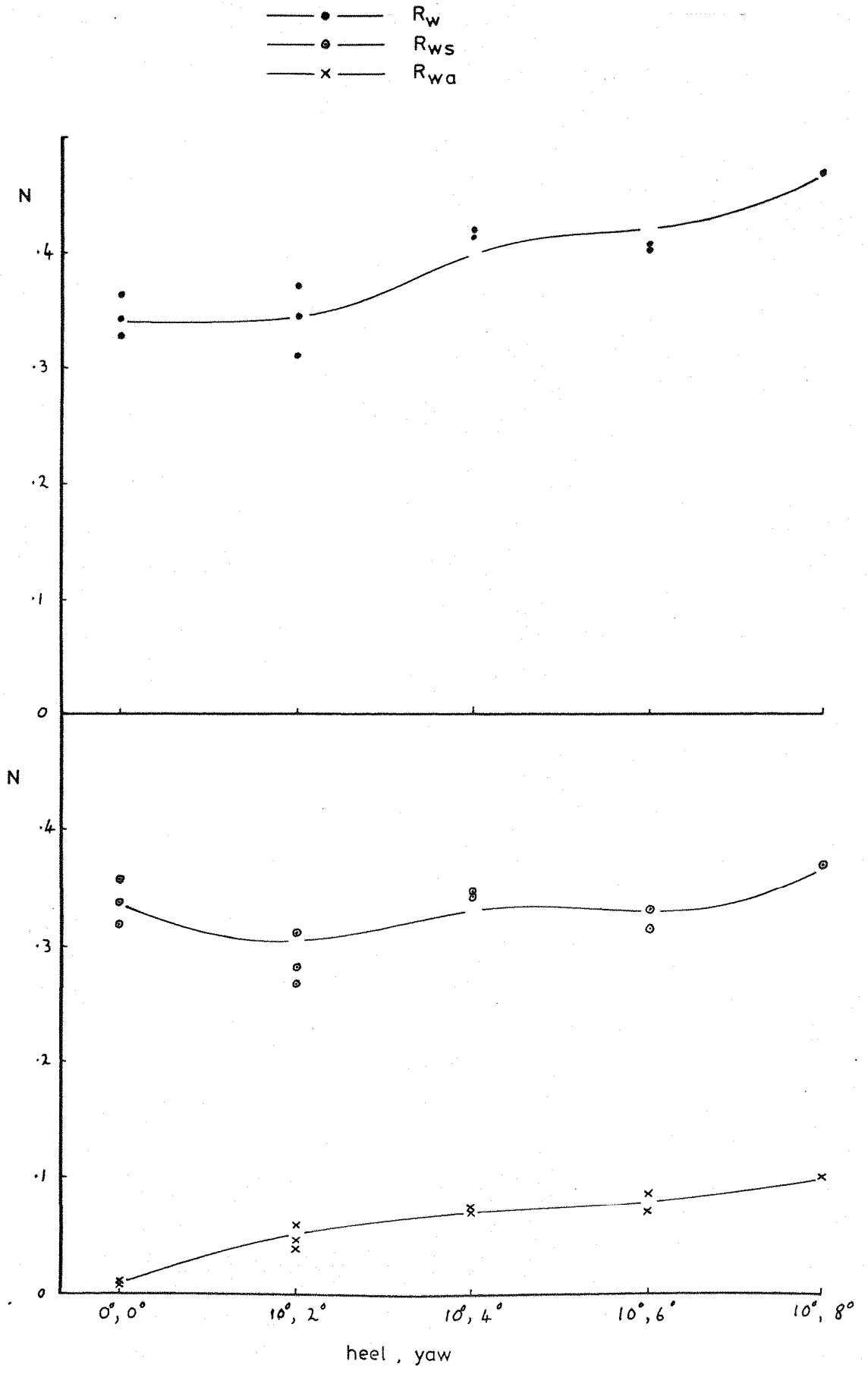

FIG 36

SYMMETRIC, ANTISYMMETRIC AND TOTAL WAVE RESISTANCE AGAINST ASPECT

$U = 1{\cdot}27\ m/s$ $\quad F_r = 0{\cdot}38$

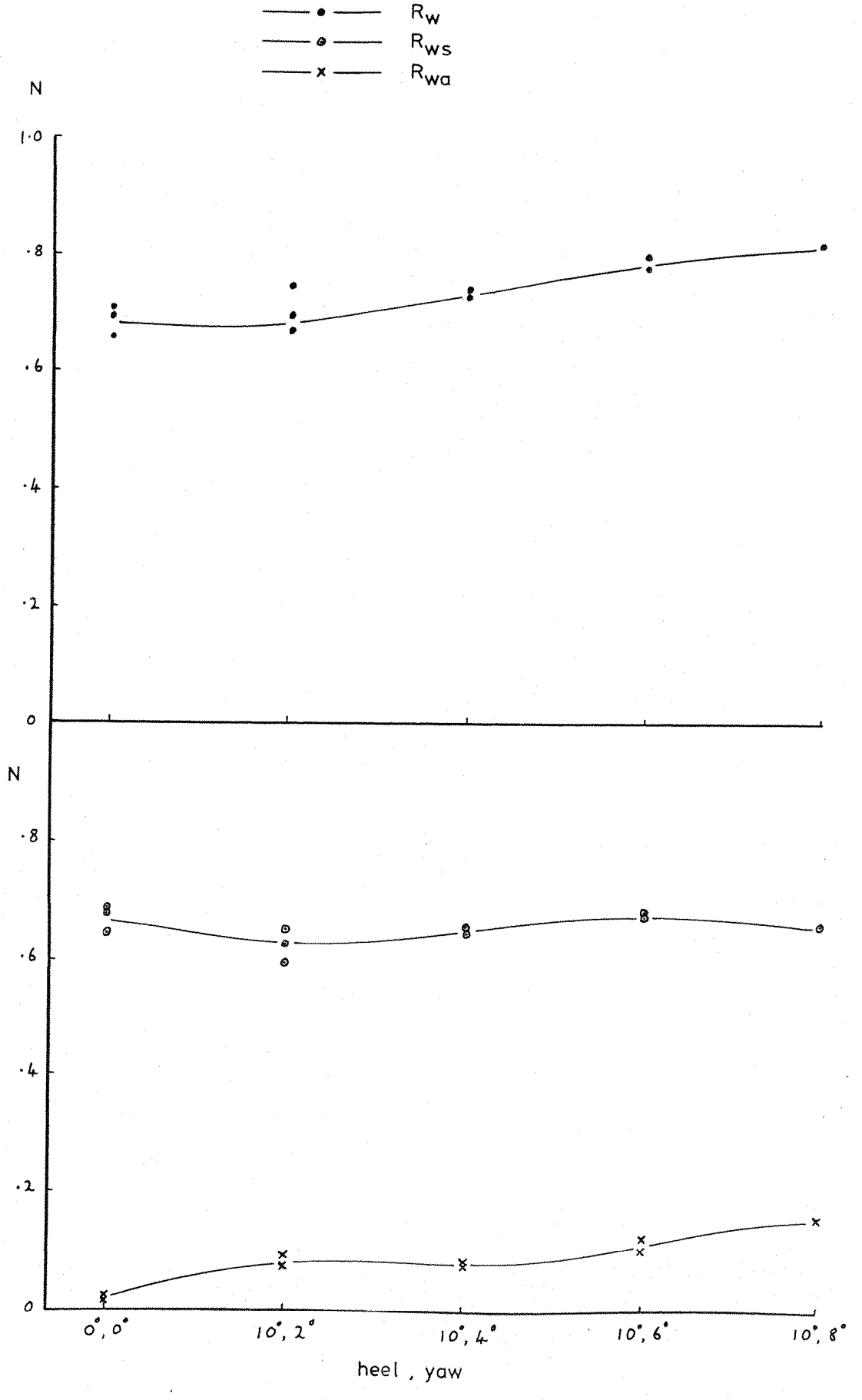

FIG 37

SYMMETRIC, ANTISYMMETRIC AND TOTAL WAVE RESISTANCE AGAINST ASPECT

U = 1·34 m/s F_r = 0·4

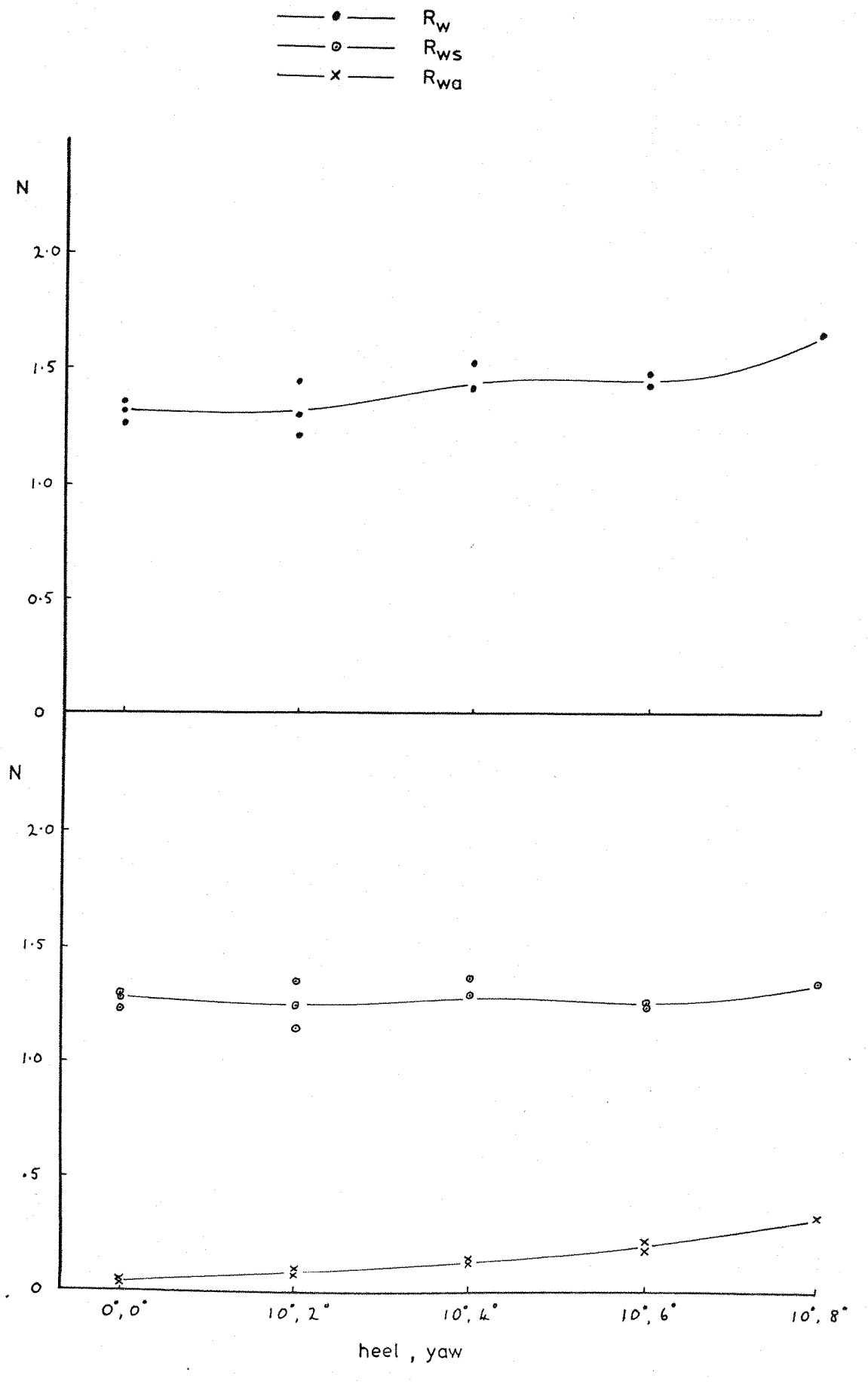

FIG 38

SYMMETRIC, ANTISYMMETRIC AND TOTAL WAVE RESISTANCE AGAINST ASPECT

U = 1·4 m/s F_r = 0·42

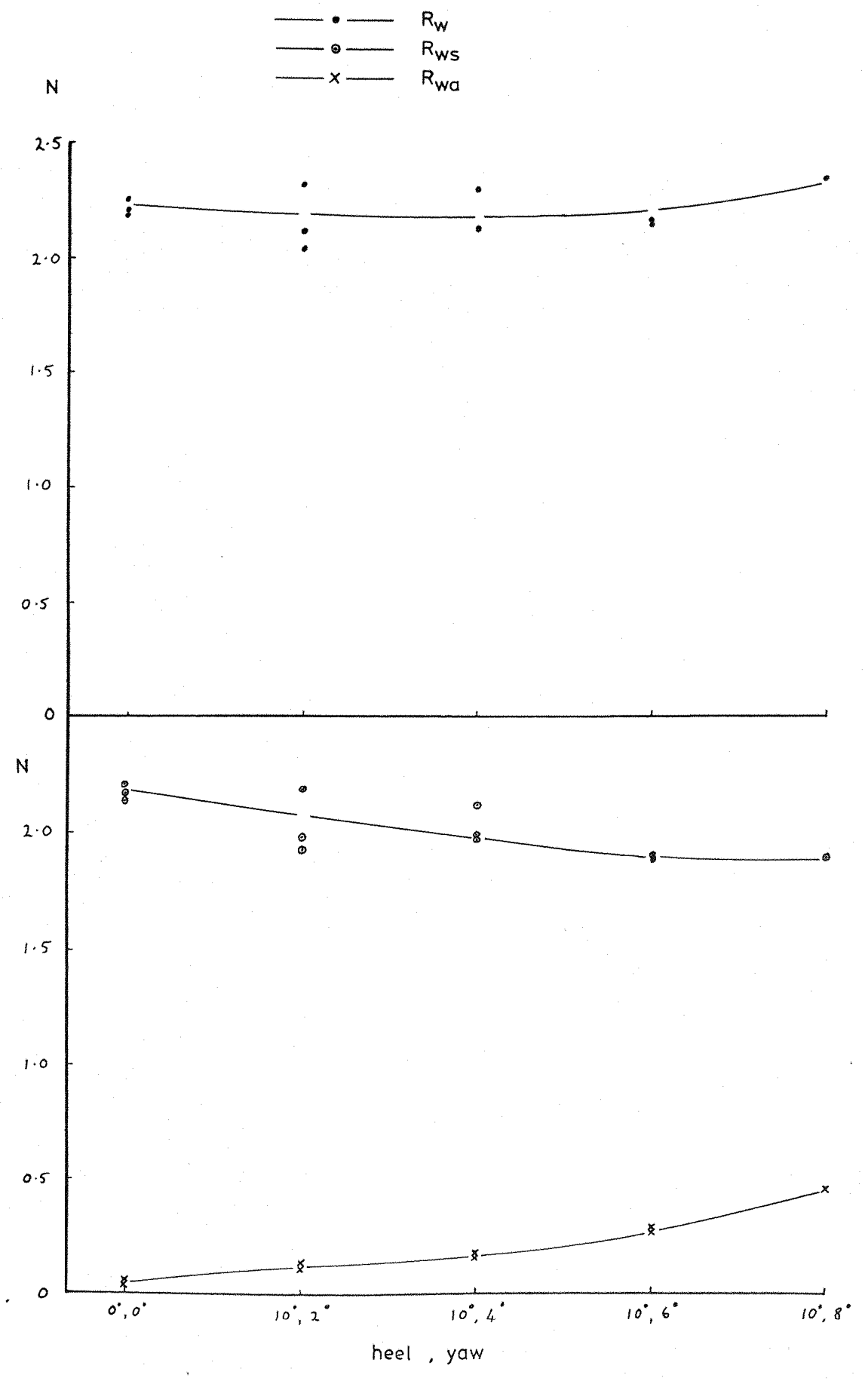

FIG 39

SYMMETRIC, ANTISYMMETRIC AND TOTAL WAVE RESISTANCE AGAINST ASPECT

U = 1·48 m/s F_r = 0·44

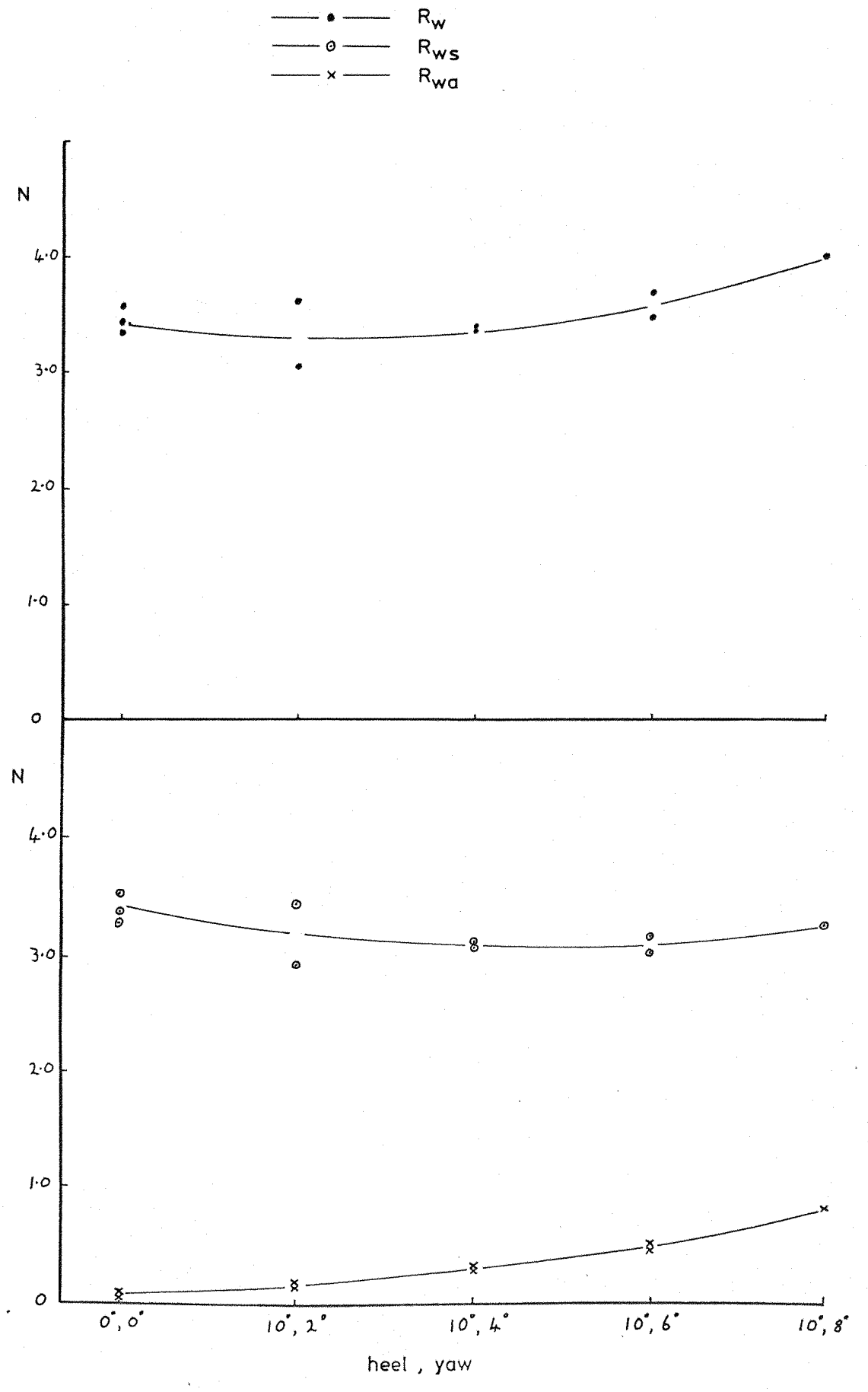

FIG 40 COMPONENTS OF TOTAL RESISTANCE AGAINST SPEED FOR THE UPRIGHT MODEL

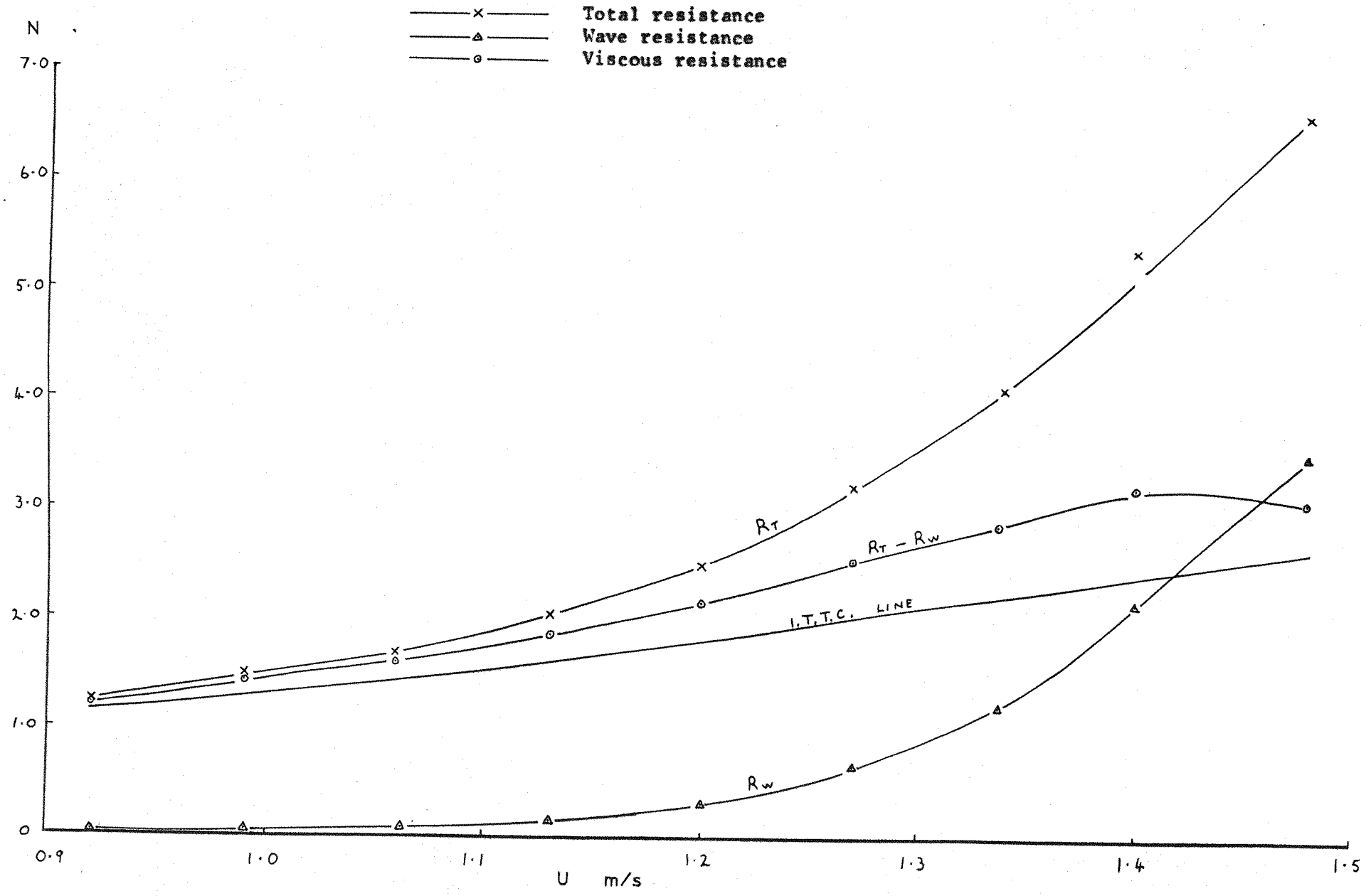

FIG 41 COMPARISON WITH WIND TUNNEL TESTS

U = 1·27 m/s F_r = 0·38

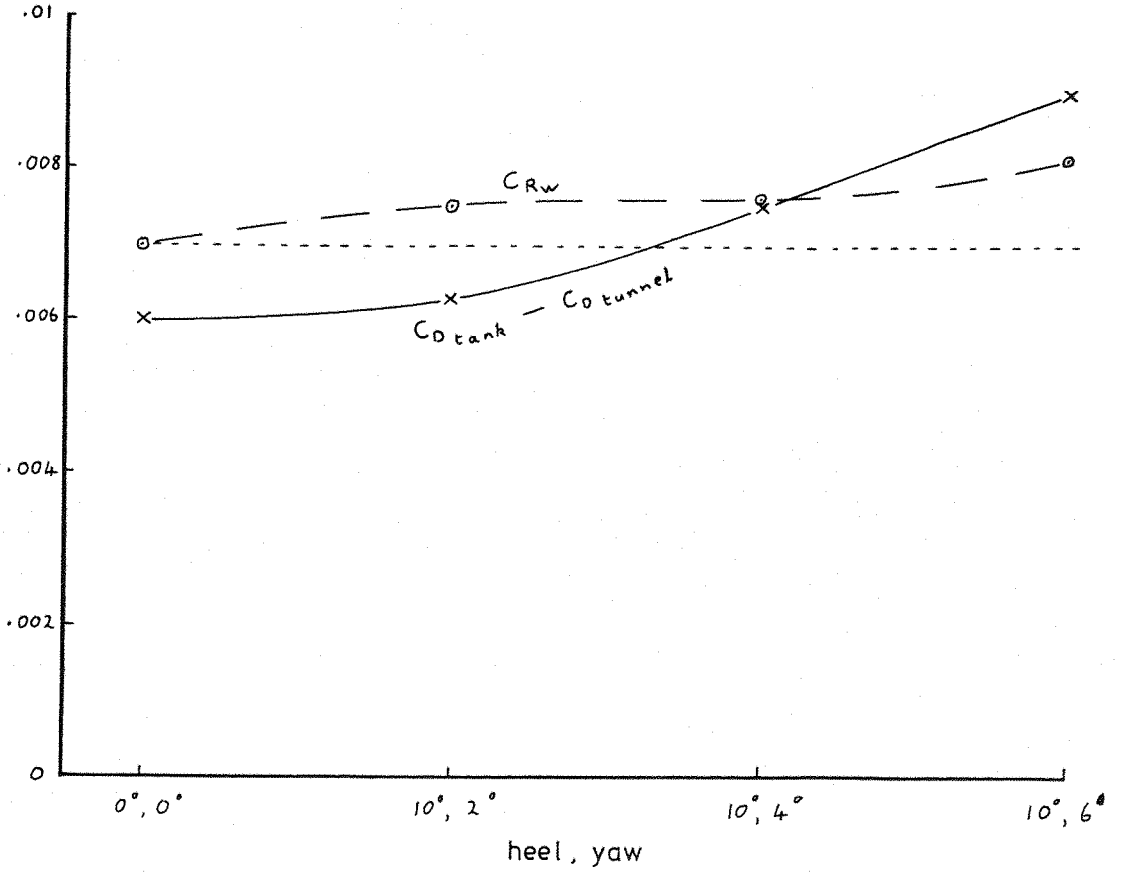

FIG 42 COMPARISON WITH WIND TUNNEL TESTS

U = 1·06 m/s F_r = 0·315

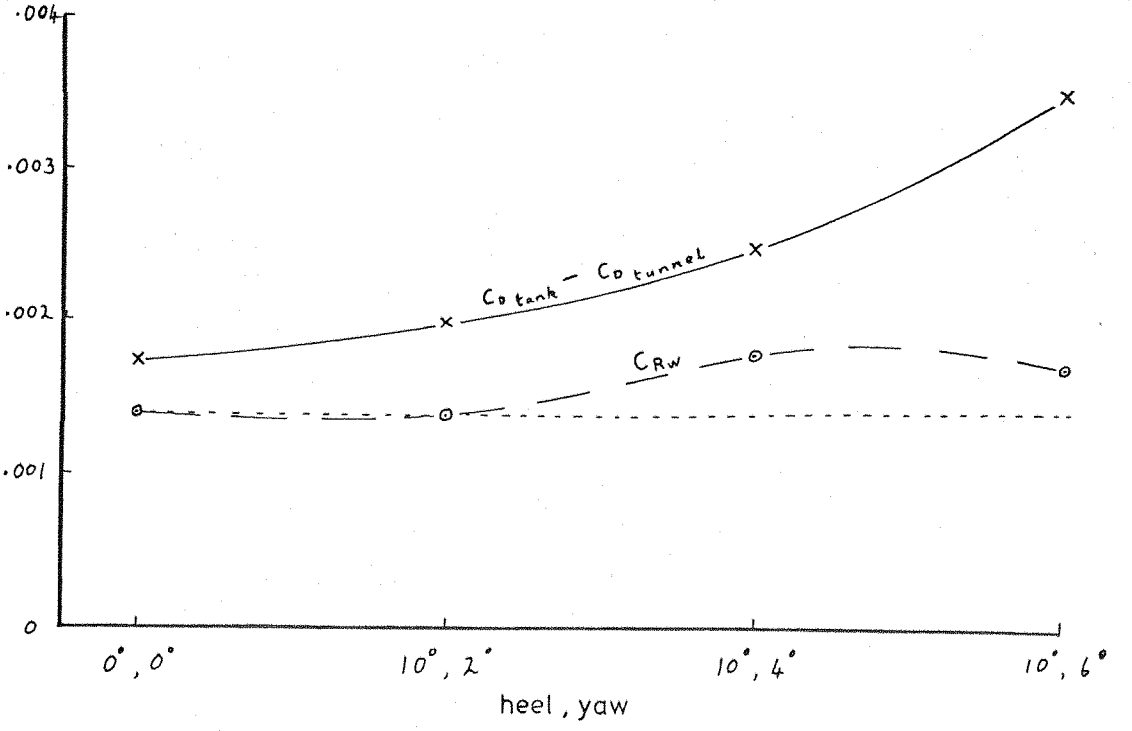

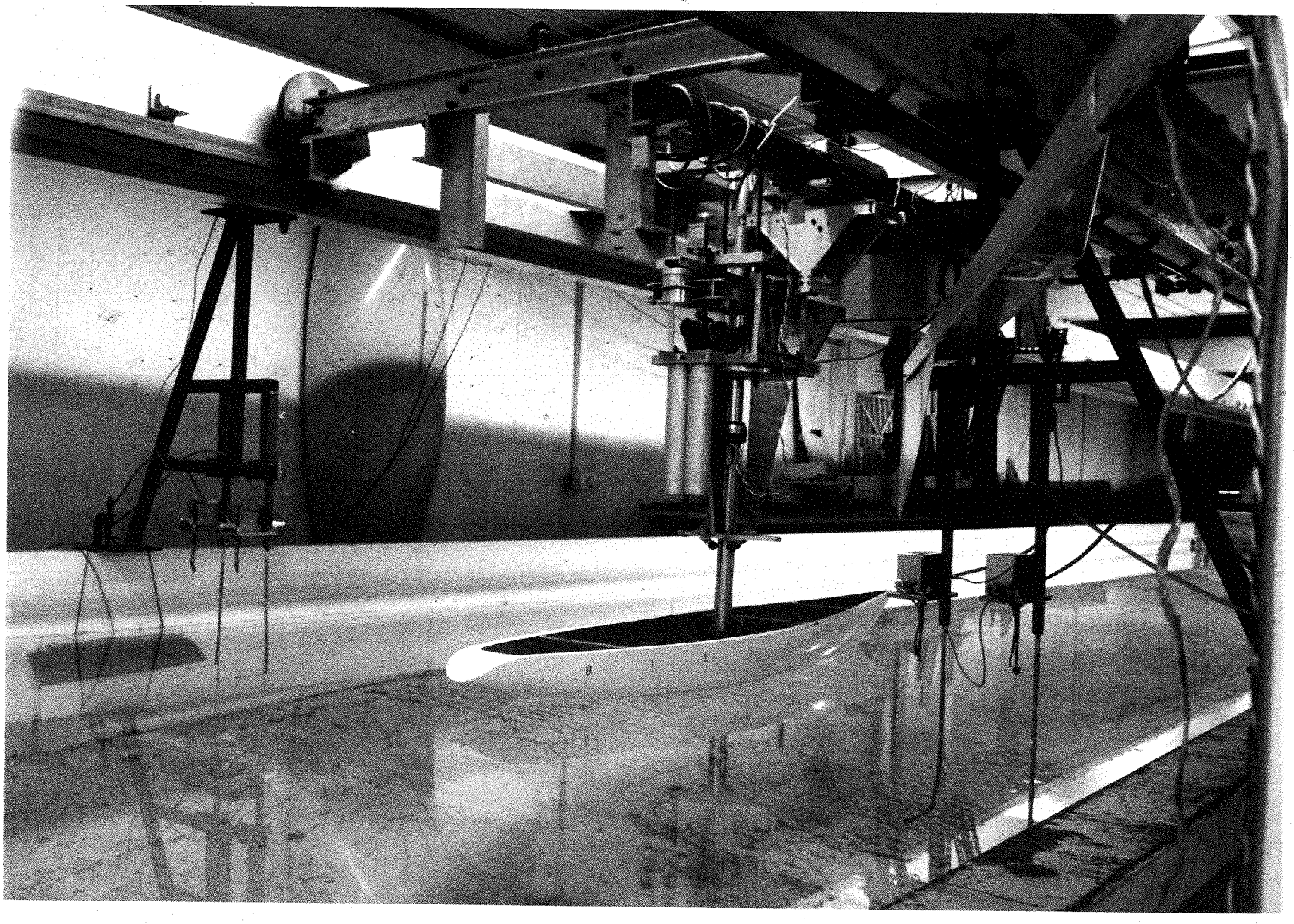

Plate 1 THE WAVE PROBES AND MODEL

Plate 2 UPRIGHT U = 1.06 m/s

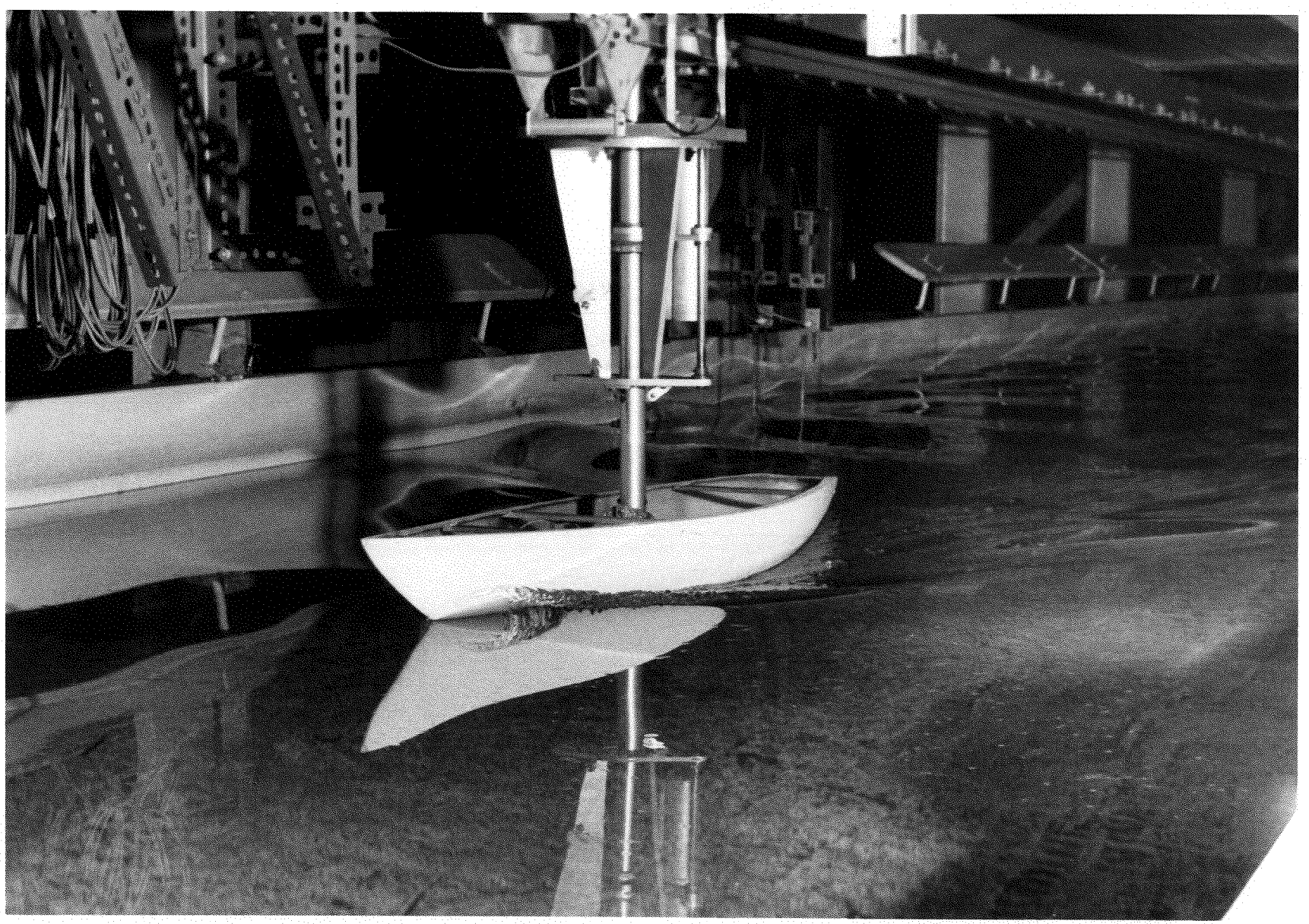

Plate 3 UPRIGHT U = 1.27 m/s

Plate 4 10^{o} HEEL 4^{o} YAW U = 1.06 m/s

Plate 5 10° HEEL 4° YAW U = 1.27 m/s